University of Rome
"Sapienza"

Department of Chemistry

PhD Thesis in Chemical Sciences

XXV Cycle

Novel Classes of Porphyrazine Macrocycles: Effect of π-Delocalization, Exocyclic Coordination and Quaternization Processes

Supervisor

Dr. Maria Pia Donzello

PhD Student

Dr. Giorgia De Mori

Reviewer

Prof. Giampaolo Ricciardi

Academic Year

2011-2012

INDEX

CHAPTER 1

INTRODUCTION

The profile of the work conducted in the present thesis is intimately connected and draws its motivation having as a basis the huge amount of relevant results cumulated in the last ten years on the octapyridinated pyrazinoporphyrazine macrocycle shown in Figure 1.1 and derivatives from.[1]

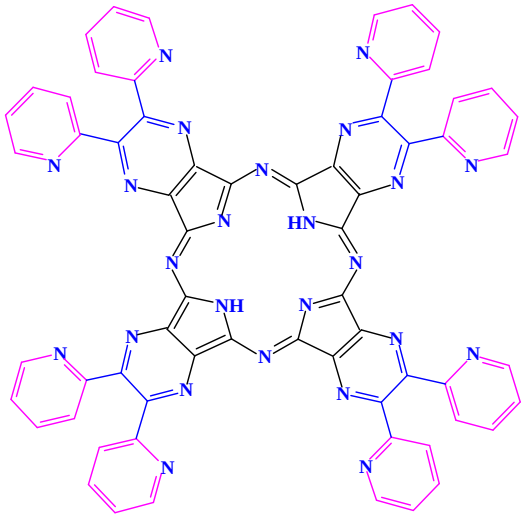

Figure 1.1. [$Py_8TPyzPzH_2$].

The world of the tetrapyrrolic macrocycles in terms of basic research and human and technological applications has been dominated in the last century and even at earlier times by the “naturally” occurring and “new lab prepared” porphyrins. Although the work of this PhD thesis scarcely concerns the *porphyrin* macrocycles, a short presentation of their structural and electronic features and the relevant role played in the many fields of the scientific area of utility for basic research and related applications is believed useful; this will clearly appear when reference will be made to the series of the *porphyrazine* macrocycles, a parallel class of tetrapyrrolic materials, to which belongs the molecular structure shown in Figure 1.1. The porphyrazines include the extremely interesting family of macrocycles named “*phthalocyanines*”, an ensemble of molecular structures so highly investigated in the last 60-70 years for reasons which will also require some short illustration below.

A crucial difference in the structure of porphyrins and porphyrazines, both carrying two central opposite NH groups, resides on the fact that their tetrapyrrolic cores see the pyrrole rings held together by four bridging *meso* =CH- groups in the porphyrins (see "porphine" in Figure 1.2A), and by the isosteric and isoelectronic N atoms instead of the =CH- groups in the case of porphyrazines (see "porphyrazine" in Figure 1.2B). This apparently limited difference in terms of composition for the two types of macrocycles, generates important specific prerogatives for the two tetrapyrrolic species in terms of physicochemical, structural and electronic properties and potentialities for practical and technological applications, as it has been established by the intense investigation carried out for years and years on the immense number of derivatives built on the central body of the two structures shown in Figure 1.2A,B. As can be evidenced looking at the structures in Figure 1.2, extensive π-electron delocalization is possible throughout the molecular framework for both of them. As a consequence, both types of macrocycles are practically forced to assume a planar or *quasi*-planar molecular arrangement. The σ/π-electron distribution, however, is different in the two macrocycles due to the fact that the bridging N atoms in the porphyrazine are more electronegative than the bridging =CH- groups in the porphine. As a result, electron distribution in the porphyrazine macrocycles (the one of Figure 1.2B or derivatives from) is less uniform than in the corresponding porphyrin compounds, with the electron density more shifted to the periphery of the macrocycle for the former species. As a consequence, porphyrins and porphyrazines, normally brown and blue/green respectively as solid materials, show quite different UV-visible solution spectral behaviour as will be detailed below.

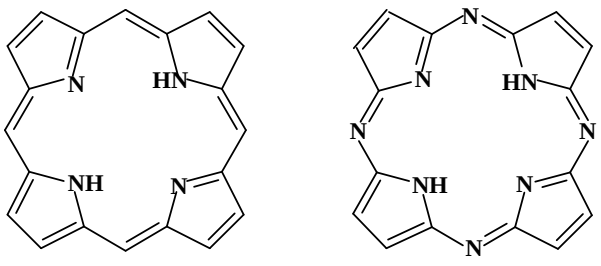

A B

Figure 1.2. A) Porphine; B) Porphyrazine.

Derivatives from the central porphyrin and porphyrazine cores (Figure 1.2A,B) can be built up in two ways; either by insertion of metal ions by substitution of the central H atoms on the NH groups, or by bearing external appropriate substituents on the *meso* positions or at the β-C atoms of the pyrrole rings. Reviewing work has shown the mosaic of the multifaceted investigations directed to an understanding of the role played by porphyrin macrocycles in fundamental biological processes and for the curative biomedical modalities of advantage for the living systems (*Porphyrins and Metalloporphyrins* (Falk, 1962); *"The Porphyrins*")[2] published by Dolphin, *"The Porphyrin Handbook"*.[3] Different important classes of macrocycles strictly connected to porphyrins, like chlorines and bacteriochlorines (see Figure 1.3A,B) were also extensively studied especially for biological and bacteriological aspects.[4] Even a short presentation of the above types of studies would lead out of the scope of this Introduction. Nevertheless, reference to some specific aspects concerning the work conducted on porphyrins will be made especially in connection with their UV-visible spectral features and utilization in photophysical applications, a subject of importance in the present PhD work.

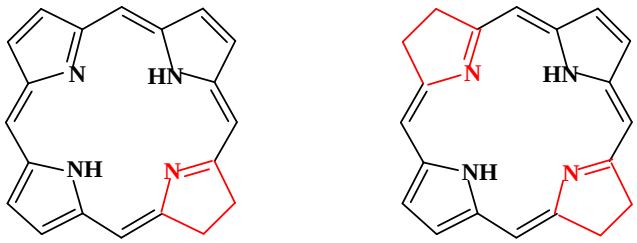

A B

Figure 1.3. A) Chlorine; B) Bacteriochlorine.

Part A. Phthalocyanines and Porphyrazines

A.1 Phthalocyanines

For several decades scientific work and possible applications on porphyrazines has been mostly focused on the phthalocyanine class of macrocycles, the basic structures of which are shown in Figure 1.4 (A: free base [PcH_2]; B: metal derivative [PcM], M = bivalent metal center).

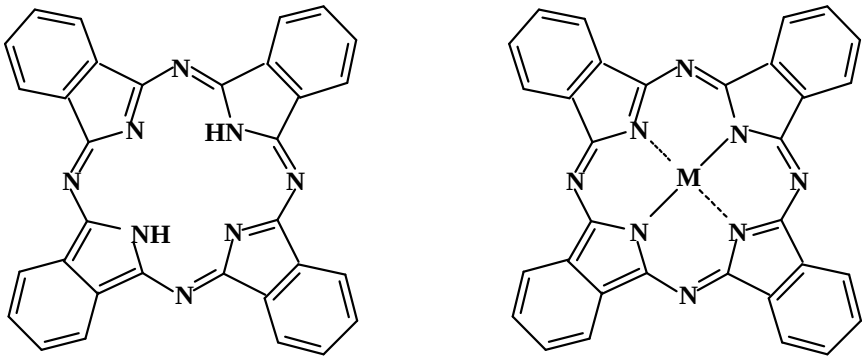

A B

Figure 1.4. A) [PcH_2]; B) [PcM] (M = bivalent metal ion).

The phthalocyanine macrocycle carries four benzene rings annulated to the pyrrole rings. The entire macrocycle is the site for a further extended π-electron delocalization with respect to that present in the porphyrazine central core shown in Figure 1.2B. Several reasons explain the prevalent attention devoted to the study of phthalocyanines with respect to that spent on the porphyrazines in general. First, they are often easily accessible by one-step reactions starting from phthalodinitrile in the presence of the appropriate metal center. Interestingly, [PcM] compounds can be purified by sublimation at 400-450 °C under vacuum (~10^{-2} mmHg) and they can be classified among the most thermally stable organic compounds having the presence of a metal center by about 10%. This thermal stability depends on the molecular structure made rigidly planar by the strong electron delocalization extended to the entire macrocycle. Since the first syntheses of the [PcM] series by R. P. Linstead and coworkers in 1930-1935 [5] and associated concomitant X-ray crystallographic work by J. M. Robertson,[6] it could be established that the [PcM] compounds exist in the

solid state in at least two solid state forms, the α and the β forms in which the molecules are stacked as shown in Figure 1.5, the β form being the one normally isolated as single crystals by sublimation under the above specified experimental conditions.

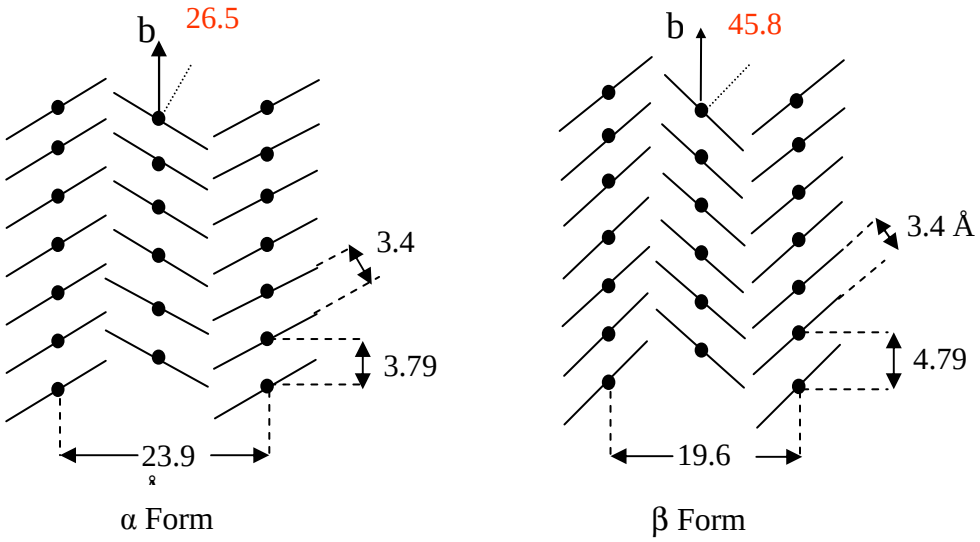

Figure 1.5

The arrangements shown in Figure 1.5 indicate that the molecular sheets of the phthalocyanine macrocycle can stay at a distance of about 3.4 Å. This is a distance apt to determine π-π interaction between adjacent molecules. This type of interaction can be frequently observed in solution studies, in which the phthalocyanine macrocycles can manifest tendency to aggregation with formation of dimeric species or forms of aggregation of higher order. UV-visible solution studies can be useful to detect the presence of aggregation and can provide information to distinguish in which solvents aggregation is a persistent effect and those solvents which give rise to spectra indicative of the exclusive presence of the monomeric species. It must be noted that aggregation is often occurring for porphyrazines in general.

The UV-visible spectrum of [PcZn] in solution of pyridine is shown in Figure 1.6. The spectrum shows intense absorptions in the Soret region (300-450 nm) and the Q-band region (600-700 nm). In the absence of aggregation, as is the case for [PcZn] in Figure 1.6, the Q band at 674 nm appears narrow and sharp and clearly indicates that the Zn(II)-phthalocyanine is present in solution essentially in its monomeric form. The presence of

aggregation can determine for the Q band limited or quite evident broadening. In case of the presence of two distinct absorptions in the Q-band region this might suggest an equilibrium monomer/dimer which needs to be studied as a function of the concentration in order to achieve information about the relative stability of the two forms. For these problematic aspects and others related to problems of stability of the monomeric species with the time or reactivity in general, UV-visible spectral studies represent a compulsory methodology of research and an excellent scientific instrument for investigation. The spectrum reported in Figure 1.6 is normally found for metal phthalocyanines in their monomeric form, and is the one appearing for simple porphyrazine macrocycles not significantly involved in some form of aggregation.

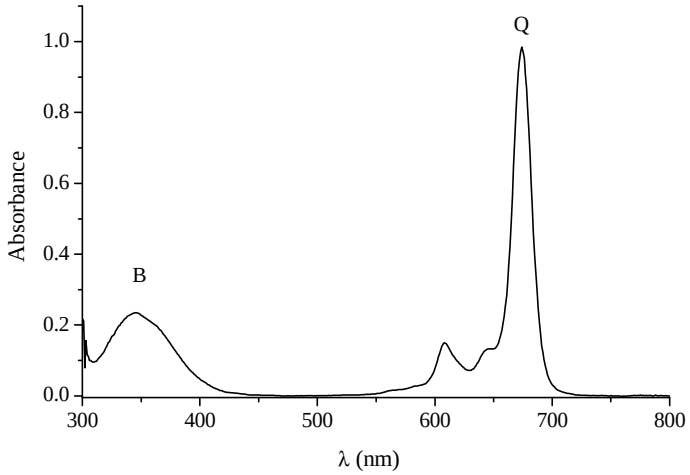

Figure 1.6. UV-visible spectrum of [PcZn] in pyridine.

It should be reminded here that phthalocyanines and porphyrazines in general are normally insoluble in water and show low solubility in low-donor solvents (dimethyl sulfoxide, DMSO; dimethylformamide, DMF; pyridine, py), reaching rarely in these solvents concentrations > 10^{-4} M. Since normally porphyrazines, including phthalocyanines, have high intensity Soret and Q bands, with ε values of the order of 100.000, UV-visible spectra can easily be registered using concentrations of the order of 10^{-5}-10^{-6} M or even lower with adequate instrumentation. The intense UV-visible absorptions in the Soret and Q-band regions are assigned as due to $\pi \rightarrow \pi^*$ intraligand transitions. Assignment of these transitions can be made based on the energy level diagram proposed by Gouterman[7] (four orbital model; Scheme 1.1) for the porphyrin macrocycles but then made applicable also to

the phthalocyanine and porphyrazine system. Such diagram easily allows to identify the HOMO-LUMO transitions for [PcM] compounds and also for [PcH_2], and in general for the parallel porphyrazine species. As can be seen, the lowering of the symmetry for the change [PcM] (D_{4h} symmetry) $\rightarrow$ [PcH_2] (D_{2h} symmetry) implies the splitting of the two e_g orbitals, which means that for [PcH_2] or a related porphrazine free-base ([PzH_2]) the Q band might be seen as split into two bands named Q_x and Q_y. Depending on the Q_x-Q_y energy separation the splitting of the Q-band can be evidenced by the spectrum or not, this depending also by the type of solvent used. Noticeably, [PcH_2] /[PzH_2] have acidic character and, depending on the experimental conditions, can give dissociation, ie. they undergo deprotonation with formation of the dianions Pc^{2-}/Pz^{2-} of D_{4h} symmetry, this leading to an unsplit Q-band. It is also noticed that the shape and position of the Soret and Q bands can be modified depending on the type of metal center. More consistent changes of the spectrum can occur in case, for example, of the presence of metal-to-ligand or ligand-to metal transitions. No doubt about it, the profile of the UV-visible spectrum and its modification as a function of different elements, ie. type of metal center, solvent, temperature, aggregation, etc. , can provide abundant precious information on the structural and electronic features of the Pc/Pz materials.

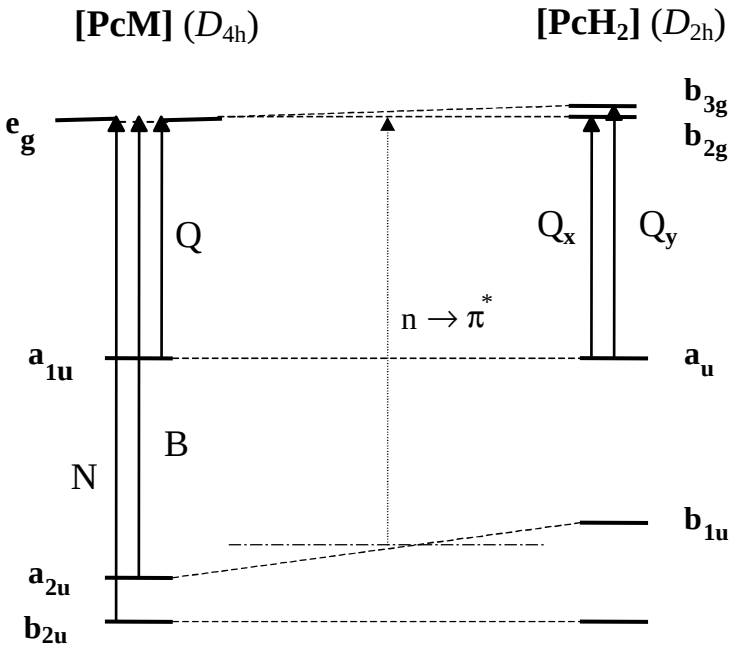

Scheme 1.1. Gouterman Orbital Energy Level Diagram for the tetrapyrrolic Pc/Pz macrocycles.

Already mentioned aspects characterizing the phthalocyanine molecules are concerned with their structural and electronic features. As already evidenced, they are intensively coloured materials, still today widely used industrially as dyes in many practical applications. They are highly thermally stable materials with positive returns in terms of environmental stability and durability. Insolubility in water can be seen as an advantage for some practical applications. As solid materials, practical uses have seen phthalocyanines studied as semiconductors, as non-linear optical materials and technically used for printers. Besides, studies are still conducted centered on their use as porphyrin-like materials in several fields. It should be taken into account that the phthalocyanine macrocycle can centrally coordinate practically all the elements of the Periodic Table known to have metallic character. In addition, introduction of a variety of substituents on the external benzene rings has allowed to expand enormously the number of phthalocyanine derivatives, this increasing the interest for the basic research and exploration of the applicative potentialities. Template macrocyclization of *o*-dicyano precursors followed by purification methods, in addition to sublimation, consisting of chromatographic techniques, has in most cases allowed to obtain highly pure materials open to technological applications. Basic research, often helped by sophisticated theoretical calculations, has led to learn a lot about their electronic structure, allowing the definition of their detailed energy level diagrams of their ground and excited states. The π-electronic delocalization in phthalocyanines, more extended than in porphyrins, favors the coplanar arrangement of the entire macrocycle, which can be seen as a “molecular sheet”.

A.2 Porphyrazines

Porphyrazine macrocycles in general, with the exclusion of the phthalocyanine compounds, were scarcely investigated until recent times. In the last two-three decades they have become the object of increasing attention. It happened in 1952 when R. P. Linstead and coworkers reported for the first time on the synthesis of simple porphyrazines, using a still today largely utilized procedure (template macrocyclization).[8] Luk'yanets *et al.* reported later on the synthesis of tetra-*t*-butyl-porphyrazines obtained by macrocyclization of 1,2-dicyano-3,3-dimethyl-1-butene, using the Linstead protocol.[9] However, a major step forward to the synthesis and structural investigation of novel classes of porphyrazine macrocycles was made by the concerted work of the A. G. M. Barrett's and B. M. Hoffman's groups with the preparation of a massive number of β-substituted porphyrazines ([R_8PzM], Figure 1.7), often implying exocyclic coordination and formation of multinuclear species. This relevant contribution to the development of the porphyrazine chemistry has been nicely reviewed.[10]

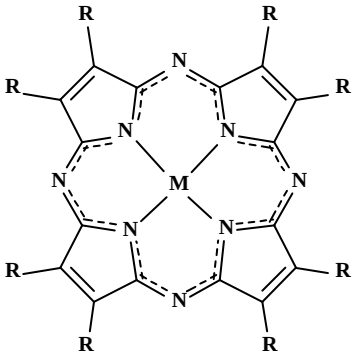

Figure 1.7. [R_8PzM].

Shown here below in Figures 1.8-1.10 are some of the most interesting macrocycles synthesized and in most cases structurally elucidated by single crystal X-ray work by the Hoffman-Barrett group.

In the previous years (1995-2000) it was believed by our group that an area of possible expansion of new classes of porphyrazine systems might be explored with the synthesis of phthalocyanine-like macrocycles carrying heterocyclic rings directly annulated to the

porphyrazine core, thus opening the route to new forms of investigations and promising potential practical applications. It must be reminded here that the first attempts directed to obtain phthalocyanine analogues in which the annulated benzene rings were substituted, for instance, by five-membered aromatic heterocycles[11] were already made in the 1930s by R. Linstead and his group. Since then only thiophene derivatives were described in some detail.[12] In more recent times mainly porphyrazine systems carrying externally annulated six-membered pyridine and pyrazine rings were reported.[13] A fairly complete overview on the porphyrazine macrocycles bearing annulated differently sized heterocyclic rings was published by P. A. Stuzhin and C. Ercolani.[14]

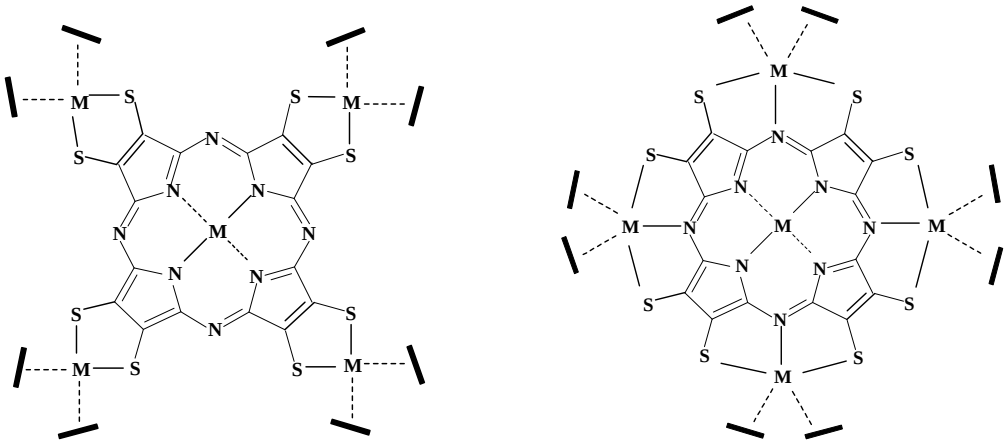

Figure 1.8. Coordination mode of the porphyrazineoctathiolate ligand: A) bidentate mode (S-S); B) tridentate mode (S-N-S).

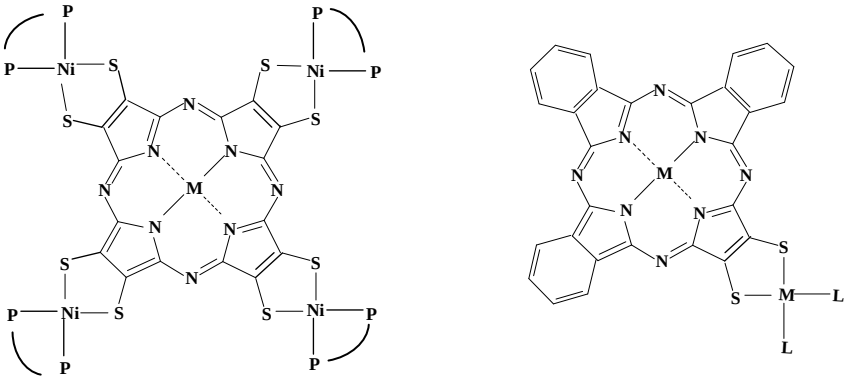

a **b**

Figure 1.9. A) *star*-porphyrazine; B) *solitaire*-porphyrazine.

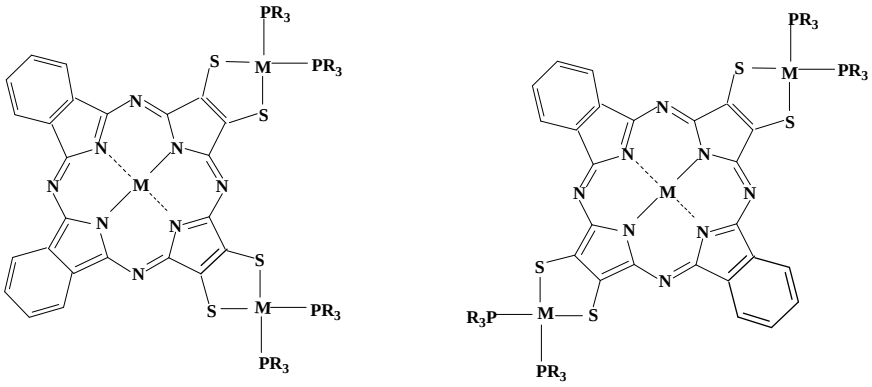

Figure 1.10. Molecular structure of *gemini*-porphyrazines.

Part B. Local experience in porphyrazine macrocycles

This piece of information is planned to provide the reader with a preliminary useful information for a better understanding of the reasons at the basis of the work project of the present PhD thesis. The effort is to clarify that the research lines, defined and developed during this thesis work, were seen in a contest of continuity with previous work carried out on a series of new classes of porphyrazines definitely representing an original as well as vast contribution to the knowledge and investigation of the potentialities of the porphyrazine macrocycles in terms of basic research and applications.

Three new classes of macrocycles were prevalently studied in the Donzello's lab during the last 10-15 years. These will be named here "thia/selenodiazolporphyrazines", carrying externally annulated thiadiazole (Figure 1.11A) and, alternatively, selenodiazole rings (Figure 1.11B), "diazepinoporphyrazines" (see further below, Figure 1.12) with externally attached diphenyldiazepino fragments, and "pyrazinoporphyrazines" (see Figure 1.1) characterized by the presence of four dipyridinopyrazine moieties annulated to the pyrrole rings of the central core. In the just cited Figures 1.11, 1.12, and 1.1, the macrocycles are represented as centrally unmetalated species. These three classes of macrocyles represent a qualified productive effort and an effective contribution to the enrichment of the knowledge of new well defined classes of porphyrazines sharing a number of structural and electronic features and potentialities in terms of applications.

B.1 Porphyrazines with annulated five-membered thiadiazole and selenodiazole rings

The first report on tetrakis(thiadiazol)porphyrazines was on the Cu^{II} complex, [TTDPzCu], prepared by a one-step macrocyclization reaction of the precursor 1,2,5-thiadiazole-3,4-dicarbonitrile with Cu powder .[15] However, purification was incomplete and the product was obtained as an impure material. A number of metal derivatives of the tetrakis(thia/selenodiazol)porphyrazines of general formulae [TTDPzM] and [TSeDPzM] carrying bivalent non transition and first transition series metal ions were prepared by our group for both types of macrocycles (S/Se) by synthesizing first the Mg^{II} complex by a template reaction and then expanding the two new classes of compounds by using the sequence Mg^{II} complex $\rightarrow$ free-base $\rightarrow$ metal derivative. The two classes of S/Se porphyrazines, described in several publications and patents, are the type of macrocycles most closely recalling the phthalocyanine molecular framework. Noticeably, they are also isoelectronic with this latter type of molecular ring. All the work until the year 2006 on the S/Se-porphyrazines was reported in detail in a review article.[16]

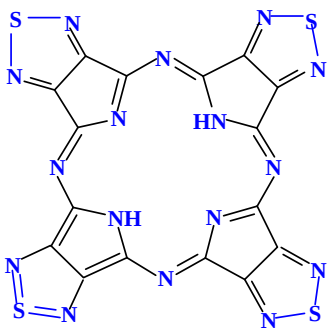

A

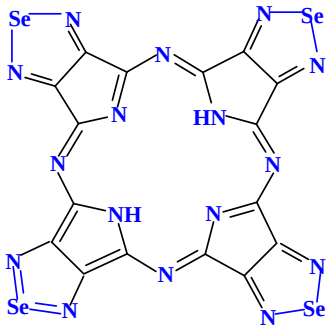

B

Figure 1.11. A) Tetrakis(thiadiazol)porphyrazine, [$TTDPzH_2$]; B) Tetrakis(selenodiazol)porphyrazine, [$TSeDPzH_2$].

The two new classes of S/Se compounds share with phthalocyanines insolubility in water and very low solubility in organic low-donor solvents and, similarly, exhibit very high thermal stability. The S-porphyrazines, similarly to phthalocyanines, are easily sublimable, although under fairly drastic experimental conditions (10^{-2} mmHg, ca. 400 °C).

Sublimability allowed isolation of single crystals for a number of the S-porphyrazines and X-ray crystallographic work led to elucidation of the structure of different solid state forms of several [TTDPzM] complexes.[17] Presently, the crystallographic information for the S-porphyrazines is much more extended than that obtained in several decades on the phthalocyanine compounds having similar formulation [PcM]. Crystallographic work has been further enriched by detailed UV-visible spectral, electrochemical and theoretical DFT and TDDFT studies for the accurate investigation of their electronic structure.[18] The UV-visible spectra of all the S/Se complexes show intense absorptions in the Soret (300-450 nm) and Q-band regions (600-700 nm), assigned to the allowed HOMO-LUMO intraligand π–π^* transitions, this behaviour closely approaching the usual spectral pattern observed for the class of phthalocyanine species.

The structural arrangement in the solid between adjacent molecules for the [TTDPzM] compounds, often suggestive of the formation of dimers, indicates the role played by the π-π interaction and explains the frequently observed aggregation in solution studies, a phenomenon common to the porphyrazine macrocycles in general, as above outlined. Another important common feature of the S-and Se-porphyrazines and also of and the other porphyrazine macrocycles considered in this section of the thesis, is their tendency to behave as "electron-deficient" macrocycles, due to the presence of the peripheral heterocyclic rings containing the highly electronegative N, S, and Se atoms. The effect is an increment of the σ/π electron density distribution towards the periphery of the macrocycle with the consequence that the tendency to reduction of these macrocycles is enahanced with respect to what is observed for the parent phthalocyanine species.

B.2 Porphyrazines with annulated seven-membered diazepine rings

Synthetic work was also extended in our laboratory to the preparation of a new class of porphyrazine macrocycles carrying annulated seven-membered diazepine rings, ie. the tetrakis-2,3-(5,7-diphenyl-6*H*-1,4-diazepino)porphyrazine, [Ph_8DzPzH_2] (see schematic representation in Figure 1.12) and its metal derivatives [Ph_8DzPzM] (M = $Mg^{II}(H_2O)$, Mn^{II}, Co^{II}, Cu^{II} and Zn^{II}).[19]

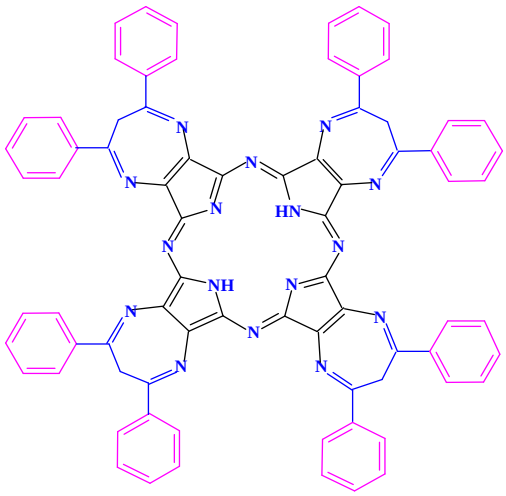

Figure 1.12. Schematic representation of the **"**diazepinoporphyrazine" free-base [Ph_8DzPzH_2].

Differently from the S/Se-porphyrazines, the diazepinoporphyrazine macrocycles are appreciably soluble (c = 10^{-3}-10^{-4} M) in non donor ($CHCl_3$, CH_2Cl_2) and low donor solvents (DMSO, DMF, CH_3CN). Solubility values even higher were observed in pyridine. Like S-, Se-porphyrazines and phthalocyanines, the "diazepinoporphyrazines" show intense absorptions in the Soret (300-400 nm) and Q-band (600-700 nm) regions. The interesting new characteristic spectral feature is that they show remarkable differences in the Q-band region, where they exhibit two peaks, one in the range 630-640 nm and the other one in the range 660-680 nm. The presence of these two peaks cannot be due to a Q band splitting, since it is also observed for the metallic derivatives. It has been suggested that the absorption at lower wavelenghts is due to the π-π^* transition ("normal" Q band), while the long-wave absorption is due to the n-π^* transition (Q_n-band).

The diazepine macrocycles are thermally stable up to temperatures of 250-300 °C in an inert atmosphere or under vacuum. They show no tendency to sublimation due to the presence of clathrated water molecules. The electrochemical and spettroelectrochemical behaviour[20] indicate that the observed reversible multistep one-electron reduction processes take place at remarkably more positive potentials than those of the parallel series of metal phthalocyanines. This provide evidence of the electron-withdrawing effect determined by the presence of the diazepinic rings.

From the structural point of view, the new "diazepinoporhyrazine" macrocycles, differently from the above mentioned "thia/selenodiazolporphyrazines", are far from

complete coplanarity of the macrocycle due to the presence of the boat-shaped diazepine rings in their 6H conformation (see the schematic representation of the precursor in Figure 1.13) and the external variable positions of the benzene rings. Reasonably, the four diphenyldiazepino fragments can have different orientation with respect to the plane of the central porphyrazine core; correspondingly, different isomers are possibly formed, coinciding with a different symmetry of the entire macrocycle. This aspect waits for further research work for a better clarification. ^{1}H-NMR studies performed in solution of different solvents under variable experimental conditions indicate that the diazepine rings can undergo a tautomeric equilibrium between the 6H and 1H forms (**I** and **II** in Figure 1.14, respectively). Protonation of the diazepine rings can lead to their full coplanarity (see forms **III** and **IV** in Figure 1.14).

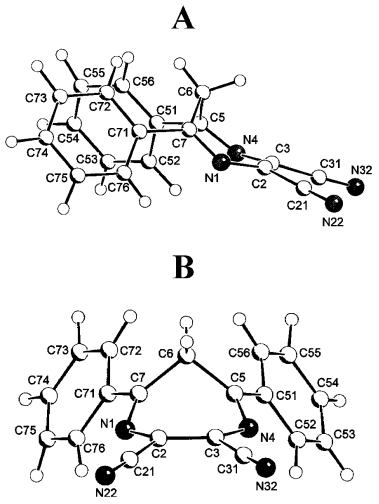

Figure 1.13. SCHAKAL side (A) and front-top (B) views of the 2,3-Dicyano-5,7-diphenyl-6*H*-1,4-diazepine.

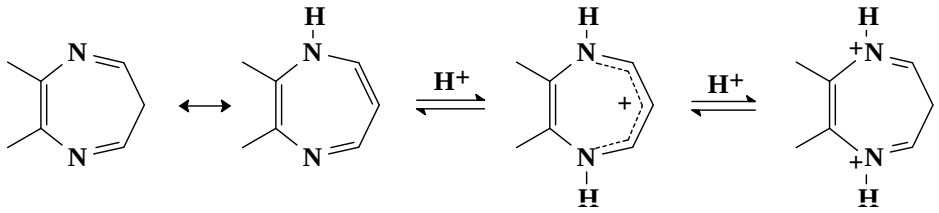

Figure 1.14

Part C. Pyrazinoporphyrazines with Externally Appended Pyridine Rings

It was several years ago when the lab group planned to start a synthetic approach leading to the formation of the free-base pyrazinoporphyrazine macrocycle tetrakis-2,3-[5,6-di(2-pyridyl)pyrazino]porphyrazine, [$Py_8TPyzPzH_2$], shown in Figure 1.1. It was established that this free-base macrocycle can be straightforwardly obtained in high yield by direct autocyclotetramerization of its precursor, the 2,3-dicyano-5,6-di(2-pyridyl)-1,4-pyrazine, [$(CN)_2Py_2Pyz$)], in the presence of 1,8-diazabicyclo[5.4.0] undec-7-ene (DBU) as catalyst (Scheme 1.2).[1] Thus, the route was open from [$Py_8TPyzPzH_2$] to the synthesis of a new series of mononuclear species of formula [$Py_8TPyzPzM$] (M = $Mg^{II}(H_2O)$, Mn^{II}, Co^{II}, Cu^{II}, Zn^{II}).[21] These "pyrazinoporphyrazine" macrocycles are very scarcely soluble in non-aqueous non-polar solvents ($CHCl_3$, CH_2Cl_2) and slightly better soluble in low-donor solvents (DMSO, DMF, pyridine). Molecular aggregation is observed in many cases depending on the particular species and the solvent.

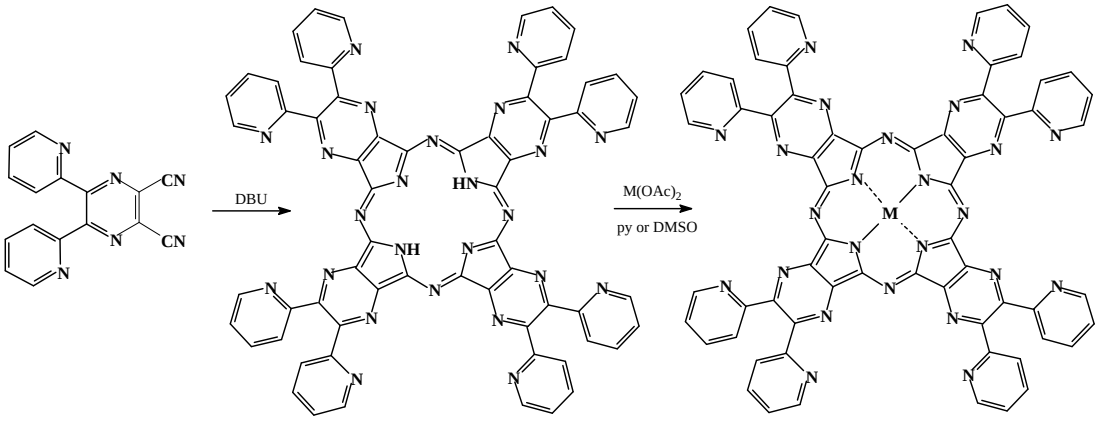

Scheme 1.2. Synthesis of "pyrazinoporphyrazine" macrocycles.

The UV-visible spectral changes followed as a function of time indicate, in all cases, a one-way disaggregation process, ending with formation of clean monomeric macrocyclic units. The final spectrum is as expected for a normal porphyrazine macrocycle of D_{4h} symmetry for the metal complexes [$Py_8TPyzPzM$], and D_{2h} symmetry in the case of the free-base ligand [$Py_8TPyzPzH_2$], showing narrow Q bands (600-700 nm) and B bands (300-450 nm)

due to the HOMO-LUMO π-π* transitions (Scheme 1.1). A spectrally monitored titration of [$Py_8TPyzPzH_2$] in CH_2Cl_2 with TBA(OH) shows the loss of two protons from the macrocyclic core and quantitative conversion of [$Py_8TPyzPzH_2$] to its corresponding dianion [$Py_8TPyzPz]^{2-}$. Cyclic voltammetry and thin-layer spectroelectrochemical measurements show that [$Py_8TPyzPzH_2$] is present in its neutral form in CH_2Cl_2, while deprotonation takes place in pyridine with formation of the dianion [$Py_8TPyzPz]^{2-}$. Both forms, neutral and dianionic, of the compound, exhibit identical electrochemical behavior, consistent with a conversion of the dianion to the neutral porphyrazine in pyridine prior to electroreduction via four reversible one-electron transfer steps.[1] A comparison of the electrochemical behavior of the macrocycles [$Py_8TPyzPzH_2$] and [$Py_8TPyzPzM$] (M = $Mg^{II}(H_2O)$, Mn^{II}, Co^{II}, Cu^{II} and Zn^{II}) with that of the phthalocyanine analogs indicates a more facile trend of the observed stepwise reversible or *quasi*-reversible reductions leading to the formation of the species $[Py_8TPyzPzM]^{n-}$ (n = 1-4). This, in keeping with the observed UV-visible spectral behaviour, highlights the remarkable electron-deficient properties of the new series of "pyrazinoporhyrazine" macrocycles.

A special chapter of the investigations conducted on the species [$Py_8TPyzPzM$] is related to the definition of the role played by the external pyridine rings in terms of coordination properties and possible formation of octacationic species, obtained upon quaternization of the pyridine N atoms by reaction with CH_3I. As will be shortly reported here below, these two aspects were given accurate attention, which consistently enlarged the work conducted on these "pyrazinoporphyrazine" macrocycles with added information of great interest.

C.1 Exocyclic coordination of metal centers (Pd^{II}, Pt^{II})

C.1.a Coordination properties of the dipyridinopyrazine fragment

Before entering the aspect of the possible coordination of metal centers to the dipyridinopyrazine fragment, it is useful remind that for the entire pyrazinoporphyrazine macrocycle a detailed structural information about bond distances and bond angles,

arrangement of the central tetrapyrazinoporphyrazine core, and orientation of the pyridine rings relative to one another and to the central quasi-planar porprhyrazine core, could be obtained by the single-crystal X-ray work carried out on the Co^{II} complex $[Py_8TPyzPzCo(DMSO)_2]$ (Figure 1.15).[22]

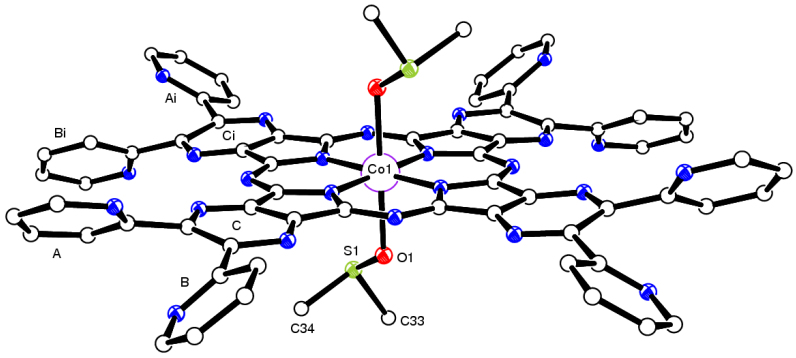

Figure 1.15. ORTEP drawing of the molecular structure of $[Py_8TPyzPzCo(DMSO)_2]$ (hydrogen atoms omitted).

As can be seen from the structure, the orientation of the pyridine rings can be such that one pyrazine N atom and one pyridine N atom can generate a bidentate coordination site able to attract a metal center (pyz-py coordination). Alternatively, the dipyridinopyrazine fragment can appropriately orient the two pyridine N atoms forming a donor center able to fix the metal center (py-py coordination). Literature reports cited[23] have shown that in most cases, for molecules containing the dipyirinopyrazine fragment or related molecules (quinoxaline, etc.), py-py coordination frequently occurs, but rare cases are known in which pyz-py coordination is also occurring. An important piece of information has been obtained by our group by isolating single crystals and elucidating by X-ray work the structure of the $PdCl_2$ and $PtCl_2$ derivatives of the precursor $[(CN)_2Py_2Pyz]$, i.e $[(CN)_2Py_2PyzPdCl_2]$[24] and $[(CN)_2Py_2PyzPtCl_2]$.[23] In both compounds a practically identical py-py coordination occurs. The front and side view of the structure of the Pd^{II} species is reported in Figure 1.16.

Worth of notice, the structure of $[(CN)_2Py_2PyzPdCl_2]$ shows a non coplanar positioning of the pyrazine and pyridine rings. In addition, the $N_{2(py)}PdCl_2$ square planar coordination site lies nearly perpendicular to the plane of the pyrazine ring. This is a privileged base of

information when considering the exocyclic coordination of $PdCl_2$ and $PtCl_2$ units in the octapyridinated "pyrazinoporphyrazine" macrocycle shown in the Figures 1.1 and 1.15.

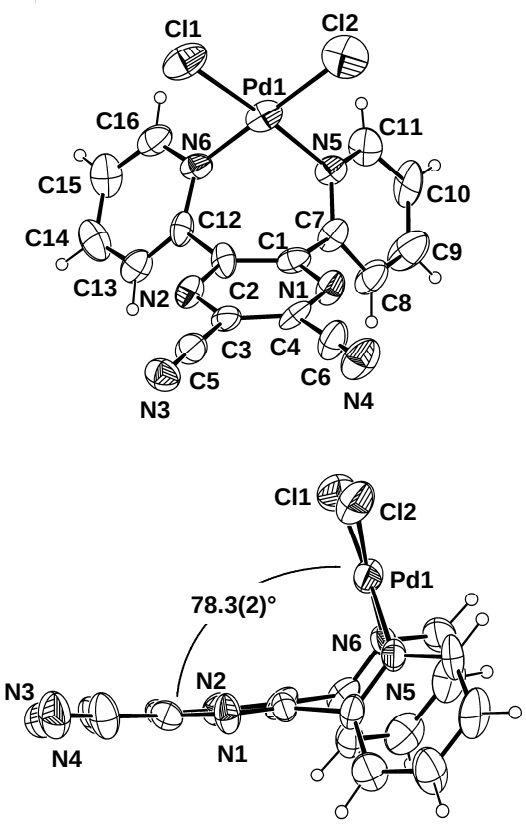

Figura 1.16. ORTEP front (top) and side (bottom) views (30% probability ellipsoid) of $[(CN)_2Py_2PyzPdCl_2]$.

C.1.b Exocyclic coordination of $PdCl_2$ and $PtCl_2$ units in the pentanuclear "pyrazinoporphyrazine" macrocycles

A triad of complexes of the pyrazinoporhyrazine macrocycle $[Py_8TPyzPzH_2]$ carrying centrally Pd^{II} could be obtained in the sequence $[(PdCl_2)_4Py_8TPyzPzPd] \rightarrow [Py_8TPyzPzPd] \rightarrow [(2\text{-Mepy})_8TPyzPzPd]^{8+}$ (the latter neutralized by I^- ions).[24] Mainly focusing on the aspect of the structural features in terms of the type of exocyclic coordination of the $PdCl_2$ units in the pentanuclear compound $[(PdCl_2)_4Py_8TPyzPzPd]$, it should be noted that the information achieved from NMR spectral studies revealed with certainty the equivalent involvement of contiguous pyridines in the macrocycle in the

ligation to Pd^{II}; this conclusively indicating the formation of all four external $N_{2(py)}PdCl_2$ coordination sites in the macrocycle, in line with the findings for the $PdCl_2$ and $PtCl_2$ derivatives of the precursor $[(CN)_2Py_2Pyz]$ (see Figure 1.16).

Illustrative demonstration of the stated py-py coordination is shown by the exemplifying response of the ^{1}H-NMR spectra shown in Figure 1.17, where the spectra of the three species $[(CN)_2Py_2Pyz]$ (A), $[(CN)_2Py_2PyzPdCl_2]$ (B) and the pentapalladated complex $[(PdCl_2)_4Py_8TPyzPzPd]$ (C) are shown. Four main resonance peaks are present in all three species proving the equivalent involvement of the pyridine rings in the coordination of the $PdCl_2$ units.

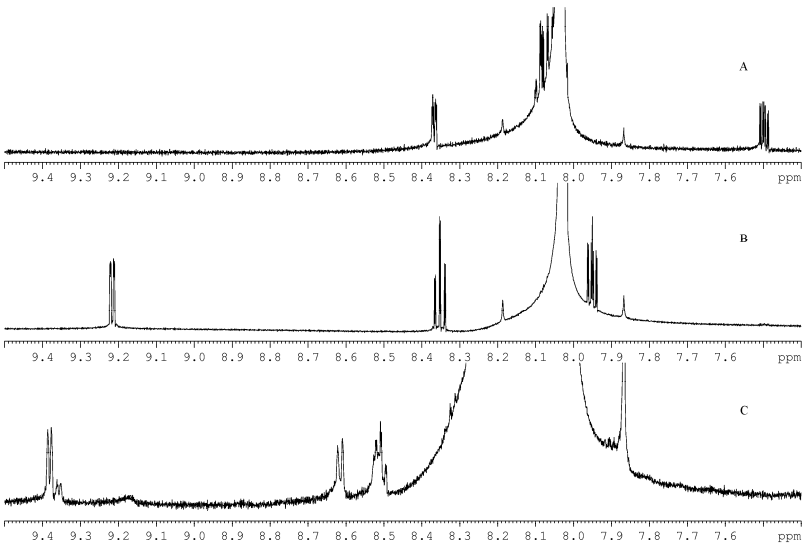

Figure 1.17. ^{1}H NMR spectra in DMF-d_7 of A) $[(CN)_2Py_2Pyz]$, B) $[(CN)_2Py_2PyzPdCl_2]$ and C) the pentapalladated species $[(PdCl_2)_4Py_8TPyzPzPd]$.

It should be taken into account that an unrestricted relative orientation of the four $N_{2(py)}PdCl_2$ square planar sites with respect to the central porphyrazine core might give rise to the formation of different isomers (see schematic representation in Figure 1.18).

^{1}H-NMR spectral data combined with accurate DFT calculations definitely prove that the largely prevalent arrangement is the 4:0 of Figure 1.18 with the four external metalated residues all directed on the same side with respect to the centralporphyrazine core, as shown in Figure 1.19.

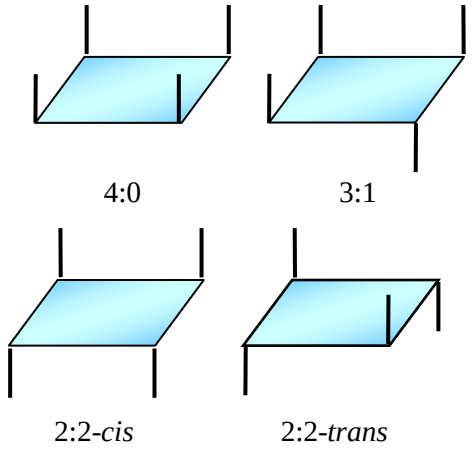

Figure 1.18. Structural isomers generated by the arrangement of the dipyridino-$PdCl_2$ fragments in the pentapalladated species.

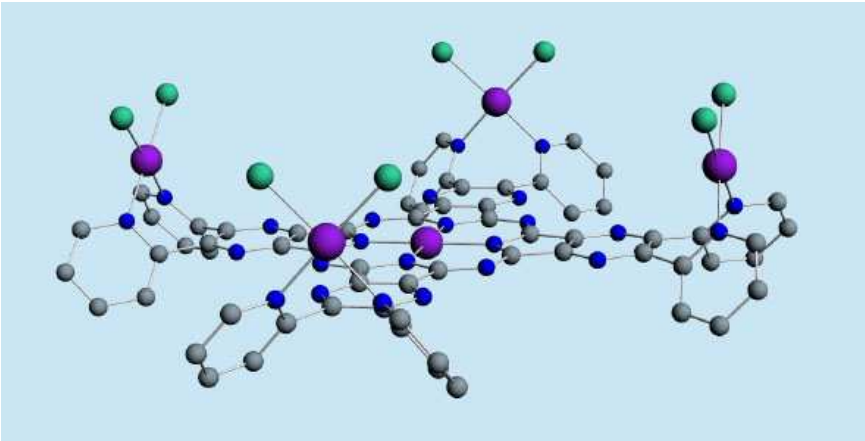

Figura 1.19. Predominant structural component present in the mixture of isomers of $[(PdCl_2)_4Py_8TPyzPzPd]$ having the four external $N_{2(py)}PdCl_2$ moieties all oriented on the same side of the central pyrazinoporphyrazine core.

The above triad of Pd^{II} pyrazinoporphyrazines were the object of detailed UV-visible and electrochemical studies. From the achieved information it was learned that the complexes behave as highly electron-deficient macrocycles, with evident effects in terms of increasing electron-deficiency moving from the mononuclear species $[Py_8TPyzPzPd]$ to either the pentanuclear complex $[(PdCl_2)_4Py_8TPyzPzPd]$ or to the octacation $[(2\text{-}Mepy)_8TPyzPzPd]^{8+}$. Quite interesting studies have been conducted on this triad of Pd^{II} compounds exploring their role as photosensitizers for the generation of singlet oxygen, $^1O_2$, the citotoxic agent in photodynamic therapy (PDT).[25] Specific reference to the role of this present class of pyrazinoporphyrazine macrocycles to these biochemical aspects will be made as a separate section in the final part of the present Introduction.

It should be noted here that the type of out-of-plane exocyclic coordination observed for the pentanuclear complex [($PdCl_2$)$_4$Py$_8$TPyzPzPd] was at the time[24] unprecedented. In fact, the numerous examples of multinuclear porphyrazine macrocycles studied by Barrett and Hoffman[10] (see some of the structures in Figures 1.8-1.10) always see the external metal coordination sites lying coplanarly with the central porphyrazine core, without exceptions. The vast physicochemical information collected on the above triad of Pd^{II} species suggested an expansion of the synthesis and study of related pentanuclear analogs. Thus, the series of new complexes externally carrying $PdCl_2$ and $PtCl_2$ units having formula [(M'Cl_2)$_4$Py$_8$TPyzPzM] (M = Mg^{II}(H_2O), Zn^{II}, Cu^{II}, Cd^{II}; M' = Pd^{II} and M = M' = Pt^{II}) (Figure 1.20) were prepared and widely investigated as to their stability in the solid state and in solution of different solvents.[26] Based mainly on the achieved NMR spectral information, it can be concluded that the tendency of the new series of pentanuclear species of the present pyridinated pyrazinoporphyrazine macrocycle exhibit, as a largely prevalent structural arrangement, that already found for the pentapalladated species [($PdCl_2$)$_4$Py$_8$TPyzPzPd] (Figure 1.19). UV-visible solution spectra and electrochemical measurements confirmed their behavior as electron-deficient macrocycles, in line with expectation. Their photosensitizing properties for the generation of $^1O_2$ will be referred to in the last section of this Introduction (see below).

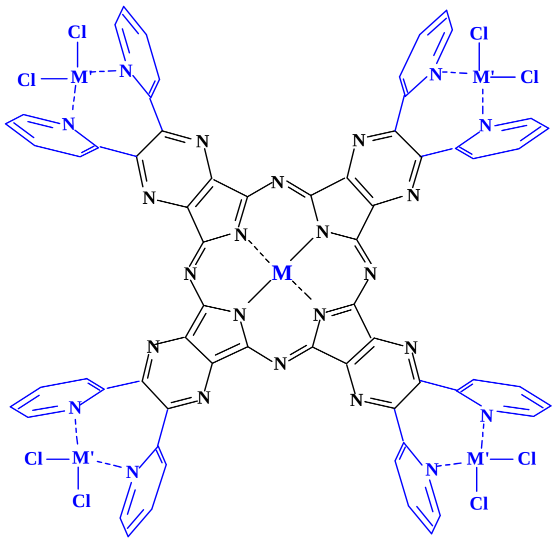

Figure 1.20. [(M'Cl_2)$_4$Py$_8$TPyzPzM] (M = Mg^{II}(H_2O), Zn^{II}, Cu^{II}, Cd^{II}; M' = Pd^{II} and M = M' = Pt^{II}).

C.2 Octacationic pyridinated pyrazinoporphyrazines

Water-soluble porphyrins have been widely investigated in the fields of biochemistry and medicine both as naturally occurring and synthetic mono or multiply charged porphyrins,[27] whereas water-soluble phthalocyanines and porphyrazines have been much less studied. Among the phthalocyanine systems, sulfonated ($-SO_3^-$) macrocycles, in particular the tetrasulfophthalocyanine [$TSPcH_2$] (Figure 1.21) and its iron, cobalt, nickel, and copper derivatives have been prepared and their reactivity and applicative properties studied.[28,29] Other few examples of water-soluble phthalocyanines are reported in literature.

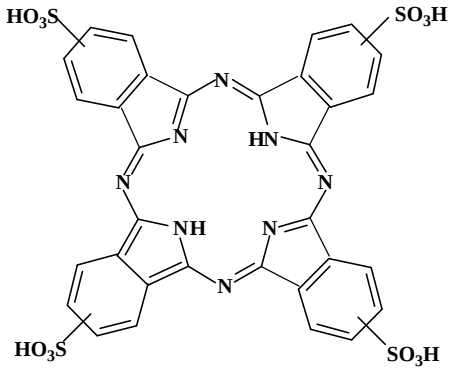

Figure 1.21. Schematic representation of tetrasulfophthalocyanine, [$TSPcH_2$].

The first example of an octacationic porphyrazine, water-soluble over a wide pH range, is represented by the macrocycle shown in Figure 1.22, which was obtained upon quaternization of the external pyridine N atoms by CH_3I.[30] Aggregation studies confirm the monomeric nature of these novel cationic porphyrazines in water, making them excellent candidates for a wide variety of applications.

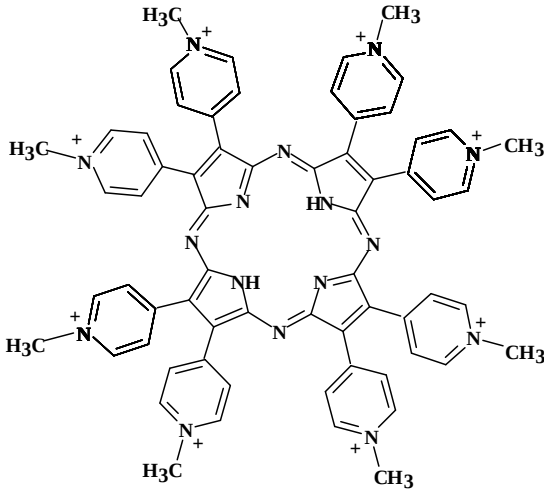

Figure 1.22. Schematic representation of the octakis(N-methyl-4-pyridiniumyl)porphyrazine, $[(4\text{-Mepy})_8PzH_2]^{8+}$.

Quaternization by methyl iodide of the pyridine N atoms of the pyridinated "pyrazinoporphyrazines" [Py_8TPyzPzM] of reference for this work (see the free-base in Figure 1.1), leads to the formation of the corresponding moderately water-soluble salt-like species of formula $[(2\text{-Mepy})_8\text{TPyzPzM}](I)_8$ (M = $2H^I$, $Mg^{II}(H_2O)$, Co^{II}, Cu^{II}, Zn^{II}); 2-Mepy = 2-(N-methyl)pyridiniumyl fragment) containing the octacation $[(2\text{-Mepy})_8\text{TPyzPzM}]^{8+}$ (Figure 1.23)[31]. The free-base $[(2\text{-Mepy})_8\text{TPyzPzH}_2]^{8+}$ (in the form of its iodide salt) shows solubility in water; depending on the range of pH explored, this macroycles undergoes easy deprotonation behaving as a strong acid and its acidity strength is definitely higher than that found for the octacation $[(4\text{-Mepy})_8PzH_2]^{8+}$in comparable experimental conditions. The facilitated deprotonation process is determined by the exceptionally strong electron-deficient properties of the pyridinated "pyrazinoporphyrazine" macrocycle, as determined by the concomitant electron-withdrawing effects due to the presence of the pyrazine rings, the pyridine rings and quaternization of the pyridine N atoms.

Studies of all charged metal derivatives $[(2\text{-Mepy})_8\text{TPyzPzM}]^{8+}$ in aqueous media at ca. 10^{-5} M concentration provide evidence for the occurrence of molecular aggregation, but the formation of monomeric species is generally favoured upon dilution of the solutions. These octacations are essentially monomeric in solutions of pyridine or DMSO.

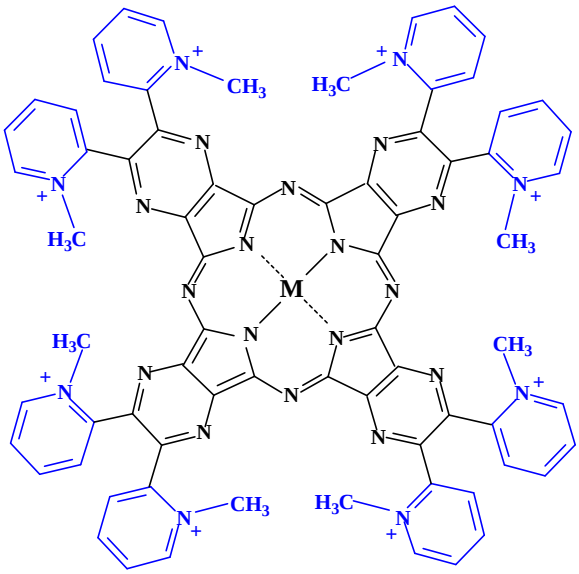

Figure 1.23. $[(2\text{-Mepy})_8\text{TPyzPzM}]^{8+}$.

Cyclic voltammetry and thin-layer spectroelectrochemical data in DMSO show well-resolved reversible multi-step one-electron reductions, all of which appear to be ligand-centered, the only exception being reduction of the Co^{II} octacation $[Py_8TPyzPzCo]^{8+}$.[31a] Similarly to what is observed for the related neutral species $[Py_8TPyzPzCo]$,[21,31b] the first one-electron reduction for this species is a metal-centered $Co^{II} \rightarrow Co^{I}$ process which implies formation of the heptacation $[Py_8TPyzPzCo^{I}]^{7+}$. This process is reversed during the second one-electron reduction and leads to the formation of the -2 charged species $[Py_8TPyzPzCo^{II}]^{6+}$ with the two excess electrons localized on the macrocycle. As can be seen from the data in DMSO (Table 1.1), the $E_{1/2}$ values for the octacations with different M are, at all steps of reduction, sensibly less negative than those of the corresponding neutral compounds, ie. reductions are facilitated by the quaternization process. These findings parallel the results of the observed UV-visible spectral changes, mainly consisting of the bathochromic shift of the Q bands in going from the spectra of the neutral species to those of the related octacations. These observations are particularly relevant, if account is taken that the electronic perturbation determined on the macrocycle by the quaternization process, is generated at the pyridine rings located at the extreme periphery of the molecule and oriented out-of-plane of the central macrocyclic framework.

Table 1.1. Half-wave Potentials ($E_{1/2}$, V vs SCE) for the complexes [Py_8TPyzPzM] and the corresponding octacationic species [(2-Mepy)$_8$TPyzPzM]$^{8+}$.

Compound	**Solvent**	**Oxid**	**Reduction**				
			1st	2nd	3rd	4th	5th
[Mg^{II}]	Py		-0.40	-0.79	-1.43	-1.70	
[Mg^{II}]	DMSO		-0.33	-0.70	-1.39	-1.67	
[Mg^{II}]$^{8+}$	DMSO	0.31	-0.19	-0.47	-0.84	-1.28	
[Zn^{II}]	Py		-0.34	-0.72	-1.38	-1.66	-1.83
[Zn^{II}]	DMSO		-0.26	-0.67	-1.38	-1.64	
[Zn^{II}]$^{8+}$	DMSO	0.33	-0.10	-0.44	-0.81	-1.24	-1.59
[Cu^{II}]	Py		-0.30	-0.68	-1.28	-1.61	
[Cu^{II}]	DMSO		-0.22	-0.58	-1.22	-1.58	
[Cu^{II}]$^{8+}$	DMSO	0.30	-0.04	-0.38	-0.85	-1.22	
[Co^{II}]	Py		-0.26	-0.87	-1.37	-1.83	
[Co^{II}]	DMSO	0.67	-0.06	-0.76	-1.31	-1.77	
[Co^{II}]$^{8+}$	DMSO	0.32	0.05	-0.51			
[Mn^{II}]	Py		-0.21	-0.91	-1.35	-1.64	
[Mn^{II}]	DMSO	0.36	-0.16	-0.89	-1.33	-1.80	

Part D. Pyrazinoporphyrazines as Photosensitizers in Photodynamic Therapy (PDT)

Photodynamic therapy (PDT) is a very promising anticancer therapy nowadays in use and under investigation for further improvement.[32] The therapy requires the combined action of light, dioxygen, ($^3O_2$), and a photosensitizer which is able to absorb energy in the phototherapeutic spectral window (600-850 nm) and release energy to dioxygen, generating singlet oxygen, ($^1O_2$), believed to be the initial cytotoxic agent in PDT.

Irradiation of the sensitizer in the presence of molecular oxygen ($^3O_2$) determines the formation of highly *reactive oxygen species* (ROS) and *singlet oxygen* ($^1O_2$), all of these species being strong cytotoxic agents able to cause irreversible damage to any nearby biologic molecule. As a result, a phototoxic effect occurs in the immediate vicinity of drug localization and the tumour is selectively destroyed. Excitation by light of a molecular system leads to a competition between physical (radiative and nonradiative) and chemical reaction modes of deactivation (see below Figure 1.24). The efficiency of each process for a given compound is expressed by the quantum yield of the process itself, Φ:

$$\Phi = \frac{\text{molecules undergoing the process}}{\text{total photons absorbed by the molecules}}$$

So, the singlet oxygen quantum yield, Φ_Δ, of a photosensitizer is defined as

$$\Phi_\Delta = \frac{^1O_2 \text{ molecules generated}}{\text{total photons absorbed by the sensitizer}}$$

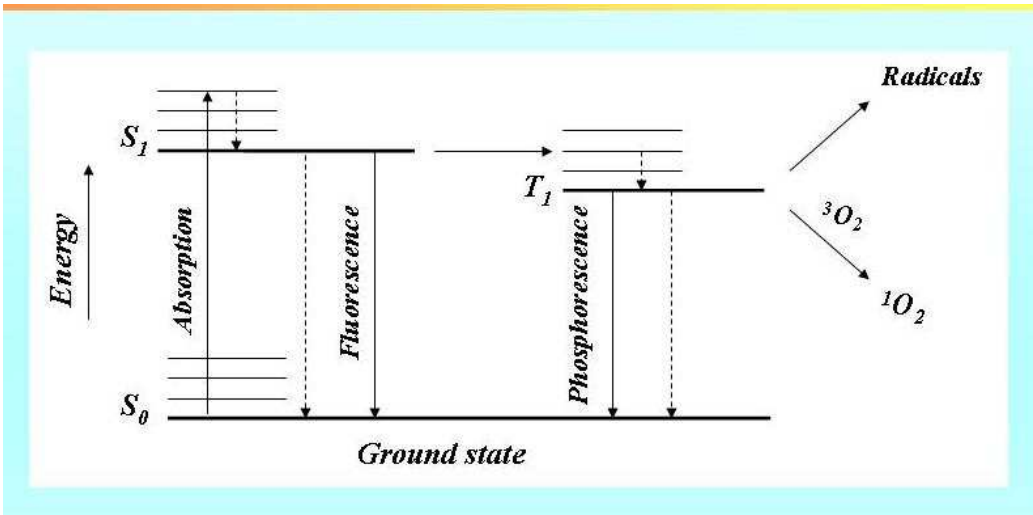

Figure 1.24. Physical and chemical processes involved in PDT.

A good photosensitizer should preferably be constituted by a single compound, having constant composition and high degree of purity, sufficiently stable under physiological conditions, non-toxic in the dark and capable of giving a selective accumulation in the diseased tissues. Moreover a good photosensitizer have to be equipped with an intense absorption in the therapeutic window (600 - 850 nm), actually used for irradiation, in which biological tissues have an increased transparency to light radiation; on the contrary, it must have poor absorption in the range 400-600 nm, to avoid skin sensitization during the treatment period. Finally, regarding the photophysical properties, it must possess a first excited electronic state of triplet with appropriate energy and time of life, to enable an efficient energy transfer in respect of molecular oxygen $^3O_2$.

Porphyrins have been intensively studied as photosensitizers, [32,33] and some of them like Photofrin®, an oligomer of natural hematoporphyrin, have found clinical applications. However, they have weak absorptions in the phototherapeutic window and induce long-lasting skin photosensitivity.[34] Besides, phthalocyanines[32b,c,33,35] have been actively considered as promising photosensitizers in PDT, because they show intense absorption bands in the therapeutic window. The attention has also been directed to investigate the photoactivity for the production of singlet oxygen in different media of differently

substituted tetrapyrazinoporphyrazines,[36] secoporphyrazines,[37] and benzonaphthoporphyrazines.[38]

As has been anticipated above, the photosensitizing activity of the octapyridinated pyrazinoporphyrazines was studied for the first time using the Pd^{II} compounds [Py_8TPyzPzPd], [$(PdCl_2)_4Py_8$TPyzPzPd], and the octacation [(2-Mepy)$_8$TPyzPzPd]$^{8+}$. Data at hand proved that these complexes are excellent photosensitizers in DMF solution. Due to reducibility of the species in DMF, experiments required to perform the measurements in acidified solution (HCl).[25] A series of related pentanuclear species carrying externally $PdCl_2$ and $PtCl_2$ units having formula [(M'Cl_2)$_4Py_8$TPyzPzM] (M' = Pd^{II}, Pt^{II}; M = Zn^{II}, Mg^{II} (H_2O), Pd^{II}, Pt^{II}) were also recently studied in detail as to their physicochemical behaviour and as photosensitizers in PDT.[26b,39] Their fluorescence response was also examined. Wide reference to the significance of these results will be considered in the Discussion Section later in the thesis.

Part E. The Target of the Present Thesis

The present Introduction has above illustrated, although in a condensed manner and certainly in an incomplete form, the achieved information in terms of basic research and potential applicative aspects available on the mononuclear "pyrazinoporphyrazines" [Py_8TPyzPzM] and related pentanuclear and supercharged water-soluble species. Structural and electronic features were studied by single crystal X-ray work, spectral (IR, UV-visible, NMR) and electrochemical investigations, and contributed by detailed theoretical DFT and TDDFT studies. The important role of the external pyridine rings has been examined by considering their capability of electronic contact with the central pyrazinoporphyrazine core. Their ability to coordinate metal centers or to undergo quaternization processes at the N atoms has sensibly enriched the knowledge of the level of electronic perturbation induced by the peripheral changes to the central framework of the pyrazinoporphyrazine macrocycle. The attention for applicative aspects has been particularly devoted to learn about their behavior as photosensitizers in PDT, and potentialities for their role in multimodal anticancer therapy is an open problematic aspect with perspectives of further expansion and therefore far from being concluded.

The present thesis work has selected as the main subject the synthesis of two novel types of porphyrazine macrocycles, strictly related to the above considered "pyrazinoporphyrazine" macrocycle, but showing a narrower ("restricted" macrocycle) or more extended porphyrazine core ("expanded" macrocycle"). The two macrocycles, in the form of unmetalated species are schematically shown in Figure 1.25A and 1.25C, whereas the widely referred to "pyrazinoporphyrazine" macrocycle is given in Figure 1.25B. The target of the present project is multifaceted. In fact, aspects of interest were:

a) how the change in the expansion or contraction of the central planar or quasi-planar π-conjugated skeleton, with respect to that of the pyrazinoporphyrazine core, will modify stability, solubility, tendency to aggregation, general physicochemical and redox behaviour of the new species and their applicative potentialities, with attention centered on their photoactivity properties;

b) how the presence of the external pyridine rings directly attached to the porphyrazine core (“restricted” macrocycle; Figure 1.24A) or more far away than in the already studied “pyrazinoporphyrazine” macrocycle (“expanded” macrocycle; Figure 1.24C) added of local metal coordination or quaternization processes, can produce consistent effects on the structural and electronic features of the new macrocyclic skeletons;

c) how do the data concerning the response of the new species as photosensitizers compare with those already known for the original “pyrazinoporphyrazine” macrocycles.

These and other problematic aspects, even those related to the effective access in terms of preparative procedures to the new macrocycles, plus other general information will be considered and widely illustrated in the Results and Discussion section.

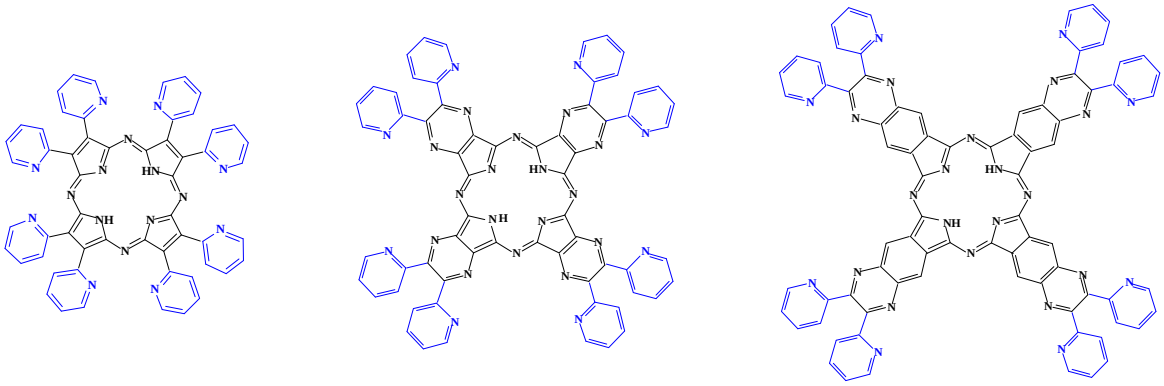

A: [Py_8PzH_2] B: [$Py_8TPyzPzH_2$] C: [$Py_8TQuinPzH_2$]

Figure 1.25

Concomitant work was conducted on “pyrazinoporphyrazine” macrocycles carrying externally thienyl rings (Figure 1.26). Whereas in the work conducted on the “restricted” and “expanded” pyrazinoporphyrazine macrocycles the attention was confined to modifications of the central π-conjugated porphyrazine core, the new work on the thienyl pyrazinoporphyrazine macrocycles involved modifications of the peripheral part of the molecule, focusing on the ligating properties of the S atoms inserted in the external 2-thienyl rings, in an interesting comparison with those seen for the pyridine rings in the pyridinated “pyrazinoporphyrazines”.

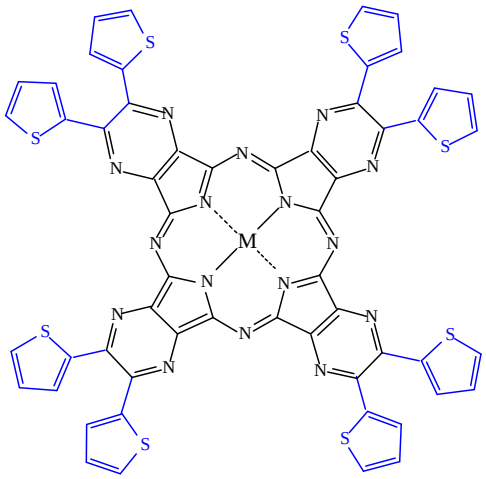

Figure 1.26. [Th_8TPyzPzM].

The attention was directed to explore the aspects concerning external metal ion coordination and involved also the examination of the coordinating capabilities of the thienyl precursor. The work on the thienyl macrocycles was the object of the graduation thesis and will be reported here only for the aspects which were developed during the PhD thesis.

CHAPTER 2

EXPERIMENTAL SECTION

Part A. Solvents and Reagents

Solvents and reagents were used as purchased unless otherwise specified. Pyridine was dried by refluxing over CaO. Dimethylformamide (DMF, RPE C. Erba) was used as purchased. Dimethyl sulfoxide (DMSO, RPE C. Erba) was freshly distilled over CaH_2. Methanol was dried over sodium. Anhydrous diethyl ether was purchased by Aldrich. Diaminomaleonitrile 98%, 2,2'-pyridil 97% and 2,2'-pyridylacetonitrile 99% were commercial products from Aldrich and were used without further purification. 1,2 Diamino-4,5-dicyanobenzene 97% was a commercial product by Bosche scientific. Palladium(II) chloride, 99.9+% and Platinum(II) chloride were commercial products respectively from Sigma Aldrich and Pressure Chemical C.o. Magnesium acetate tetrahydrate [$Mg(OAc)_2 \cdot 4H_2O$; Carlo Erba 99.99%, p.f. 80 °C], zinc acetate [$Zn(OAc)_2 \cdot 2H_2O$; Merck 99.5%] and cobalt acetate [$Co(OAc)_2 \cdot 4H_2O$; Fluka, 99%] were used as received.

Part B. Syntheses

This Section describes the synthesis of two novel classes of porphyrazine macrocycles, the "quinoxalinoporphyrazine"(B.1), and the "pyridylporphyrazine"(B.2).

The last set of synthetic procedures (B.3) describes the synthesis of the already reported[40] "thienylpyrazinoporphyrazine" macrocycle and its mono- and multinuclear complexes of formulae [$Th_8TPyzPzM$] (M = $2H^I$, $Mg^{II}(H_2O)$, Co^{II}, Cu^{II}, Zn^{II}) and [$(PdCl_2)_4Th_8TPyzPzM$] (M = $Mg^{II}(H_2O)$, Zn^{II}) respectively.

B.1 MONO- AND PENTANUCLEAR HOMO- AND HETEROMETALLIC "QUINOXALINOPORPHYRAZINES"

B.1.a The Precursor [$(CN)_2Py_2Quin$] and its Pd(II) and Pt(II) Derivatives

B.1.a.1 *Synthesis of the precursor 2,3-di(2-pyridyl)-6,7-dicyano-1,4-quinoxaline, [$(CN)_2Py_2Quin$]*

The synthesis of [$(CN)_2Py_2Quin$], reported elsewhere[41] was carried out according to the following reaction scheme:

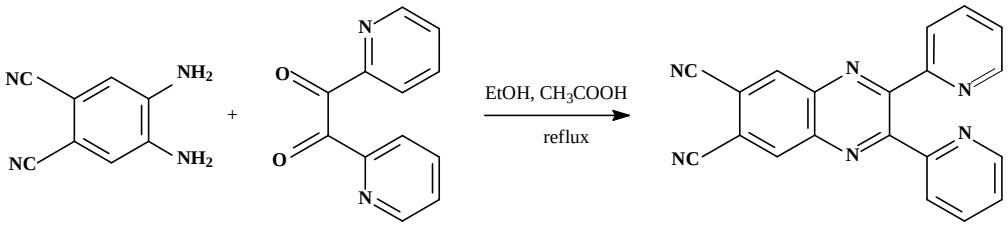

4,5-diaminophthalonitrile (0.69 g, 4.39 mmol) and 2,2'-pyridil (1.08 g, 5.09 mmol) were added to 95% ethanol (40 mL) and glacial acetic acid (6 mL) and the mixture was kept refluxing for 4 h at 85 °C. After cooling, the yellow solid formed was separated by filtration, washed with ice ethanol and brought to constant weight under vacuum (10^{-2} mmHg; 1.20 g, yield 82%). Calcd for [$(CN)_2Py_2Quin$], $C_{20}H_{10}N_6$: C, 71.85; H, 3.01; N, 25.14. Found: C, 71.69; H, 3.03; N, 24.83%. IR (KBr, cm^{-1}): 2236 (w-m; ν_{CN}), 1583 (s), 1568 (w), 1550 (w), 1473 (s), 1435 (w-m), 1421 (w), 1396 (s), 1346 (s), 1294 (w-m), 1286 (w-m), 1248 (w), 1221 (w-m), 1151 (w), 1099 (w-m), 1078 (s), 1043 (m), 1001 (vs), 988 (w), 921 (m-s), 897 (m-s), 848 (w-m), 829 (w-m), 794 (s), 758 (vs), 748 (s), 712 (w), 683 (w), 623 (w-m), 578 (m), 550 (w-m), 536 (vs), 494 (vw), 463 (vw), 416 (m), 399 (w-m), 349 (vw), 325 (vw), 300 (vw).

B.1.a.2 ***Synthesis of bis-(benzonitrile)palladiumdichloride, [(C$_6$H$_5$CN)$_2$PdCl$_2$]***

According to the procedure reported in literature,[42] $PdCl_2$ (426 mg, 2.40 mmol) was dissolved in the minimum amount of hot benzonitrile (ca. 8 mL). Upon concentration of the red-brown solution, a crystalline yellow solid was formed. Additional solid material was obtained by pouring ether into the separated solution. The total amount of solid material was washed with ether and brought to constant weight under vacuum (10^{-2} mmHg; 711 mg, yield 78%).

B.1.a.3 ***Synthesis of the palladated precursor of formula [(CN)$_2$Py$_2$QuinPdCl$_2$]***

This complex was prepared by a different procedure respect that reported in the literature,[41] following the reaction scheme below:

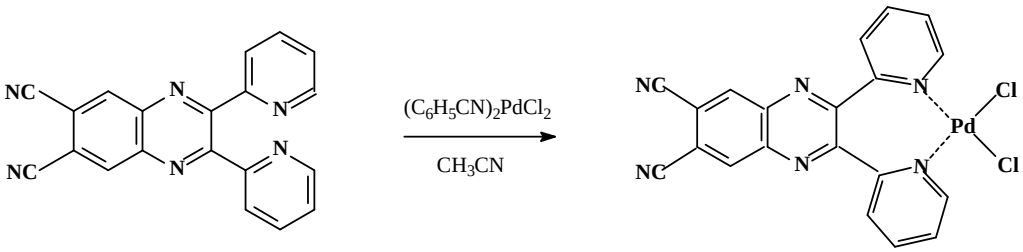

[(CN)$_2$Py$_2$Quin] (53 mg, 0.158 mmol) and [(C$_6$H$_5$CN)$_2$PdCl$_2$] (66 mg, 0.172 mmol) were added to CH_3CN (10 mL) and the mixture was heated at 100 °C with stirring for 4 h. After cooling and filtration, the solid material was washed repeatedly with CH_3CN and THF and then brought to constant weight under vacuum (10^{-2} mmHg; 53 mg, yield 65%). Calcd for [(CN)$_2$Py$_2$QuinPdCl$_2$], $C_{20}H_{10}Cl_2N_6Pd$: C, 46.95; H, 1.97; N, 16.43; Pd, 20.79. Found: C, 46.58; H, 2.36; N, 16.67; Pd, 19.87%. IR (KBr, cm^{-1}): 2237 (m-s; ν_{CN}), 1598 (s), 1572 (m), 1543 (w), 1485 (s), 1442 (w), 1398 (w), 1348 (vs), 1288 (m), 1275 (m-s), 1251 (s), 1161 (m), 1109 (m), 1082 (vs), 1059 (s), 1036 (w-m), 987 (m), 933 (w), 899 (m), 848 (w-m), 819 (w-m), 775 (s), 760 (vs), 729 (vw), 712 (w), 675 (w), 658 (w), 619 (w), 578 (w), 553 (m), 538 (s), 489 (w), 463 (w), 438 (w), 341 (s, ν_{Pd-Cl}), 305 (m), 257 (w).

B.1.a.4 ***Synthesis of bis-(benzonitrile)platinumdichloride, [(C$_6$H$_5$CN)$_2$PtCl$_2$]***

According to the procedure reported in literature,[42] $PtCl_2$ (502 mg, 1.88 mmol) was dissolved in the minimum amount of hot benzonitrile (ca. 8 mL). Upon concentration of the red-brown solution, a crystalline yellow solid was formed. Additional solid material was obtained by pouring ether into the separated solution. The total amount of solid material was washed with ether and brought to constant weight under vacuum (10^{-2} mmHg; 571 mg, yield 64%).

B.1.a.5 ***Synthesis of the palladated precursor of formula [(CN)$_2$Py$_2$QuinPtCl$_2$]***

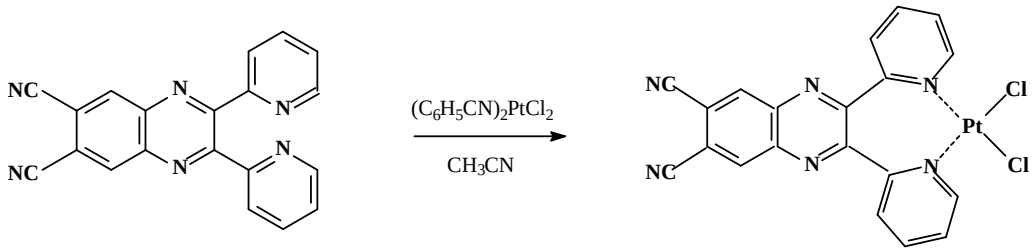

[$(CN)_2Py_2Quin$] (54 mg, 0.162 mmol) and [$(C_6H_5CN)_2PtCl_2$] (85 mg, 0.180 mmol) (molar ratio: 1/1.1) were added to CH_3CN (10 mL) and the mixture was kept at 100 °C with stirring for 4 h. After cooling and centrifugation, the solid yellow material was washed repeatedly with CH_3CN and THF and then brought to constant weight under vacuum (10^{-2} mmHg; 43 mg, yield 44%). Calcd for [$(CN)_2Py_2QuinPtCl_2$], $C_{20}H_{10}Cl_2N_6Pt$: C, 40.01; H, 1.68; N, 13.99; Pt, 32.49. Found: C, 40.09; H, 1.85; N, 14.27; Pt, 31.26%. IR (KBr, cm^{-1}): 2237 (s; ν_{CN}), 1600 (s), 1572 (w), 1545 (w), 1487 (s), 1441 (w), 1396 (m-w), 1348 (s), 1288 (m-s), 1273 (m-s), 1251 (m-s), 1161 (m-s), 1111 (m), 1084 (vs), 1065 (s), 1035 (w-m), 987 (m-s), 905 (m-s), 848 (w-m), 818 (w-m), 771 (vs), 760 (vs), 727 (vw), 712 (w), 675 (vw), 661 (vw), 619 (w), 578 (w), 553 (m-s), 538 (s), 486 (w), 469 (vw), 443 (vw), 376 (vw), 341 (s, ν_{Pt-Cl}), 314 (m-s), 260 (w).

B.1.b Synthesis of the Tetrakis[2,3-di(2-pyridyl)quinoxalino]porphyrazine and its Metal Derivatives

B.1.b.1 *Synthesis of the Hydrated Tetrakis[2,3-di(2-pyridyl)quinoxalino]porphyrazinato-monoaquo-Mg^{II}, $[Py_8TQuinPzMg(H_2O)]\cdot 4H_2O$*

The hydrated Mg^{II} complex was directly obtained by autocyclotetramerization of the precursor $[(CN)_2Py_2Quin]$ as follows :

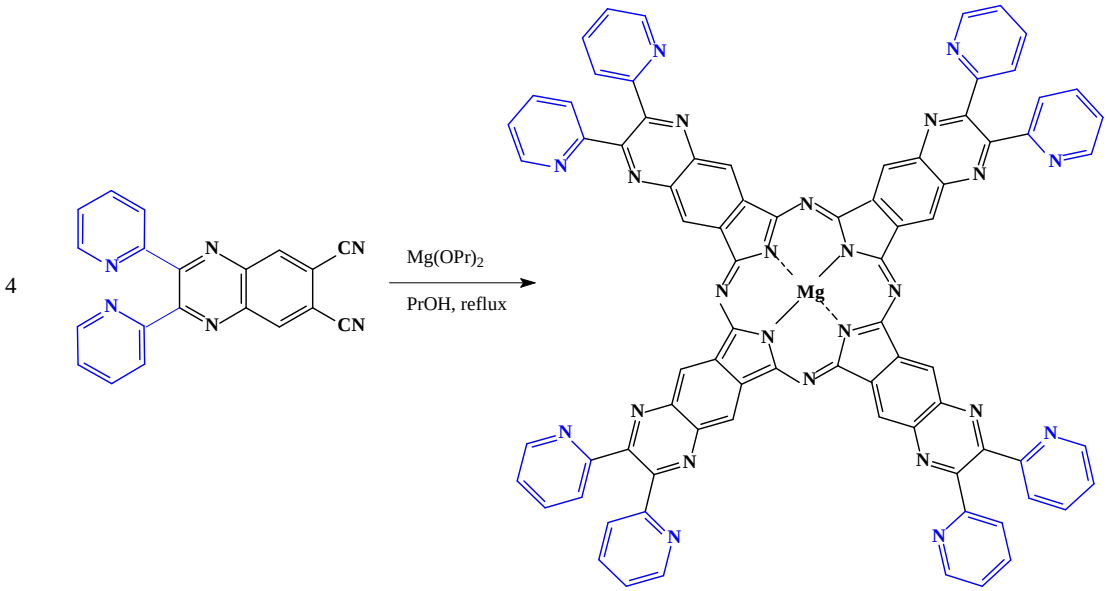

Magnesium (90 mg, 3.720 mmol), propyl alcohol (15 mL) and a few crystals of iodine were introduced in a small flask (25 mL) and the mixture was heated to reflux under stirring for 16 h. The obtained suspension was then added of the precursor $[(CN)_2Py_2Quin]$ (310 mg, 0.927 mmol) and heated to reflux again for 8 h. The mixture, brought to room temperature, was poured in air in a vessel and the solvent was left to evaporate completely. The solid residue was added of 10% CH_3COOH (5 mL) and the mixture was kept under stirring for 1h. The solid, separated by centrifugation and washed repeatedly with water, then with THF, and finally with acetone was brought to constant weight under vacuum (10^{-2} mmHg; 264.2 mg, yield. 81%). Calcd for $[Py_8TQuinPzMg(H_2O)]\cdot 4H_2O$, $C_{80}H_{50}MgN_{24}O_5$: C, 66.19; H, 3.47; N, 23.15. Found: C, 66.59; H, 3.59; N, 21.83%. IR (KBr, cm^{-1}): 3400

(broad), 1772 (vw), 1726 (vw), 1585 (s), 1566 (s), 1473 (m-s), 1383 (w), 1346 (vs), 1280 (vvw), 1248 (vw), 1145 (w), 1103 (vs), 1034 (s), 999 (m), 983 (vw), 893 (w), 875 (w-m), 839 (vvw), 821 (w), 791 (m), 746 (s), 708 (m-s), 596 (m), 548 (w), 501 (vw), 426 (vw), 403 (w), 279 (vw).

B.1.b.2 *Synthesis of the Hydrated Tetrakis[2,3-di(2-pyridyl)quinoxalino]porphyrazine, [$Py_8TQuinPzH_2$]·$6H_2O$*

The synthesis of this macrocycle, previously reported elsewhere,[41] was carried out by our group with a slightly different procedure, as follows:

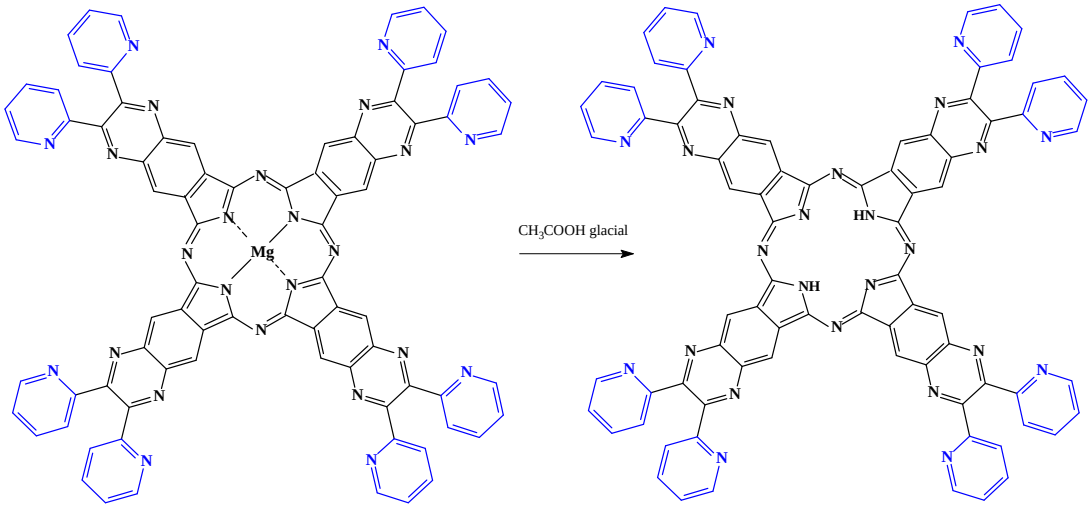

The Mg^{II} complex**,** [$Py_8TQuinPzMg(H_2O)$]·$4H_2O$ (251 mg, 0.173 mmol) was suspended, partly dissolved, in glacial CH_3COOH (9 mL). The mixture was kept to reflux under stirring for 20 h and, after cooling, was poured in a vessel and the solvent was left mostly to evaporate in air. The blue solid was separated from the mixture by centrifugation, washed several times with water to neutrality, then with acetone, and brought to constant weight under vacuum (10^{-2} mmHg; 152 mg, yield 61%). Calcd for [$Py_8TQuinPzH_2$]·$6H_2O$, $C_{80}H_{52}N_{24}O_6$: C, 66.57; H, 3.39; N, 21.31. Found: C, 66.38; H, 3.76; N, 23.22%. IR (KBr, cm^{-1}): 3290 (vw, ν_{NH}), 1774 (vw), 1726 (vw), 1629 (vvw), 1585 (m), 1566 (m), 1506 (w), 1471 (m), 1431 (w-m), 1396 (w), 1344 (s), 1317 (m), 1244 (w), 1224 (vw), 1203 (vw), 1167 (m), 1095 (vs), 1078 (vs), 1041 (w-m), 1008 (s), 997 (vs), 981 (s), 883 (m), 856 (m), 821

(m), 789 (s), 775 (s), 740 (s), 700 (vs), 634 (w), 609 (vw), 592 (vs), 548 (s), 494 (w), 428 (w-m), 403 (w).

B.1.b.3 ***Synthesis of the Hydrated Tetrakis[2,3-di(2-pyridyl)quinoxalino]porphyrazinato-Zn^{II}, [Py$_8$TQuinPzZn]·6H$_2$O***

$$[Py_8TQuinPzH_2]\cdot 6H_2O \xrightarrow[DMSO,\ 120\ °C,\ 6\ h]{Zn(OAc)_2\cdot 2H_2O} [Py_8TQuinPzZn]\cdot 6H_2O$$

[Py$_8$TQuinPzH$_2$]·6H$_2$O (53 mg, 0.037 mmol) and Zn(OAc)$_2$·2H$_2$O (53 mg, 0.240 mmol) were suspended in freshly distilled DMSO (3 mL) and the mixture was heated under stirring at 120°C for 6 h. After cooling and centrifugation, the dark green solid was washed repeatedly with water and acetone and brought to constant weight under vacuum (10^{-2} mmHg; 31 mg, yield 55%). Calcd for [Py$_8$TQuinPzZn]·6H$_2$O, C$_{80}$H$_{52}$N$_{24}$O$_6$Zn: C, 63.59; H, 3.47; N, 22.25. Found: C, 63.82; H, 3.15; N, 21.77%. IR (KBr, cm^{-1}): 3440 (broad), 1585 (m), 1566 (m), 1471 (w-m), 1383 (w), 1346 (vs), 1248 (vw), 1145 (w), 1109 (s), 1034 (m-s), 999 (w-m), 891 (w), 872 (w-m), 821 (w), 791 (w-m), 742 (m), 707 (m), 596 (w-m), 545 (w), 501 (vw), 426 (vvw), 401 (vvw).

B.1.b.4 ***Synthesis of the Hydrated Tetrakis[2,3-di(2-pyridyl)quinoxalino]porphyrazinato Co^{II}, [Py$_8$TQuinPzCo]·5H$_2$O***

$$[Py_8TQuinPzH_2]\cdot 6H_2O \xrightarrow[DMSO,\ 120\ °C,\ 6\ h]{Co(OAc)_2\cdot 4H_2O} [Py_8TQuinPzCo]\cdot 5H_2O$$

[Py$_8$TQuinPzH$_2$]·6H$_2$O (46 mg, 0.032 mmol) and Co(OAc)$_2$·4H$_2$O (50 mg, 0.200 mmol) were suspended in freshly distilled DMSO (3 mL) and the mixture was heated under stirring at 120°C for 6 h. After cooling and centrifugation, the dark blue solid separated was washed repeatedly with water and acetone and brought to constant weight under vacuum (10^{-2}

mmHg) (40 mg, yield 83%). Calcd for $[Py_8TQuinPzCo]\cdot 5H_2O$, $C_{80}H_{50}CoN_{24}O_5$: C, 64.64; H, 3.96; N, 22.61. Found: C, 64.91; H, 2.81; N, 22.57%. IR (KBr, cm^{-1}): 3400 (w, broad), 1585 (m), 1568 (m), 1525 (w), 1471 (w-m), 1427 (w-m), 1388 (w), 1346 (s), 1246 (w), 1159 (w), 1107 (s), 1078 (m-s), 1053 (w), 1041 (w), 1014 (w-m), 999 (m-s) , 983 (w-m), 889 (w-m), 856 (vw), 848 (vw), 821 (w), 791 (m), 777 (w-m), 740 (m), 710 (w-m), 700 (w-m), 661 (vw), 632 (vvw), 592 (w-m), 548 (w), 492 (vw), 430 (vw), 403 (vw).

B.1.c Homo-and Heteropentanuclear Pd(II) "Quinoxalinoporphyrazines" of Formula $[(PdCl_2)_4Py_8TQuinPzM]$ (M = $Mg^{II}(H_2O)$, Zn^{II}, Pd^{II})

The heteropentanuclear title complexes with M = $Mg^{II}(H_2O)$ and Zn^{II} were prepared starting from the corresponding monometallic species $[Py_8TQuinPzM]$ by reaction with $PdCl_2$ in DMSO, according to the following reaction scheme:

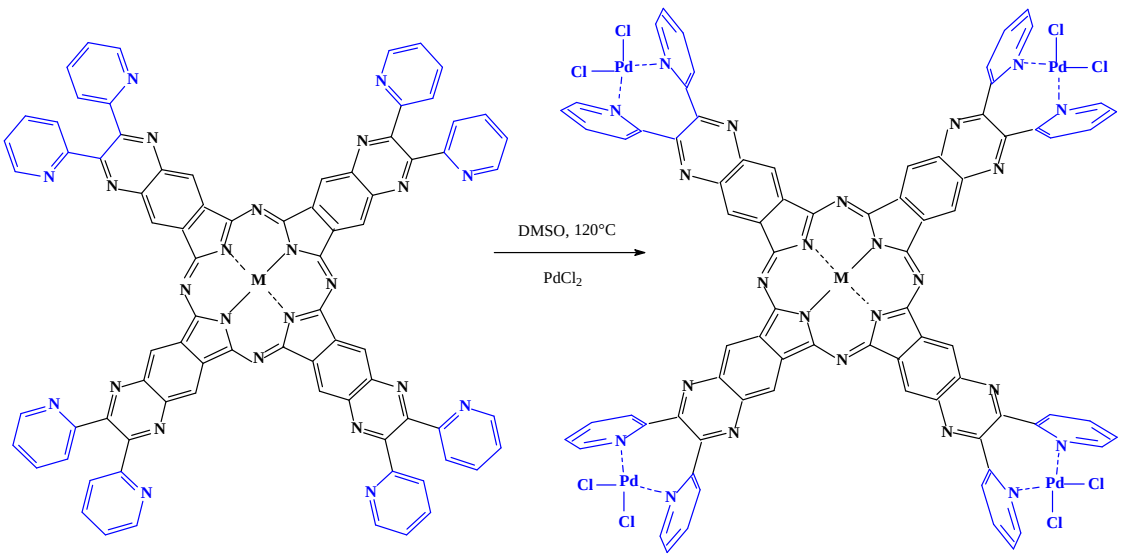

The homopentanuclear analog having Pd^{II} centrally coordinated, was prepared starting from the free-base ligand by reaction with $PdCl_2$ in DMSO under the experimental conditions specified below.

B.1.c.1 ***Synthesis of [(PdCl$_2$)$_4$Py$_8$TQuinPzMg(H$_2$O)]·5H$_2$O·2DMSO***

$$[Py_8TQuinPzMg(H_2O)]\cdot 4H_2O \xrightarrow[DMSO,\ 120\ °C,\ 7\ h]{PdCl_2} [(PdCl_2)_4Py_8TQuinPzMg(H_2O)]\cdot 5H_2O\cdot 2DMSO$$

$[Py_8TQuinPzMg(H_2O)]\cdot 4H_2O$ (53 mg, 0.036 mmol) was suspended (partly dissolved) in freshly distilled DMSO (3 mL). The mixture, added of $PdCl_2$ (33 mg, 0.187 mmol), was heated at 120 °C for 7 h. After cooling, the solid material was washed with water and acetone and brought to constant weight under vacuum (10^{-2} mmHg; 19 mg, yield 23%). Calcd for $[(PdCl_2)_4Py_8TQuinPzMg(H_2O)]\cdot 5H_2O\cdot 2DMSO$, $C_{84}H_{64}Cl_8MgN_{24}O_8Pd_4S_2$: C, 43.20; H, 2.76; N, 14.39; S, 2.74, Pd, 18.22. Found C, 42.26; H, 2.16; N, 18.46; S, 3.19, Pd, 17.60%. IR (KBr, cm^1): 3400 (broad), 1693 (m), 1599 (w), 1568 (w), 1485 (m), 1381 (w), 1348 (s), 1284 (vw), 1253 (vw), 1161 (vw), 1101 (s), 1068 (vw), 1059 (w), 1036 (m), 983 (vvw), 874 (w), 839 (vw), 814 (vw), 787 (vw), 769 (w), 746 (w-m), 719 (w), 699 (vvw), 598 (w), 551 (vw), 449 (vvw), 337 (w, $\nu_{Pd\text{-}Cl}$).

B.1.c.2 ***Synthesis of [(PdCl$_2$)$_4$Py$_8$TQuinPzZn]·10H$_2$O***

$$[Py_8TQuinPzZn]\cdot 6H_2O \xrightarrow[DMSO,\ 120\ °C,\ 7\ h]{PdCl_2} [(PdCl_2)_4Py_8TQuinPzZn]\cdot 10H_2O$$

$[Py_8TQuinPzZn]\cdot 6H_2O$ (18 mg, 0.012 mmol) was suspended (partly dissolved) in freshly distilled DMSO (3 mL). The mixture, added of $PdCl_2$ (12 mg, 0.066 mmol), was heated at 120 °C for 7 h. At the end of the reaction, the solvent was distilled off under vacuum at 100 °C and the solid residue was washed with water and acetone and brought to constant weight under vacuum (10^{-2} mmHg; 11 mg, yield 42%). Calcd for $[(PdCl_2)_4Py_8TQuinPzZn]\cdot 10H_2O$, $C_{80}H_{60}Cl_8MgN_{24}O_{10}Pd_4$: C, 41.91; H, 2.85; N, 14.66, Pd,

18.57. Found: C, 41.74; H, 2.30; N, 13.56; Pd, 19.95%. IR (KBr, cm^{-1}): 3450 (broad), 1598 (w), 1566 (w), 1483 (vvw), 1450 (vvw), 1427 (vvw), 1381 (w), 1344 (s), 1278 (vw), 1251 (vw), 1161 (vw), 1099 (vw), 1057 (m), 1032 (w), 1010 (vw), 893 (w), 869 (vw), 812 (w), 777 (w), 766 (w), 740 (w), 700 (w), 594 (w), 551 (w), 339 (w, $\nu_{Pd\text{-}Cl}$).

B.1.c.3 ***Synthesis of [(PdCl$_2$)$_4$Py$_8$TQuinPzPd]·11H$_2$O***

$$[Py_8TQuinPzH_2]\cdot 6H_2O \xrightarrow[DMSO,\ 120\ °C,\ 8\ h]{PdCl_2} [(PdCl_2)_4Py_8TQuinPzPd]\cdot 11\ H_2O$$

$[Py_8TQuinPzH_2]\cdot 6H_2O$ (35 mg, 0.024 mmol) was suspended (partly dissolved) in freshly distilled DMSO (1.5 mL). The mixture, added of $PdCl_2$ (32 mg, 0.182 mmol), was heated at 120 °C for 8 h. After cooling and evaporation of the solvent under vacuum (100 °C), the solid residue was washed with water and acetone and brought to constant weight under vacuum (10^{-2} mmHg; 41 mg, yield 79%). Calcd for $[(PdCl_2)_4Py_8TQuinPzPd]\cdot 11H_2O$, $C_{80}H_{62}Cl_8N_{24}O_{11}Pd_5$: C, 40.70; H, 2.74; N, 14.06; Pd, 22.26. Found: C, 40.62; H, 2.24; N, 13.04; Pd, 21.20%. IR (KBr, cm^{-1}): 3450 (s), 1658 (w), 1627 (m), 1597 (m), 1566 (w), 1537 (vw), 1483 (m), 1423 (w), 1385 (w), 1344 (s), 1282 (vw), 1253 (w), 1157 (w), 1120 (m), 1082 (w), 1058 (m), 1032 (vw), 1012 (vw), 895 (w), 848 (vvw), 812 (vw), 766 (w), 746(w), 704 (vvw), 598 (vw), 550 (w), 335 (w-m, $\nu_{Pd\text{-}Cl}$).

B.1.d Homo- and Heteropentanuclear Pt(II) "Quinoxalinoporphyrazines" of Formula [(PtCl$_2$)$_4$Py$_8$TQuinPzM] (M = Mg^{II}(H$_2$O), Zn^{II}, Pt^{II})

By analogy with the synthetic work carried out on the Pd^{II} species described above, a series of new pentametallic complexes of formula $[(PtCl_2)_4Py_8TQuinPzM]$ (M = $Mg^{II}(H_2O)$, Zn^{II}, Pt^{II}) has been prepared.

The $Mg^{II}(H_2O)$ and Zn^{II} complexes have been synthesized starting from the corresponding monometallic species $[Py_8TQuinPzM]$ by reaction with $PtCl_2$, in DMSO, according to the

reaction scheme here below; for the pentaplatinated species $[(PtCl_2)_4Py_8TQuinPzPt]$ the starting material was the free-base ligand, $[Py_8TQuinPzH_2]$.

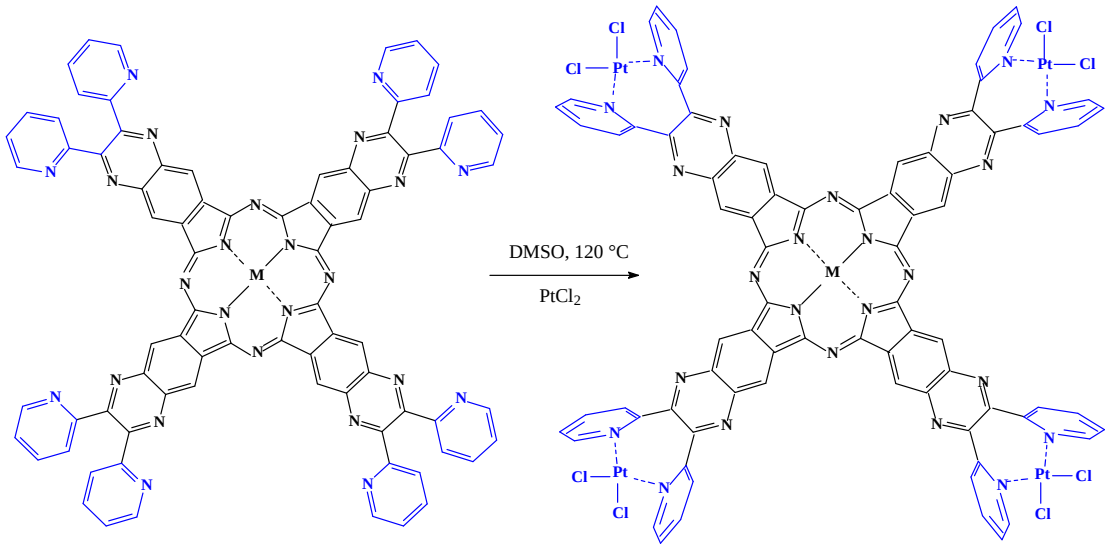

B.1.d.1 ***Synthesis of $[(PtCl_2)_4Py_8TQuinPzMg(H_2O)]\cdot 12H_2O\cdot DMSO$***

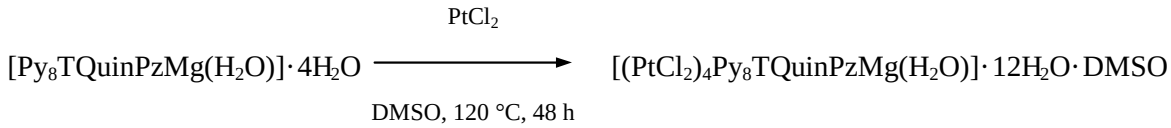

$[Py_8TQuinPzMg(H_2O)]\cdot 4H_2O$ (47 mg, 0.032 mmol) was suspended (partly dissolved) in freshly distilled DMSO (1.5 mL). The mixture, added of $PtCl_2$ (50 mg, 0.188 mmol), was heated at 120°C for 48 h. After cooling and evaporation of the solvent under vacuum (10^{-2} mmHg; 100°C) the solid residue was washed with water and acetone and brought to constant weight under vacuum (10^{-2} mmHg; 59 mg, yield 68%). Calcd for $[(PtCl_2)_4Py_8TQuinPzMg(H_2O)]\cdot 12H_2O\cdot DMSO$, $C_{82}H_{72}Cl_8MgN_{24}O_{14}Pt_4$: C, 35.95; H, 1.92; N, 11.21; S,1.15; Pt, 28.64. Found: C, 35.97; H, 2.65; N, 12.28; S,1.17; Pt, 28.50%. IR (KBr, cm^{-1}): 3400 (broad), 1600 (w-m), 1566 (w), 1483 (m), 1379 (w), 1346 (s), 1280 (vw), 1252 (vw), 1159 (vvw), 1099 (s), 1072 (w), 1031 (m), 983 (vw), 893 (w), 873 (w), 837 (vw), 812 (vw), 783 (w), 765 (w), 746 (w-m), 702 (w), 597 (w), 551 (w), 337 (w, $\nu_{Pt\text{-}Cl}$).

B.1.d.2 ***Synthesis of [(PtCl$_2$)$_4$Py$_8$TQuinPzZn]·18H$_2$O·6DMSO***

$$[Py_8TQuinPzZn]\cdot 5H_2O \xrightarrow[DMSO,\ 120\ °C,\ 48\ h]{PtCl_2} [(PtCl_2)_4Py_8TQuinPzZn]\cdot 18\ H_2O\cdot 6DMSO$$

$[Py_8TQuinPzZn]\cdot 6H_2O$ (41 mg, 0.027 mmol) was suspended (partly dissolved) in freshly distilled DMSO (1.5 mL). The mixture, added of $PtCl_2$ (43 mg, 0.162 mmol), was heated at 120 °C for 48 h. After cooling and evaporation of the solvent under vacuum (10^{-2} mmHg; 100 °C), the solid residue was washed with water and acetone and brought to constant weight under vacuum (10^{-2} mmHg; 42 mg, yield 47%). Calcd for $[(PtCl_2)_4Py_8TQuinPzZn]\cdot 18H_2O\cdot 6DMSO$, $C_{92}H_{112}Cl_8N_{24}O_{24}Pt_4Zn$: C, 33.94; H, 2.43; N, 9.94; S, 6.05; Pt, 22.00. Found: C, 33.89; H, 3.46; N, 10.31; S, 5.90; Pt, 22.93%. IR (KBr, cm^{-1}): 3400 (broad), 1600 (w), 1566 (w), 1485 (m), 1381 (w-m), 1346 (s), 1250 (vw), 1103 (s), 1074 (vw), 1034 (m), 895 (vw), 869 (w), 839 (vw), 812 (vw), 783 (w), 767 (vw), 740 (w-m), 702 (w), 623 (vvw), 596 (w), 553 (w), 503 (vw), 439 (vw), 337(w, $\nu_{Pt\text{-}Cl}$).

B.1.d.3 ***Synthesis of [(PtCl$_2$)$_4$Py$_8$TQuinPzPt]·13H$_2$O·3DMSO***

$$[Py_8TQuinPzH_2]\cdot 6H_2O \xrightarrow[DMSO,\ 120\ °C,\ 7g]{PtCl_2} [(PtCl_2)_4Py_8TQuinPzPt]\cdot 13\ H_2O\cdot 3DMSO$$

$[Py_8TQuinPzH_2]\cdot 6H_2O$ (30 mg, 0.021 mmol) was suspended (partly dissolved) in freshly distilled DMSO (3 mL). The mixture, added of $PtCl_2$ (38 mg, 0.143 mmol), was heated at 120 °C for 7 days. After cooling and evaporation of the solvent under vacuum (10^{-2} mmHg; 100 °C), the solid residue was washed with water and acetone and brought to constant weight under vacuum (10^{-2} mmHg; 48 mg, yield 53%). Calcd for $[(PtCl_2)_4LPt]\cdot 13\ H_2O\cdot 3DMSO$, $C_{86}H_{84}Cl_8N_{24}O_{16}Pt_5$: C, 33.57; H, 2.29; N, 10.56; S, 3.10; Pt, 33.25. Found: C, 33.31; H, 2.86; N,10.84; S, 2.90; Pt, 32.45%. IR (KBr, cm^{-1}): 3500 (broad), 1660 (w), 1598 (w) ,1566 (w) ,1483 (m), 1425 (vw), 1394 (vw), 1342 (s), 1315 (vw), 1282 (vw), 1251

(vw), 1161 (vw), 1098 (s), 1062 (vw), 1014 (s), 981 (w), 891 (w), 854 (w), 810 (w), 692 (w), 592 (w), 551 (w), 438 (w), 378 (vw), 337 (w-m, $\nu_{Pt\text{-}Cl}$).

B.1.e Synthesis of Quaternized "Quinoxalinoporphyrazines" of Formula $[(2\text{-Mepy})_8\text{TQuinPzM}](I)_8$ (M = $Mg^{II}(H_2O)$, Zn^{II})

The quaternized "quinoxalinoporphyrazines" were prepared by methylation at the pyridine N atoms of the corresponding neutral complexes [Py_8TQuinPzM], by using CH_3I in DMF, according to the following reaction scheme:

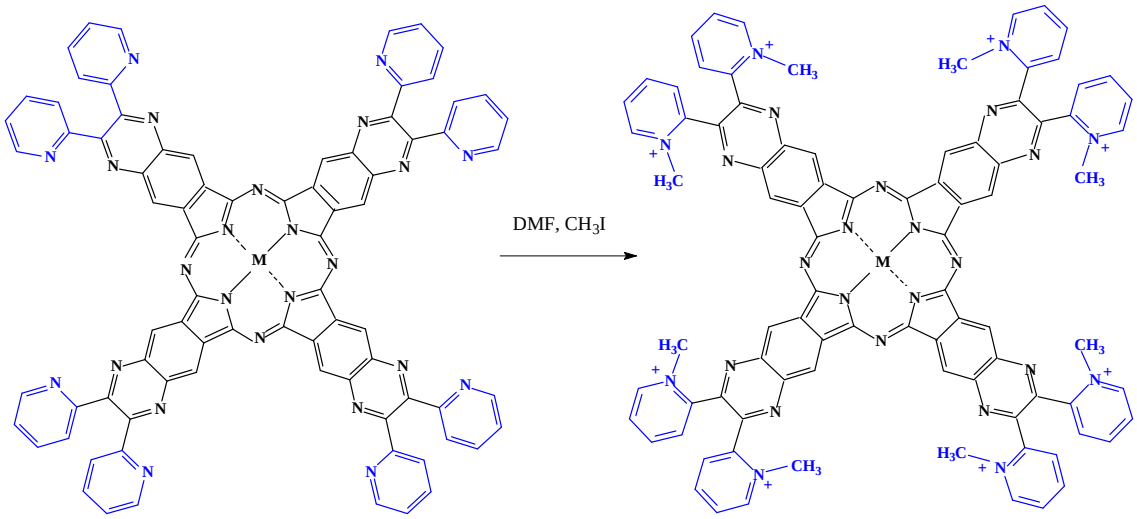

B.1.e.1 *Synthesis of $[(2\text{-Mepy})_8\text{TQuinPzMg}(H_2O)](I)_8 \cdot 13H_2O$*

$$[Py_8\text{TQuinPzMg}(H_2O)]\cdot 4H_2O \xrightarrow[60°C,\ 4\ days]{CH_3I,\ DMF} [(2\text{-Mepy})_8\text{TQuinPzMg}(H_2O)](I)_8\cdot 13H_2O$$

$[Py_8\text{TQuinPzMg}(H_2O)]\cdot 4H_2O$ (50 mg, 0.034 mmol) and CH_3I (0.55 mL, 8.83 mmol) were added to DMF (1 mL) and the mixture was kept at 60 °C for 4 days. After evaporation of the excess CH_3I in air at room temperature, the solution was added of benzene and kept in the refrigerator overnight. The solid material was separated by centrifugation, washed with benzene and brought to constant weight under vacuum (10^{-2} mmHg; 81 mg, yield 86%). Calcd for $[(2\text{-Mepy})_8\text{TQuinPzMg}(H_2O)](I)_8\cdot 13H_2O$, $C_{88}H_{92}I_8MgN_{24}O_{14}$: C, 38.44; H,

3.37; N, 12,22. Found: C, 38.19; H, 3.14; N, 12.19%. IR (KBr, cm^{-1}): 3405 (w-m), 1618 (m), 1577 (w), 1508 (w), 1458 (w-m), 1400 (w-m), 1342 (s), 1275 (w-m), 1163 (m), 1093 (s), 1076 (s), 1008 (w), 997 (m), 981 (w), 943 (w), 887 (w), 816 (w), 773 (w), 748 (w-m), 692 (w-m), 586 (w).

B.1.e.2 ***Synthesis of [(2-Mepy)$_8$TQuinPzZn](I)$_8$·20H$_2$O***

$$[Py_8TQuinPzZn]\cdot 6H_2O \xrightarrow[\text{r.t., 4 days}]{CH_3I,\ DMF} [(2\text{-}Mepy)_8TQuinPzZn](I)_8\cdot 20H_2O$$

$[Py_8TQuinPzZn]\cdot 6H_2O$ (30 mg, 0.020 mmol) and CH_3I (0.55 mL, 8.83 mmol) were added to DMF (1 mL) and the mixture was kept at room temperature for 4 days. After evaporation of excess CH_3I in air at room temperature, the solution was added of benzene and kept in the refrigerator overnight. The solid material separated by centrifugation, was washed with benzene and brought to constant weight under vacuum (10^{-2} mmHg; 81 mg, yield 62%). Calcd for $[(2\text{-}Mepy)_8TQuinPzZn](I)_8\cdot 20H_2O$, $C_{88}H_{104}I_8N_{24}O_{20}Zn$: C, 36.32; H, 3.77; N, 13.24. Found: C, 36.46; H, 3.62; N, 11.60 %. IR (KBr, cm^{-1}): 3430 (s), 2979 (m-s), 2763 (m), 1624 (m), 1579 (w-m), 1509 (vw), 1460 (vw), 1381 (w), 1346 (s), 1250 (vw), 1140 (w), 1101 (s), 1034 (m), 1016 (m), 997 (w), 983 (vvw), 879 (vvw), 819 (vw), 779 (w), 740 (m), 698 (w), 590 (w), 501 (vw), 430 (vvw).

B.2 MONO- AND PENTANUCLEAR HOMO- AND HETEROMETALLIC "PYRIDYLPORPHIRAZINES"

B.2.a The Precursor [$(CN)_2Py_2Et$] and its Pd(II) and Pt(II) Derivatives

B.2.a.1 *Synthesis of the precursor 1,2-di(2-pyridyl)-1,2-dicyanoethylene, [$(CN)_2Py_2Et$]*

The synthesis of [$(CN)_2Py_2Et$] was carried out following a previously reported procedure[43] according to the reaction scheme:

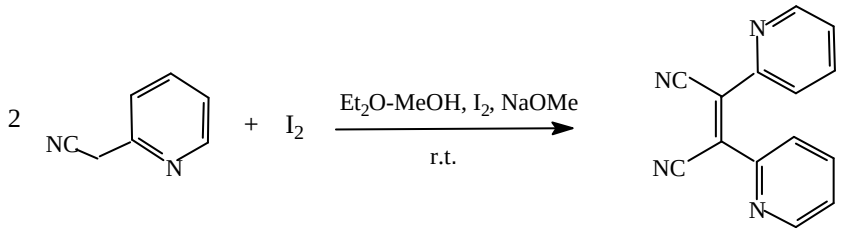

2-Pyridylacetonitrile (3.3 mL, 0.030 mmol) and bisublimed iodine (7.5 g, 0.029 mol) were added under N_2 in a 50 mL flask to a solution of methanol (10 mL) and anhydrous ether (10 mL) and the mixture was kept at room temperature for 1 h. The mixture was then added of a solution of CH_3ONa prepared in a 50 mL flask by dissolving under N_2 and with stirring, metallic sodium (1.4 g) in 14 mL of methanol (preliminarly dried over Na). The resulting mixture was kept overnight in the refrigerator. The precipitate was separated by filtration under vacuum, and the brown crystalline solid was washed with ice methanol and brought to constant weight under vacuum (10^{-2} mmHg; 1.59 g, yield 45%). Calcd for [$(CN)_2Py_2Et$] $C_{14}H_8N_4$: C, 72.4; H, 3.47; N, 24.12; Found: C, 70.93 ; H, 3.45; N, 23.89%. IR (KBr, cm^{-1}): 2216 (w-m, ν_{CN}), 1579 (s), 1467 (s), 1438 (s), 1302 (w), 1294 (w), 1226 (w-m), 1160 (w), 1103 (m), 1055 (m), 1026 (vw), 995 (s), 974 (w), 893 (vw), 850 (vw), 781 (vvs), 737 (vs), 652 (vw), 619 (s), 580 (w), 489 (s), 470 (vs), 397 (m-s), 377 (vw), 272 (m).

B.2.a.2 ***Synthesis of the palladated precursor of formula [(CN)$_2$Py$_2$EtPdCl$_2$]***

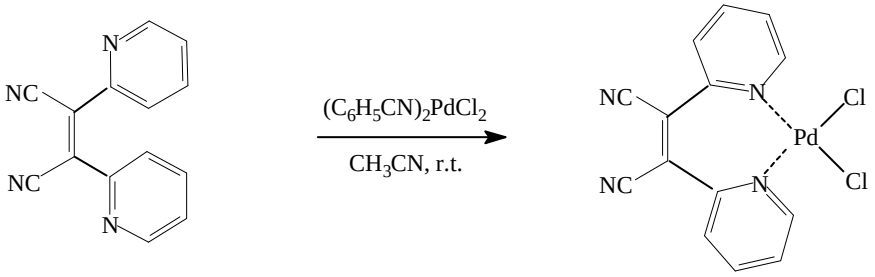

[(CN)$_2$Py$_2$Et] (52 mg, 0.225 mmol) and [(C$_6$H$_5$CN)$_2$PdCl$_2$] (85 mg, 0.222 mmol) were added to CH$_3$CN (10 mL) in a 50 mL flask and the mixture was kept at room temperature under stirring until the solution was clear. After cooling in the refrigerator, the formed precipitate was separated by filtration under vacuum, washed repeatedly with ice CH$_3$CN and brought to constant weight under vacuum (10^{-2} mmHg; 63 mg, yield 68%). Calcd for [(CN)$_2$Py$_2$EtPdCl$_2$], C$_{14}$H$_8$Cl$_2$N$_4$Pd: C, 41.06; H, 1.97; N, 13.68; Pd, 25.98. Found: C, 39.56; H, 2.23; N, 13.14; Pd, 25.21%. IR (KBr, cm^{-1}): 2210 (s,ν_{CN}), 1757 (vvw), 1594 (s), 1508 (m), 1477 (s), 1432 (m-s), 1325 (w), 1277 (m), 1242 (m-s), 1165 (m), 1107 (w), 1066 (vw), 1041 (w), 993 (vvw), 966 (vvw), 858 (vw), 775 (vs), 752 (m), 649 (w), 621 (vw), 578 (vw), 495 (vw), 447 (vw), 413 (vw), 347 (m-s; ν_{Pd-Cl}).

B.2.a.3 ***Synthesis of the platinated precursor of formula [(CN)$_2$Py$_2$EtPtCl$_2$]·H$_2$O***

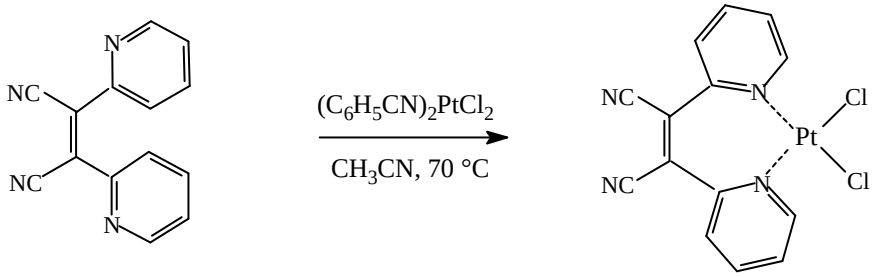

The precursor [(CN)$_2$Py$_2$Et] (50 mg, 0.22 mmol) and [(C$_6$H$_5$CN)$_2$PtCl$_2$] (101 mg, 0.222 mmol) were added to CH$_3$CN (10 mL) in a 50 mL flask and the mixture was kept at 70 °C for 1 h. After cooling, the suspension was filtrated under vacuum and the brown solid material was washed repeatedly with CH$_3$OH and brought to constant weight under vacuumn (10^{-2} mmHg; 63 mg, yield 56%). Calcd for [(CN)$_2$Py$_2$EtPtCl$_2$]·H$_2$O,

$C_{14}H_{10}Cl_2N_4OPt$: C, 32.57; H, 1.95; N, 10.85; Pd, 37.79. Found: C, 32.02; H, 2.19; N, 12.23; Pd, 36.95% . IR (KBr, cm^{-1}): 2213 (m, ν_{CN}), 1593 (w-m), 1506 (vvw), 1481 (vw), 1467 (vw), 1446 (w-m), 1435 (w), 1407 (vw), 1354 (vvw), 1294 (vw), 1236 (vw), 1189 (m), 1176 (w), 1163 (w), 1103 (vw), 1068 (vvw), 1056 (vvw), 1027 (w-m), 995 (w), 935 (vw), 852 (vw), 783 (m), 762 (vs), 737 (w), 684 (s), 619 (w), 549 (m), 534 (w), 490 (w), 468 (w), 399 (vw), 350 (s; $\nu_{Pt\text{-}Cl}$,), 277 (w).

B.2.b Synthesis of the Tetrakis[di(2-pyridyl)]porphyrazine and its Metal Derivatives

B.2.b.1 *Synthesis of the Hydrated Tetrakis[2,3-di(2-pyridyl)]porphyrazinato-monoaquo-Mg^{II}, $[Py_8PzMg(H_2O)]\cdot 4H_2O$*

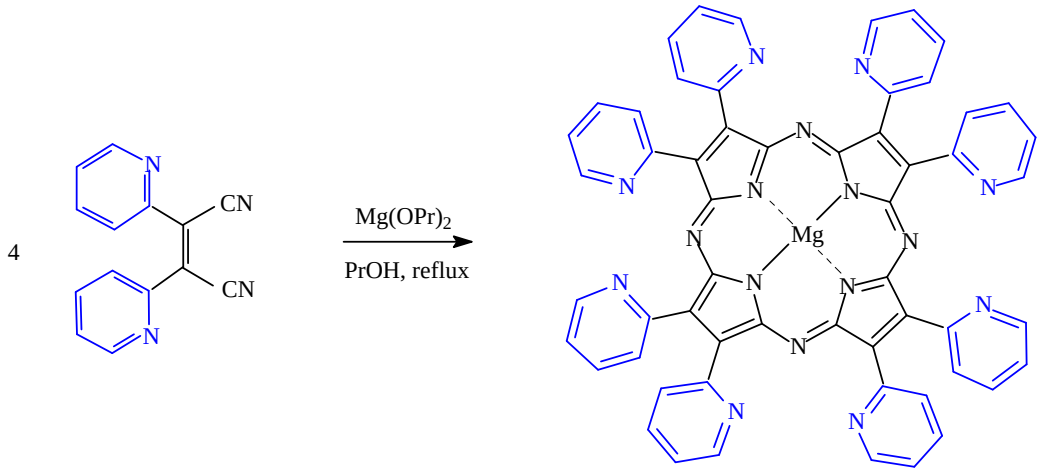

Propyl alcohol (15 mL), metallic magnesium (120 mg, 4.94 mmol), and a few crystals of iodine were introduced in a small flask (25 mL) and the mixture was heated to reflux under stirring for 16 h. After addition of the precursor $[(CN)_2Py_2Et]$ (300 mg, 1.29 mmol), the suspension was heated to reflux again for 8 h. The mixture, brought to room temperature, was poured in air in a vessel and the solvent was left to evaporate completely. The solid residue was added of 10% CH_3COOH (5 mL) and the mixture was kept under stirring for 1 h. The solid was then separated by centrifugation, washed repeatedly with water until neutrality and then brought to constant weight under vacuum. The solid was purified by column chromatography using alumina (Acros, activated, neutral, 50-200 microns) as solid

phase and a solution of 20% CH_3OH in $CHCl_3$ as eluant for the first column, and a gradient from 5% to 30% of CH_3OH in $CHCl_3$ as eluant for the second column. The blue solid obtained was brought to constant weight under vacuum (10^{-2} mmHg; 50 mg, yield 15%). Calcd for $[Py_8PzMg(H_2O)]\cdot 4H_2O$, $C_{56}H_{42}MgN_{16}O_5$: C, 64.47; H, 4.06; N, 21.48. Found: C, 64.54; H, 4.22; N, 21.08%. IR (KBr, cm^{-1}): 3450 (broad), 1718 (vw), 1629 (w), 1585 (s), 1508 (w), 1463 (m), 1423 (w), 1286 (vw), 1238 (w), 1149 (m), 1095 (w), 1049 (vw), 1006 (m-s), 983 (m), 881 (w), 835 (w), 786 (m), 742 (s), 665 (vw), 607 (w), 526 (vw), 497 (vw), 403 (w).

B.2.b.2 ***Synthesis of the Hydrated Tetrakis[2,3-di(2-pyridyl)]porphyrazine, $[Py_8PzH_2]\cdot 5H_2O$***

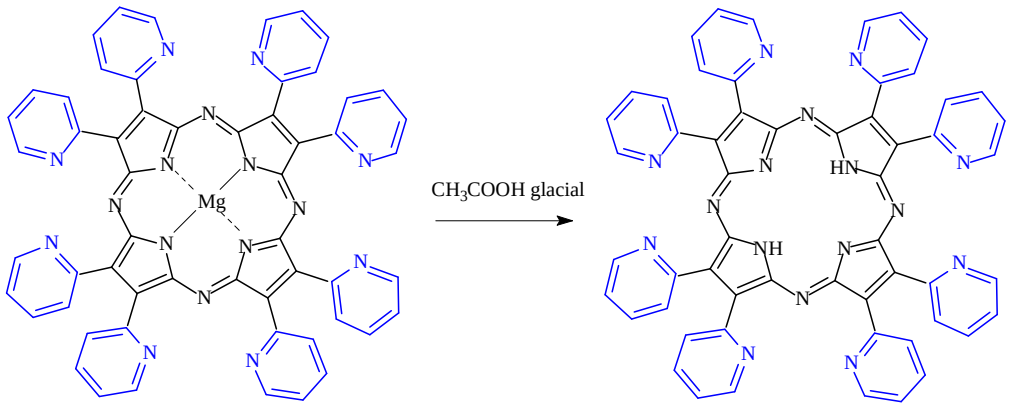

$[Py_8PzMg(H_2O)]\cdot 4H_2O$ (40 mg, 0.038 mmol) was added to glacial acid acetic CH_3COOH (1 mL) in a 10 mL flask and the mixture was kept at room temperature with stirring for 3 h. The obtained solution, brought to room temperature, was poured in air in a vessel and the solvent was left to evaporate completely. The solid material residue separated was washed repeatedly with water and acetone and brought to constant weight under vacuum (10^{-2} mmHg; 11 mg, yield 29%). Calcd for $[Py_8PzH_2]\cdot 5H_2O$, $C_{56}H_{44}N_{16}O_5$: C, 65.87; H, 4.34; N, 21.94. Found: C, 66.41; H, 3.96; N, 21.40%. IR (KBr, cm^{-1}): 3310 (w-m, ν_{NH}), 1606 (m), 1587 (vs), 1564 (m), 1547 (m), 1506 (m), 1461 (s), 1417 (m), 1371 (w), 1338 (m), 1277 (m), 1244 (w), 1174 (m), 1151 (m), 1122 (vw), 1093 (m), 1053 (w), 1020

(s), 999 (s), 968 (s), 900 (w), 860 (w), 829 (w), 771 (m-s), 740 (m), 709 (s), 623 (w), 597 (s), 526 (w), 403 (w).

B.2.b.3 *Synthesis of the Hydrated Tetrakis[2,3-di(2-pyridyl)]porphyrazinato-Zn^{II}, $[Py_8PzZn]\cdot 9H_2O$*

$$[Py_8PzMg(H_2O)]\cdot 4H_2O \xrightarrow[CH_3COOH,\ r.t.,\ 5\ h]{Zn(OAc)_2\cdot 2H_2O} [Py_8PzZn]\cdot 9H_2O$$

$[Py_8PzMg(H_2O)]\cdot 4H_2O$ (41 mg, 0.028 mmol), and $Zn(OAc)_2\cdot 2H_2O$ (20 mg, 0.09 mmol), were suspended in glacial CH_3COOH (3.5 mL). The mixture was kept at room temperature for 5 h. After evaporation of the solvent the solid material was washed with water and acetone and brought to constant weight under vacuum (10^{-2} mmHg; 22 mg, yield 49%). Calcd for $[Py_8PzZn]\cdot 9H_2O$, $C_{56}H_{50}N_{16}O_9Zn$: C, 58.16; H, 4.35; N, 19.38; Zn, 5.65. Found: C, 58.27; H, 3.34; N, 17.37; Zn 6.31%. IR (KBr, cm^{-1}): 3380 (broad), 1587 (vs),1565 (s), 1510 (w-m), 1466 (m), 1429 (w), 1392 (vw), 1344 (vvw), 1288 (vw), 1242 (m), 1151 (m), 1095 (w), 1049 (w), 1005 (m), 881 (w), 785 (w-m), 744 (s), 700 (w), 607 (w), 494 (w).

B.2.c Heteropentanuclear Pt(II) "Pyridylporphyrazines" of Formula $[(PtCl_2)_4Py_8PzM]$ ($M = Mg^{II}(H_2O), Zn^{II}$)

The heteropentanuclear title complexes having $PtCl_2$ externally coordinated, were prepared starting from the corresponding monometallic species $[Py_8PzM]$ with $M = Mg^{II}(H_2O)$ and Zn^{II}, by reaction with $PtCl_2$ in DMSO, according to the following reaction scheme:

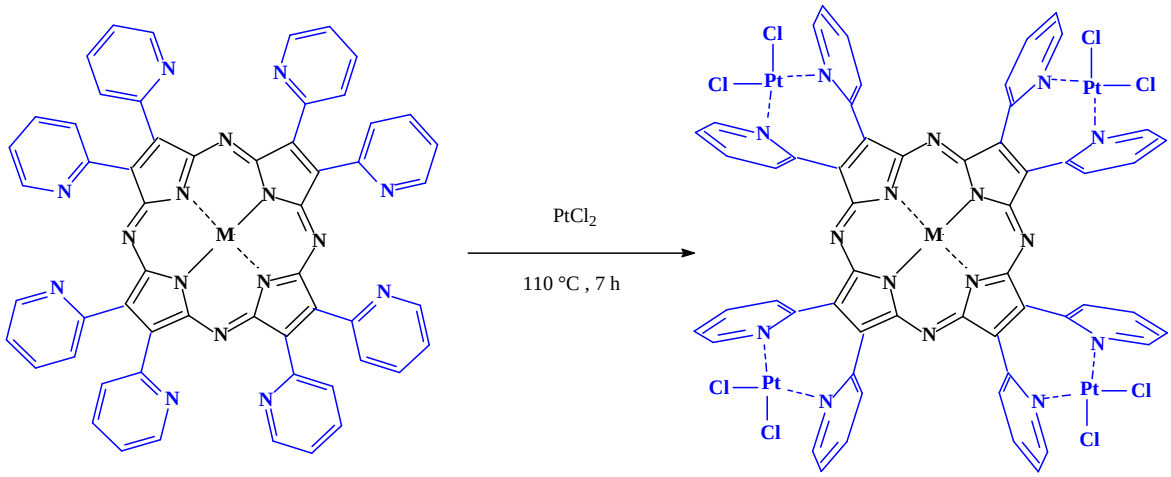

B.2.c.1 ***Synthesis of [(PtCl$_2$)$_4$Py$_8$PzMg(H$_2$O)]***

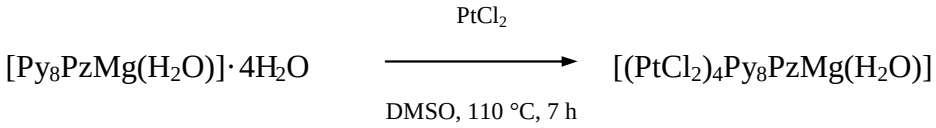

[Py$_8$PzMg(H$_2$O)]·4H$_2$O (41 mg, 0.039 mmol) was suspended (partly dissolved) in freshly distilled DMSO (1.5 mL). The mixture, added of $PtCl_2$ (55 mg, 0.210 mmol), was heated at 110 °C for 7 h. After cooling and filtration, the solid was washed with water and acetone and brought to constant weight under vacuum (10^{-2} mmHg; 16 mg, yield 20%). Calcd for [(PtCl$_2$)$_4$Py$_8$PzMg(H$_2$O)], $C_{56}H_{34}Cl_8MgN_{16}OPt_4$: C, 33.05; H, 1.68; N, 11.01; Pt, 38.34 %. Found: C, 33.74; H, 2.41; N, 9.78; Pt, 37.56. IR (KBr, cm^{-1}): 3440 (m-s), 1616 (m), 1602 (m), 1562 (m), 1527 (vw), 1494 (vw), 1473 (s), 1425 (w-m), 1398 (vw), 1367 (vw), 1288 (w), 1244 (w), 1230 (w), 1186 (w), 1163 (w), 1134 (w), 1113 (w), 1095 (vvw), 1066 (vw), 1037 (w), 1034 (w), 983 (vs), 860 (w-m), 827 (w-m), 814 (w), 775 (s), 712 (m), 677 (w), 604 (m), 571 (vw), 528 (vw), 337 (m, $\nu_{Pt\text{-}Cl}$).

B.2.c.2 ***Synthesis of [(PtCl$_2$)$_4$Py$_8$PzZn]·16H$_2$O·2DMSO***

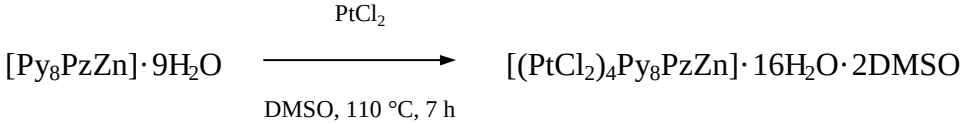

[Py_8PzZn]·$9H_2O$ (21 mg, 0.018 mmol) and $PtCl_2$ (23 mg, 0.086 mmol) were suspended (partly dissolved) in freshly distilled DMSO (1.5 mL). The mixture was heated at 110 °C for 7 h. After cooling and filtration, the separated solid was washed with water and acetone and brought to constant weight under vacuum (10^{-2} mmHg). Calcd for [$(PtCl_2)_4Py_8PzZn$]·$16H_2O$·2DMSO, $C_{60}H_{76}Cl_8N_{16}O_{18}Pt_4Zn$: C, 28.79; H, 3.06; N, 8.90; S, 2.56; Pt, 33.59. Found: C, 28.77; H, 2.44; N, 6.83; S, 2.27; Pt, 32.49%. IR (KBr, cm^{-1}): 3430 (s, broad), 1637 (m), 1612 (vvw), 1602 (m), 1560 (w-m), 1527 (vw), 1493 (w), 1471 (m), 1421(vw), 1400 (vw), 1369 (w), 1288 (vw), 1223 (w), 1155 (vw), 1115 (vw), 1078 (vw), 1041 (vw), 997 (s), 952 (vw), 881 (w-m), 833 (w-m), 773 (w-m), 727 (m), 613 (w-m), 337 (w-m, $\nu_{Pt\text{-}Cl}$).

B.2.d Synthesis of Quaternized "Pyridylporphyrazines" of Formula [(2-Mepy)$_8$PzM](I)$_8$ (M = $Mg^{II}(H_2O)$, Zn^{II})

Quaternized "pyridylporphyrazines" having the formula [(2-Mepy)$_8$PzM](I$_8$) (M = $Mg^{II}(H_2O)$, Zn^{II}) can be prepared by methylation at the pyridine N atoms of the corresponding neutral complexes, [Py_8PzM], by using CH_3I in DMF according to the following reaction scheme:

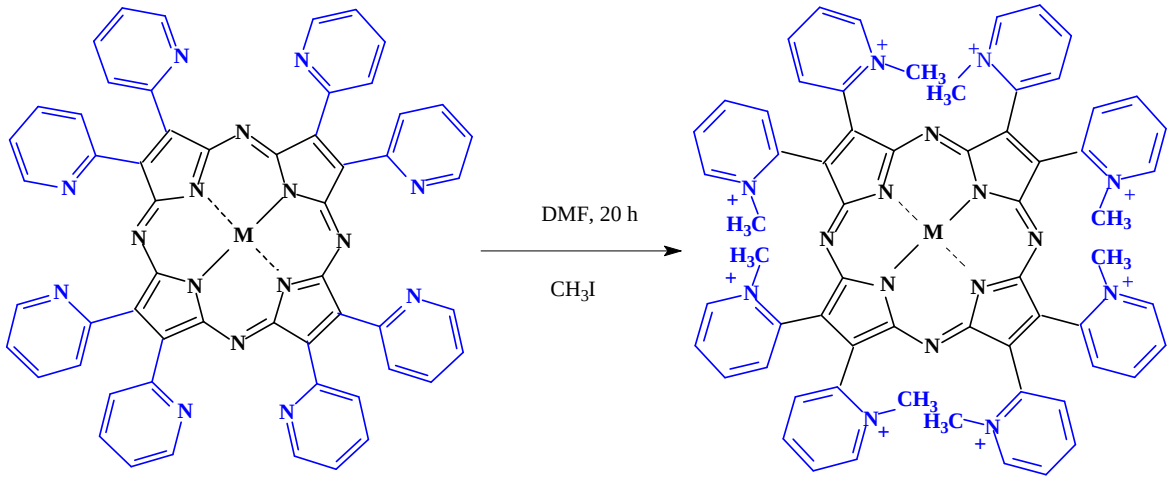

B.2.d.1 ***Synthesis of [(2-Mepy)$_8$PzMg(H$_2$O)](I)$_8$·11H$_2$O***

$$[Py_8PzMg(H_2O)]\cdot 4H_2O \xrightarrow[\text{r.t., 20 h}]{CH_3I,\ DMF} [(2\text{-}Mepy)_8PzMg(H_2O)](I)_8\cdot 11H_2O$$

The complex [Py$_8$PzMg(H$_2$O)]·4H$_2$O (30 mg, 0.029 mmol) and CH$_3$I (0.20 mL, 3.2 mmol) were added to DMF (1 mL) and the mixture was kept at room temperature for 20 h. After evaporation of excess CH$_3$I in air at room temperature, the solution was added of benzene and kept in the refrigerator. The solid material formed was separated by centrifugation, washed with benzene and brought to constant weight under vacuum (10^{-2} mmHg). Calcd for [(2-Mepy)$_8$PzMg(H$_2$O)](I)$_8$·11H$_2$O, $C_{64}H_{78}I_8MgN_{16}O_{11}$: C, 33.21; H, 3.52; N, 10.28. Found: C, 33.97; H, 3.47; N, 9.90%. IR (KBr, cm^{-1}): 3430 (m-s), 2979 (m), 1710 (w), 1624 (s), 1579 (w-m), 1512 (w), 1483 (vw), 1462 (vw), 1273 (m), 1049 (vw), 1016 (w), 1003 (m), 981 (w), 943 (w), 879 (vw), 854 (vvw), 762 (m), 700 (vw), 661 (vvw).

B.2.d.2 ***Attempted Synthesis of [(2-Mepy)$_8$PzZn](I)$_8$***

$$[Py_8PzZn]\cdot 9H_2O \xrightarrow[\text{r.t., 20 h}]{CH_3I,\ DMF} [(2\text{-}Mepy)_8PzZn](I)_8\cdot xH_2O$$

[Py$_8$PzZn]·9H$_2$O (19 mg, 0.016 mmol) and CH$_3$I (0.24 mL, 3.8 mmol) were added to DMF (1 mL) and the mixture was kept at room temperature for 20 h. After evaporation of excess CH$_3$I, the solution was added of benzene and kept in the refrigerator overnight. Due to the impossibility to isolate the solid by centrifugation, it was extracted with water in a separating funnel. The blue water solution containing the complex was then left to evaporate and the residue solid was brought to constant weight under vacuum (10^{-2} mmHg).

B.3 MONO- AND PENTAMETALLIC "THIENYLPORPHYRAZINES"

B.3.a Synthesis of "Thienylporphyrazines" of Formula [Th_8TPyzPzM] (M = $2H^I$, $Mg^{II}(H_2O)$, Co^{II}, Cu^{II}, Zn^{II})

B.3.a.1 *Synthesis of the Hydrated Tetrakis[2,3-di(2-thienyl)pyrazino]porphyrazinato-monoaquo-Mg^{II}, [Th_8TPyzPzMg(H_2O)]·3H_2O*

This Mg^{II} complex was obtained by template cyclotetramerization of the precursor [$(CN)_2Th_2Pyz$][40b] in the presence of Mg^{II} propoxide, according to a previously reported procedure:[44]

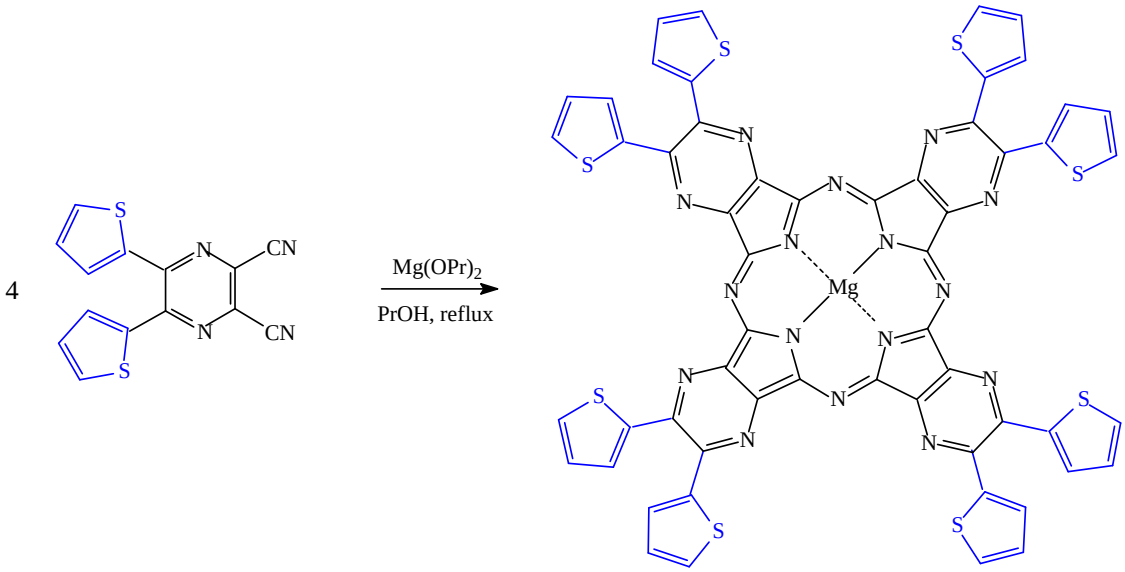

B.3.a.2 *Synthesis of the Solvated Tetrakis[2,3-di(2-thienyl)pyrazino]porphyrazine, [Th_8TPyzPzH_2]·CF_3COOH·H_2O*

The free-base macrocycle was prepared as follows: the Mg^{II} complex [Th_8TPyzPzMg(H_2O)]·3H_2O (200 mg, 0.157 mmol) was suspended, partly dissolved, in CF_3COOH (4 mL) and the mixture refluxed under stirring for 5 h. After cooling, water was added to the mixture (cautiously!) and the bluish-black solid was separated by

centrifugation, washed several times with water until neutrality of the mother liquors, then with acetone, and finally brought to constant weight under vacuum (10^{-2} mmHg; 155 mg, yield 77%). Calcd for $[Th_8TPyzPzH_2]\cdot CF_3COOH\cdot H_2O$, $C_{56}H_{26}N_{16}S_8(CF_3COOH)(H_2O)$: C, 53.12; H, 2.23; N, 17.09; S, 19.56. Found: C, 53.52; H, 2.54; N, 16.93; S, 19.64%. IR (KBr, cm^{-1}): 3400 (broad), 3300 (w, ν_{N-H}), 1736 (w-m), 1518 (m), 1423 (m), 1385 (vs), 1319 (vs), 1309 (w) (sh), 1230 (w), 1202 (w), 1175 (vw), 1136 (m-s), 1084 (w), 1022 (vw), 904 (w), 852 (m), 841 (m), 777 (w), 744 (m), 708 (s), 690 (w), 523 (w).

B.3.a.3 *Synthesis of the Hydrated Tetrakis[2,3-di(2-thienyl)pyrazino]porphyrazinato-Zn^{II}, $[Th_8TPyzPzZn]\cdot 4H_2O$*

The synthesis of the Zn^{II} complex $[Th_8TPyzPzZn]$ is described here below as a representative example of the general synthetic procedure used also for the other metal complexes all prepared starting from the free-base ligand $[Th_8TPyzPzH_2]$ in the presence of the corresponding metal acetate in DMSO at 120 °C, as described by the following reaction scheme:

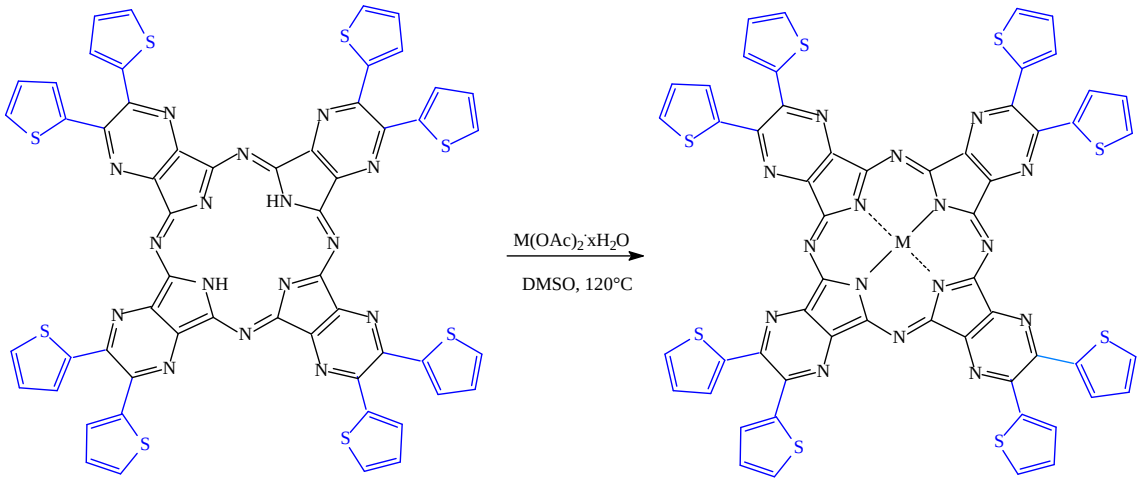

M = Co^{II}, Cu^{II}, Zn^{II}.

$[Th_8TPyzPzH_2]\cdot CF_3COOH\cdot H_2O$ (61 mg, 0.047 mmol) and $Zn(OAc)_2\cdot 2H_2O$ (56 mg, 0.250 mmol) (molar ratio 1:5) were suspended in freshly distilled DMSO (3 mL) and the mixture then heated to 120 °C and kept at this temperature while stirring for 6 h. After cooling and centrifugation, the separated dark green solid was washed repeatedly with

water and acetone and brought to constant weight under vacuum (10^{-2} mm Hg; 47 mg, yield 62%). Calcd for $[Th_8TPyzPzZn]\cdot 4H_2O$, $C_{56}H_{32}N_{16}O_4S_8Zn$: C, 51.14; H, 2.45; N, 17.04; S, 19.51. Found: C, 50.87; H, 1.99; N, 16.70; S, 20.02%. IR (KBr, cm^{-1}): 3400 (broad), 1628 (w), 1543 (vw), 1514 (w-m), 1485 (w),1455 (w), 1421 (m-s), 1362 (m), 1322 (m), 1317 (m), 1250 (m), 1232 (m), 1180 (m), 1101 (m-s), 1049 (w), 996 (vw), 951 (w), 904 (m-s), 854 (m), 812 (vw), 774 (m-s), 746 (m), 700 (s), 666 (w), 634 (w), 566 (w), 523 (w), 452 (w).

B.3.b Heteropentanuclear Pd(II) Complexes of "Thienylporphyrazines" of Formula $[(PdCl_2)_4Th_8TPyzPzM]$ ($M = Mg^{II}(H_2O), Zn^{II}$)

The pentanuclear hydrated complexes of general formula $[(PdCl_2)_4Th_8TPyzPzM]$ ($M = Mg^{II}(H_2O), Zn^{II}$) were prepared starting from the corresponding hydrated monometallic species $[Th_8TPyzPzM]$ by reaction with $PdCl_2$ in tetrahydrofuran according to the following reaction scheme:

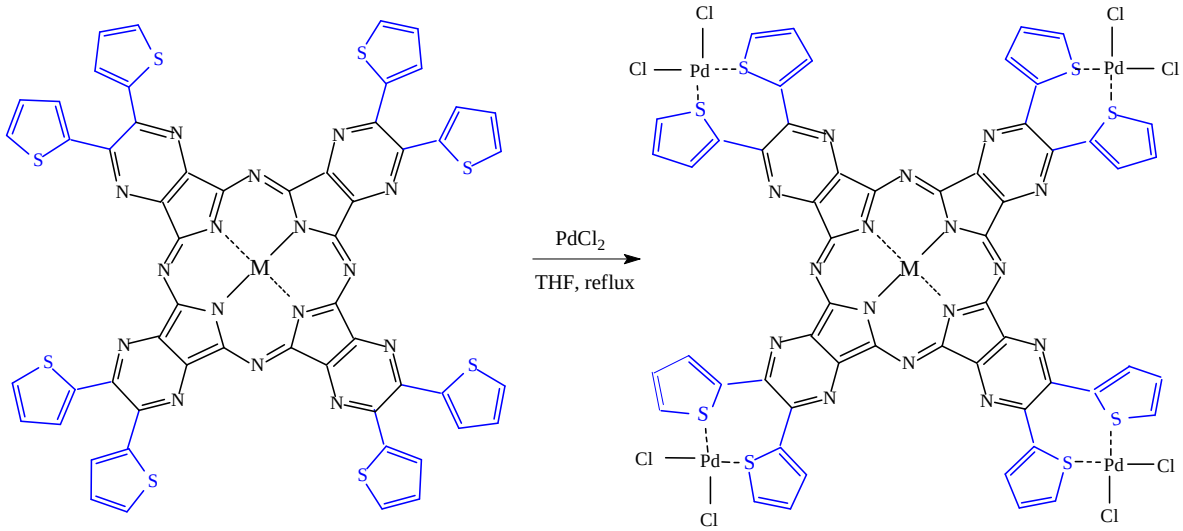

$M = Mg^{II}(H_2O), Zn^{II}$

The synthesis of the Zn^{II} complex $[(PdCl_2)_4Th_8TPyzPzZn]$ is described here below as a representative example.

B.3.b.1 ***Synthesis of [(PdCl$_2$)$_4$Th$_8$TPyzPzZn]·6H$_2$O***

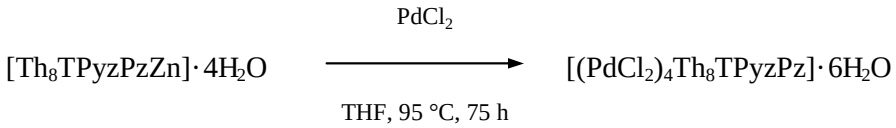

$[Th_8TPyzPzZn]\cdot 4H_2O$ (21 mg, 0.016 mmol) and $PdCl_2$ (13 mg, 0.080 mmol) (molar ratio 1:4.5) were suspended (partly dissolved) in THF (4 mL) and the mixture was heated to reflux under stirring for 75 h. After cooling and centrifugation, the dark-green solid was washed repeatedly with water, twice with acetone and brought to constant weight under vacuum (10^{-2} mmHg; 16 mg, yield 56%). Calcd for $C_{56}H_{36}Cl_8N_{16}O_6Pd_4S_8Zn$: C, 32.65; H, 1.76; N, 10.88, S, 12.45; Pd, 21.81. Found: C, 32.62; H, 1.69; N, 9.48, S, 11.24; Pd, 23.40 %. IR (KBr, cm^{-1}): 3400 (broad), 1632 (w), 1551 (vw), 1516 (w), 1419 (s), 1362 (s), 1317 (m-s), 1252 (m), 1232 (m), 1180 (m-s), 1101 (m-s), 1065 (vw), 1049 (vw), 904 (s), 856 (m), 812 (m), 773 (s), 746 (m), 713 (s), 702 (s), 667 (vw), 565 (vw), 525 (w), 335 (w, $\nu_{Pd\text{-}Cl}$).

Part C. Physical Measurements

Here below the different types of physical techniques utilized in the present work are summarized.

NMR. NMR solutions measurements were made at the CNR Research Area (Montelibretti, Roma) in collaboration with Prof. L. Mannina. NMR spectral data were obtained by dissolving the samples in 700 μL of DMF-d_7 (99.5%, CIL) or of DMSO-d_6 (99.9%, Aldrich). The ^{1}H and ^{13}C experiments were performed at 27 °C on a Bruker AVANCE AQS 600 spectrometer operating at 600.13 and 150.95 MHz, respectively, and equipped with a Bruker multinuclear, z-gradient inverse probehead. ^{1}H and ^{13}C assignments were obtained by means of HSQC experiments carried out using 1024 data points in the f2 dimension and 512 data points in the f1 dimension, a recycle delay of 1s and a coupling constant of 150 Hz. ^{1}H and ^{13}C chemical shifts are reported in parts per million (ppm) and are referred to the residual proton (2.5 ppm) and the residual CH carbon (40.40 ppm) of DMSO-d_6 respectively, or to the residual singlet proton (8.03 ppm) and to the CO (162.5 ppm) of DMF-d_7, respectively.

EXAFS Data Collection and Analysis of $[(CN)_2Th_2Pyz(PdCl_2)_2]$. XAS (X-ray Absorption Structure) spectra of solid $[(CN)_2Th_2Pyz(PdCl_2)_2]$ were collected in transmission mode at the ELETTRA Synchrotron (Trieste, Italy) on the beamline 11.1. Solid $[(CN)_2Th_2Pyz(PdCl_2)_2]$ was diluted with boron nitride to give an absorption change over the edge of about one logarithmic unit. The storage ring was operating at 2/2.4 GeV with an optimal storage beam current of between 300 and 130 mA. Measurements were carried out at the Pd K-edge and the incident beam was mono-chromatized with a Si(111) double crystal. To obtain good signal-to-noise statistic, 5 spectra were recorded and averaged. A Pd foil internal energy calibration was measured simultaneously with each spectrum. The energy was defined by assigning the first inflection point of the Pd foil spectrum to 24350 eV.

EXAFS data analysis was performed using a GNXAS program which has proven to give reliable structural information also in the high energy domain.[45] The GNXAS method accounts for multiple scattering (MS) paths by including the configurational average of all

MS signals to allow fitting of correlated distances and bond length variances described by Debye–Waller factors. Due to the short range sensitivity of the EXAFS technique only the first coordination shell up to 3.5 Å has been taken into account in the analysis. It comprises two chlorine atoms, one nitrogen and one sulphur atom. Each theoretical signal has been modeled with a gamma-like function which depends on four parameters, namely the coordination number N, the average distance R, the distance variance σ^2 and the skewness β. β is related to the third cumulant C_3 of the distance distribution through the relation $C_3 = \sigma^3/\beta$, and R is its first moment of the distance distribution. Additional nonstructural parameters were minimized, namely E_0 (core ionization threshold energy) and S_0^2. Least-squares fits of the EXAFS raw experimental data have been performed by minimizing a residual function.[46] Phase shifts were calculated using muffin-tin potentials and advanced models for the exchange-correlation self-energy (Hedin-Lundqvist). The muffin-tin radii were chosen according to the Norman criterion with 10 % of overlapping.

Theoretical Calculations. DFT and TDDFT calculations were performed in order to provide both gas phase structures and absorption spectra of the two compounds, $[(CN)_2Th_2Pyz]$ and $[(CN)_2Th_2Pyz(PdCl_2)_2]$. The calculations were done with gaussian03.[47] For the energy calculations and geometric optimizations, the DFT method was used with the B3LYP functional[48] using the 6-311+G(d)[49] basis on the first and second row atoms and the LANL ECP with a TZ basis on the Pd atom.[50] Excited state calculations were performed by means of the TDDFT method using the same functional and the same basis set.

Electrochemical and Spectroelectrochemical Measurements. The solvents used for electrochemical measurements, pyridine (99.9+%), DMSO (99.9+%) and DMF (99.8+%), were purchased from Sigma-Aldrich Co. and were used without further purification. High purity N_2 from Trigas was used to deoxygenate the solution before each electrochemical experiment. Tetra-*n*-butylammonium perchlorate (TBAP, 99%) from Fluka Chemika Co. was used as supporting electrolyte (0.1 M for cyclic voltammetry and 0.2 M for spectroelectrochemistry) and stored under vacuum at 40 ^oC prior to use.

Cyclic voltammetry (CV) was performed at 298 K with an EG&G model 173 potentiostat coupled with an EG&E model 175 universal programmer. Current-voltage curves were recorded on an EG&G Princeton Applied Research model R-0151 X-Y recorder. A

three-electrode system was used, consisting of a glassy carbon working electrode, a platinum counter electrode, and a saturated calomel reference electrode (SCE). The reference electrode was separated from the bulk solution by a fritted-glass bridge filled with the solvent/supporting electrolyte mixture.

UV-visible spectroelectrochemical experiments were carried out with a home made thin-layer[51] cell which has a light-transparent platinum gauze working electrode. The applied potential was monitored with an EG&G Model 173 potentiostat and UV-visible spectra were recorded on a Hewlett-Packard Model 8453 diode array spectrophotometer.

Singlet oxygen quantum yield measurements. Measurements of singlet oxygen quantum yield (Φ_Δ) of the complexes were carried out in DMF and/or DMF/HCl by an absolute method reported in the literature,[35b,38] recently modified by us.[52] 1,3-diphenylisobenzofuran (DPBF) was used as the scavenger of $^1O_2$. Solutions of the complexes (ca. 10^{-6}-10^{-5} M) and DPBF (ca. $5x10^{-5}$ M) in DMF were irradiated in a 10-mm path length quartz cell with monochromatic light (Premier LC Lasers/HG Lens, Global Laser). The irradiation wavelength (λ_{irr} = 635, 670, 778 nm) was close to the maximum of the Q-band absorption peaks for all the compounds. The light intensity was set to 0.300 mW and accurately measured with a radiometer (ILT 1400A/SEL100/F/QNDS2, International Light Technologies). The decay of DPBF absorption at 414 nm (ε^{DPBF}= $2.3x10^4$ mol^{-1} L cm^{-1}) was detected at 20 °C by a UV-visible spectrophotometer (Varian Cary 50 Scan).

The Φ_Δ values were obtained from the quantum yield of the photoreaction (Φ_{DPBF}) calculated with respect to different concentrations of DPBF, on the basis of Equation 2.1:

$$\frac{1}{\Phi_{DPBF}} = \frac{1}{\Phi_\Delta} + \frac{k_d}{k_r}\frac{1}{\Phi_\Delta}\frac{1}{[DPBF]} \qquad (2.1)$$

where k_d is the decay rate constant of $^1O_2$ in the solvent and k_r is the rate constant of the reaction of DPBF with $^1O_2$. The $1/\Phi_\Delta$ value was obtained as the intercept of the Stern-Volmer plot ($1/\Phi_{DPBF}$ vs 1/[DPBF] (see Figure 3.34B in Part E of the Results and Discussion section), while the k_d/k_r value, which depends exclusively on the scavenger and the solvent used, is calculated by the ratio between the slope and the intercept of each linear plot. For the experiments in DMF and DMF/HCl, the k_d/k_r value calculated was (3.3 ± 0.3) x 10^{-5} M. This value compares very well with previously published data for similar

measurements: (2.9 ± 0.3) x 10^{-5} M (DMF),[35b] (3.7 ± 0.4) x 10^{-5} M (DMF),[53] and (3.0 ± 0.2) x 10^{-5} M (DMF/HCl).[53] This optimal agreement supports the reliability of the Φ_Δ values measured for the present compounds and reported in Part E of Result and Discussion.

Fluorescence measurements. Steady-state fluorescence and excitation spectra were obtained in DMF and/or DMF/HCl with a Fluorescence Spectrophotometer (Cary Eclipse, Varian) using a 10 mm quartz SUPRASIL cuvette. The fluorescence quantum yields were determined by a comparative method with a reference standard of chlorophyll-*a* (Φ_F = 0.32, ether solution), according to Equaton 2.2, where *G* is the integrated emission area, *n* is the refractive index of the solvent, *A* is the absorbance at the excitation wavelength, *S* and *R* indicate the sample and the reference.

$$\Phi_F^S = \frac{G^S \cdot n_{DMF}^2 \cdot A^R}{G^R \cdot n_{ether}^2 \cdot A^S} \Phi_F^R \qquad (2.2)$$

In all cases the absorbances of the solution were below 0.1 at and above the excitation wavelength.

Other Physical Measurements. IR spectra of the solid materials as KBr pellets were recorded in the range of 4000-250 cm^{-1} on a Varian 660-IR FT-IR spectrometer. UV-visible solution spectra other than those for spectroelectrochemistry (see above) were recorded with a Varian Cary 5E spectrometer by using 1-cm quartz cuvettes. Thermogravimetric analyses (TGA) were performed on a Stanton Redcroft model STA-781 analyzer under a N_2 atmosphere (0.5 L/min). Elemental analyses for C, H, N and S were provided by the "Servizio di Microanalisi" at the Dipartimento di Chimica, Università "La Sapienza" (Rome) on an EA 1110 CHNS-O instrument. X-ray powder diffraction patterns were obtained on a Philips PW 1710 diffractometer by using a CuKα (Ni-filtered) radiation. The ICP-PLASMA analysis of palladium, platinum and zinc was performed on a Varian Vista MPX CCD simultaneous ICP-OES.

CHAPTER 3

RESULTS AND DISCUSSION

As will be extensively illustrated in this chapter large part of the work conducted in this thesis has been focused on the synthetic aspects, physicochemical characterization and applicative perspectives of two types of new porphyrazine macrocycles obtained from the precursors 2,3-di(2-pyridyl)-6,7-dicyano-1,4-quinoxaline, [$(CN)_2Py_2Quin$] (Chart 3.1A) and 1,2-di(2-pyridyl)-1,2-dicyanoethylene, [$(CN)_2Py_2Et$] (Chart 3.1B).

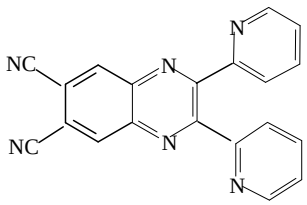

A: [$(CN)_2Py_2Quin$]

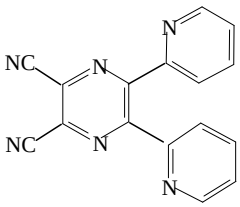

B: [$(CN)_2Py_2Et$]

Chart 3.1

Mononuclear derivatives of formulae [$(CN)_2Py_2QuinMCl_2$] and [$(CN)_2Py_2EtMCl_2$] (M = Pd^{II}, Pt^{II}) were also prepared and studied, and data available on both the compounds [$(CN)_2Py_2Quin$] and [$(CN)_2Py_2Et$] and their Pd^{II} and Pt^{II} complexes will be discussed first here below. The discussion will then be extended with the presentation of the results obtained on the new series of related porphyrazine macrocycles.

Part A. Synthesis and Characterization of 2,3-Di(2-pyridyl)-6,7-dicyano-1,4-quinoxaline, [$(CN)_2Py_2Quin$] and 1,2-Di(2-pyridyl)-1,2-dicyanoethylene, [$(CN)_2Py_2Et$] and their Pd(II) and Pt(II) Metal Complexes

A.1 Synthesis and General Properties of the Quinoxaline Derivative [$(CN)_2Py_2Quin$] and its Complexes [$(CN)_2Py_2QuinPdCl_2$] and [$(CN)_2Py_2QuinPtCl_2$]

It is known from the literature that the dipyridinopyrazine fragment can exhibit two different bidentate modes of coordination to metal ions. One mode involves the N atoms of the two vicinal pyridine rings ("py-py" coordination, Scheme 3.1A). The alternative type of coordination involves one pyrazine N atom and one pyridine N atom ("pyz-py" coordination, Scheme 3.1B). A number of examples are known in the literature in which both types of coordination take place.[23]

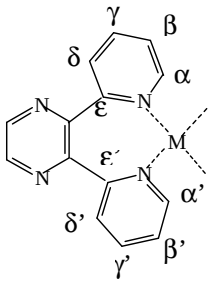

A: "py-py"

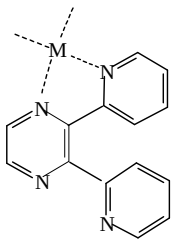

B: "pyz-py"

Scheme 3.1

The present study on the quinoxaline compound 2,3-di(2-pyridyl)-6,7-dicyano-1,4-quinoxaline, [$(CN)_2Py_2Quin$] (Chart 3.1A) and its Pd^{II} and Pt^{II} metal derivatives [$(CN)_2Py_2QuinPdCl_2$] and [$(CN)_2Py_2QuinPtCl_2$], was conducted as a work directed to achieve a well defined level of preliminary information on the coordination properties of the dipyridinoquinoxaline fragment, useful to understand its role in the tetrapyrrolic macrocyclic compounds described below and generated by using [$(CN)_2Py_2Quin$] as

precursor. The results allowed also a comparison with those previously described by our group on the parallel species 2,3-dicyano-5,6-di(2-pyridyl)-1,4-pyrazine, $[(CN)_2Py_2Pyz]$, and its corresponding mononuclear compounds $[(CN)_2Py_2PyzMCl_2]$ (M = Pd^{II}, Pt^{II}) also structurally elucidated in detail.[1,23,24] Added information was given by previous work conducted on the unmetalated compound $[(CN)_2Py_2Quin]$ and its palladated derivative $[(CN)_2Py_2QuinPdCl_2]$, this latter prepared by reaction of $[(CN)_2Py_2Quin]$ with $(DMSO)_2PdCl_2$.[41]

As described in the Experimental Section, the quinoxaline compound $[(CN)_2Py_2Quin]$ (Chart 3.1A) was prepared via a Schiff's base condensation of 2,2'-pyridil and 4,5-diaminophthalonitrile, according to the previously reported procedure.[41] The compound was converted in CH_3CN into its mononuclear derivatives $[(CN)_2Py_2QuinPdCl_2]$ and $[(CN)_2Py_2QuinPtCl_2]$ by reaction with $(C_6H_5CN)_2PdCl_2$ and $(C_6H_5CN)_2PtCl_2$, respectively.

The NMR spectra of $[(CN)_2Py_2Quin]$ and its monopalladated complex $[(CN)_2Py_2QuinPdCl_2]$ were obtained in solution of DMSO-d_6 (Figures 3.1 and 3.2, respectively). For the two compounds, the ^1H and also ^{13}C NMR spectral data were collected and are given in Table 3.1. The ^1H spectral data are in substantial agreement with those previously reported for both species in the same solvent (DMSO-d_6).[41]

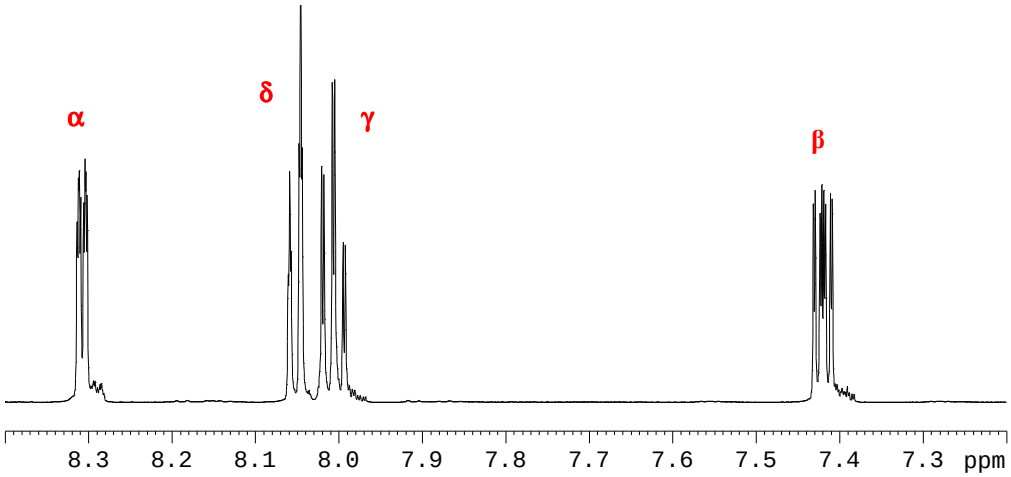

Figure 3.1. ^1H NMR spectrum of $[(CN)_2Py_2Quin]$ in DMSO-d_6 at 300 K.

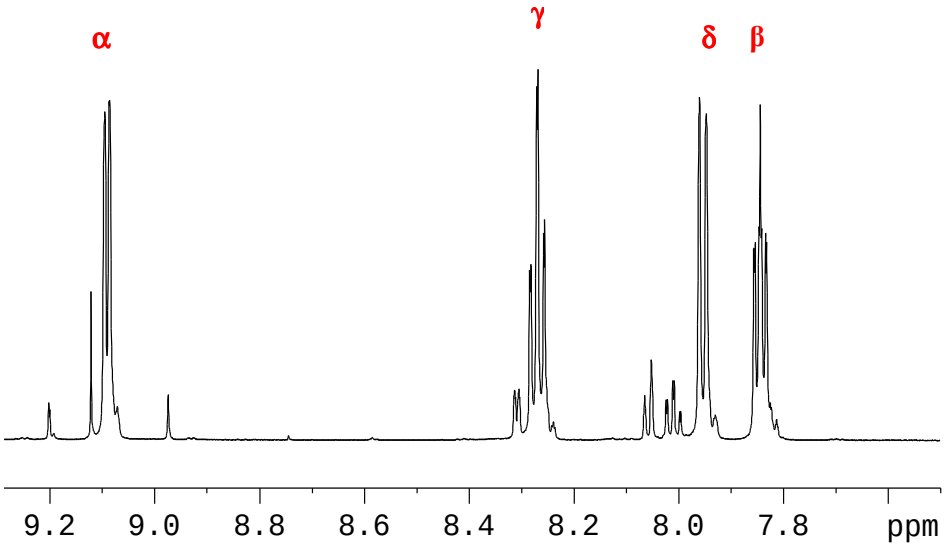

Figure 3.2. ^{1}H NMR spectrum of [$(CN)_2Py_2QuinPdCl_2$] in DMSO-d_6 at 300 K. The singlet at 9.11 ppm is assigned to the aromatic CH protons at 5 and 8 positions.The low intensity peaks detected in the spectrum are due to a little amount of [$(CN)_2Py_2Quin$] present as impurity.

Table 3.1. ^{1}H and ^{13}C NMR Assignments of [$(CN)_2Py_2Quin$] and [$(CN)_2Py_2QuinPdCl_2$] in DMSO-d_6 at 300 K.

	[$(CN)_2Py_2Quin$]				**[$(CN)_2Py_2QuinPdCl_2$]**			
	^{1}H	**m**	***J* (Hz)**	**^{13}C**	**^{1}H**	**m**	***J* (Hz)**	**^{13}C**
α[a]	8.307	ddd	4.8, 1.7, 1.0	149.0	9.080	bd	5.8	153.3
β[a]	7.420	ddd	4.8, 7.6, 1.3	122.7	7.843	ddd	5.8, 7.7, 1.3	128.0
γ[a]	8.006	ddd	7.6, 7.6, 1.7	137.7	8.269	ddd	7.7, 7.9, 1.3	141.5
δ[a]	8.052	ddd	7.6, 1.0, 1.0	124.8	7.954	ddd	7.9, 0.9, 0.9	129.5
CH, CH	9.11 0	s		137.84				

[a] See Scheme 3.1A

Figure 3.1 and 3.2 show only one set of four resonance peaks associated with the hydrogen atoms of the pyridine rings in the α, β, γ and δ positions (Scheme 3.1A). This unequivocally indicates that the pyridine rings are equivalent for the two species, which is fully in line with expectation at least for the unmetalated compound [$(CN)_2Py_2Quin$]. The identical ^{1}H NMR response of the pyridine rings for the palladated species [$(CN)_2Py_2QuinPdCl_2$] strongly suggests that the $PdCl_2$ unit forms upon ligation to [$(CN)_2Py_2Quin$] a coordination site of the

type $N_{2(pyr)}PdCl_2$ which involves the N atoms of the two vicinal pyridine rings ("py-py" coordination). This is in keeping with the findings, based on single crystal X-ray work for the crystalline solid material[41] (see the structure shown in Figure 3.3A). Looking at the chemical shifts listed in Table 3.1, it is evident that in going from the precursor to its monopalladated complex a remarkable low-field shift is observed for three of the four resonance peaks (α,α', 8.307 → 9.080; β,β', 7.420 → 7.843; γ,γ', 8.006 → 8.269), while the fourth one shows a small change in the reverse direction (δ,δ', 8.052 → 7.954). In keeping with expectation, the highest shift is observed for the α proton, which is the one closest to the coordinated N atom (Scheme 3.1A). These results fully coincide with the NMR spectral information achieved in DMF-d_7 (see data in Table 3.2) for the parallel couple of compounds 2,3-dicyano-5,6-di(2-pyridyl)-1,4-pyrazine, $[(CN)_2Py_2Pyz]$, and its related Pd^{II} derivative $[(CN)_2Py_2PyzPdCl_2]$.[24] The suggested "py-py" coordination for the latter has been confirmed by singe-crystal X-ray work on the solid;[24] the same type of coordination was established for the Pt^{II} analog, $[(CN)_2Py_2PyzPtCl_2]$, by X-rays resolution of the structure.[23]

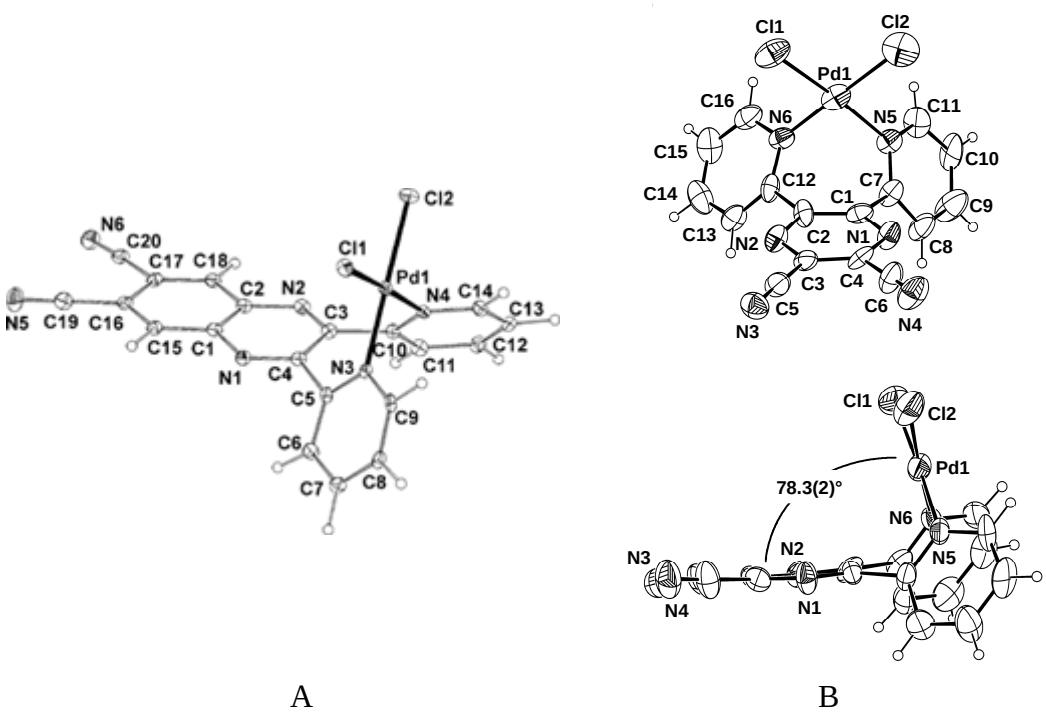

A B

Figure 3.3. An ORTEP representation (30% probability ellipsoids) of the molecular structure of A) $[(CN)_2Py_2QuinPdCl_2]$[41] and B) $[(CN)_2Py_2PyzPdCl_2]$ (top/front and bottom/side views).[24]

Table 3.2. ^{1}H NMR Assignments of $[(CN)_2Py_2Pyz]$ and $[(CN)_2Py_2PyzPdCl_2]$ in DMF-d_7 at 300 K.

	$[(CN)_2Py_2Pyz]$[a]			**$[(CN)_2Py_2PyzPdCl_2]$**[a]		
	^{1}H	**m**	***J* (Hz)**	**^{1}H**	**m**	***J* (Hz)**
α^b	8.367	ddd	4.7, 1.6, 1.4	9.216	dd	5.7, 1.5
β^b	7.497	ddd	4.7, 7.1, 1.6	7.950	ddd	5.7, 7.7, 1.5
γ^b	8.068	ddd	7.1, 7.6, 1.8	8.352	ddd	7.7, 7.7, 1.5
δ^b	8.093	ddd	7.6, 1.6, 1.3	8.027	h[c]	5.7, 1.5

[a] Data taken from ref. 3; [b] see Scheme 3.1A; [c] h = hidden: the assignment was obtained by means of ^{1}H-^{1}H COSY experiment.

With reference to the structure of the quinoxaline Pd^{II} complex,[41] the metal ion adopts a square-planar coordination geometry, the site $N_{2(pyr)}PdCl_2$ being oriented almost perpendicularly to the plane of the quinoxaline residue (dihedral angle between the pyridine rings is 87.0(2)°), as can be seen in Figure 3.3A, and the seven membered ring $C_3C_4C_5N_3Pd_1N_4$ roughly approaching a boat conformation. The described geometry for $[(CN)_2Py_2QuinPdCl_2]$ closely resembles that found for the already cited dipyridinopyrazine derivative $[(CN)_2Py_2PyzPdCl_2]$[24] (Figure 3.3B) and the corresponding Pt^{II} complex, $[(CN)_2Py_2PyzPtCl_2]$.[23] It is relevant that similar types of "py-py" coordination were also established by X-rays for the related compounds containing the quinoxaline fragment, ie. dichloro(6,7-dimethyl-2,3-di(2-pyridyl)quinoxaline)palladium(II),[54] dichloro(2,3-di(2-pyridyl)quinoxaline)platinum(II)[55] and dichloro(6,7-dimethyl-2,3-di(2-pyridyl)quinoxaline)platinum(II).[56]

The IR spectra for the $[(CN)_2Py_2Quin]$ and its Pd^{II} and Pt^{II} complexes are reported in Figure 3.4. The spectrum of the precursor shows differences with respect to those of the metal derivatives, particularly in the range 1100-750 cm^{-1}. Due to the assumed closely similar structures of the Pd^{II} and Pt^{II} complexes, it is not surprising that the IR spectra of the two compounds have an almost superimposable form. Interestingly, both Pd^{II} and Pt^{II} compounds show the presence of an absorption at 341 cm^{-1}, not observed for the unmetalated species, which can be assigned as $\nu_{Pd\text{-}Cl}$ and $\nu_{Pt\text{-}Cl}$, respectively. As the two cyano groups, the position of ν_{CN} remains practically unchanged (2336-2337 cm^{-1}) when going from the unmetalated compound to its metal derivatives.

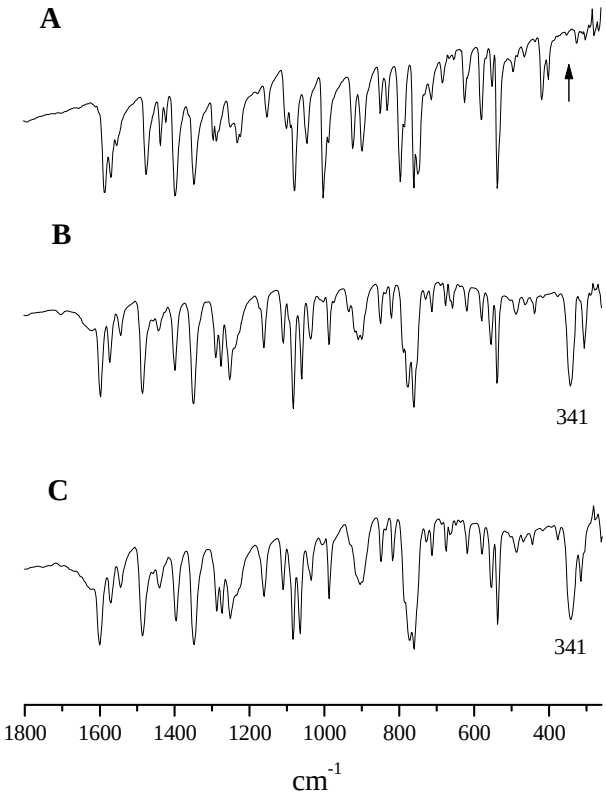

Figure 3.4. IR spectra in KBr of A) $[(CN)_2Py_2Quin]$, B) $[(CN)_2Py_2QuinPdCl_2]$, C) $[(CN)_2Py_2QuinPtCl_2]$.

The UV-visible spectra of $[(CN)_2PyQuin]$ and its Pd^{II} and Pt^{II} complexes taken in solution of CH_3CN show absorptions only in the range 200-500 nm (Figure 3.5), with three distinct absorptions in the range 200-300 nm and a broad peak at 350-390 nm (quantitative data in Table 3.3). The relative intensity of the absorptions in the range 200-300 nm changes in going from $[(CN)_2Py_2Quin]$ to its metal derivatives, whilst the absorption of lower intensity at ca. 350-390 nm becomes broader and probably covers different absorptions. These changes are evidently caused by the metal binding at the dipyridinopyrazine fragment of $[(CN)_2PyQuin]$. The observed absorptions for the three compounds can be confidently assigned to $\pi \rightarrow \pi^*$ transitions, although a definitive assignation could be made by theoretical calculations.

Table 3.3. Quantitative UV-visible Spectral Data of $[(CN)_2Py_2Quin]$, $[(CN)_2Py_2QuinPdCl_2]$, and $[(CN)_2Py_2QuinPtCl_2]$, in CH_3CN.

Compound	λ, nm (log ε)				
$[(CN)_2PyQuin]$	222 (4.47)	252 (4.65)	282 (4.42)	350 (3.98)	
$[(CN)_2Py_2QuinPdCl_2]$	212 (4.74)	250 (4.63)	279 (4.54)	347 (3.96)	360 (3.97)
$[(CN)_2Py_2QuinPtCl_2)]$	207 (4.60)	250 (4.68)	278 (4.66)	355 (3.91)	382 (3.87)

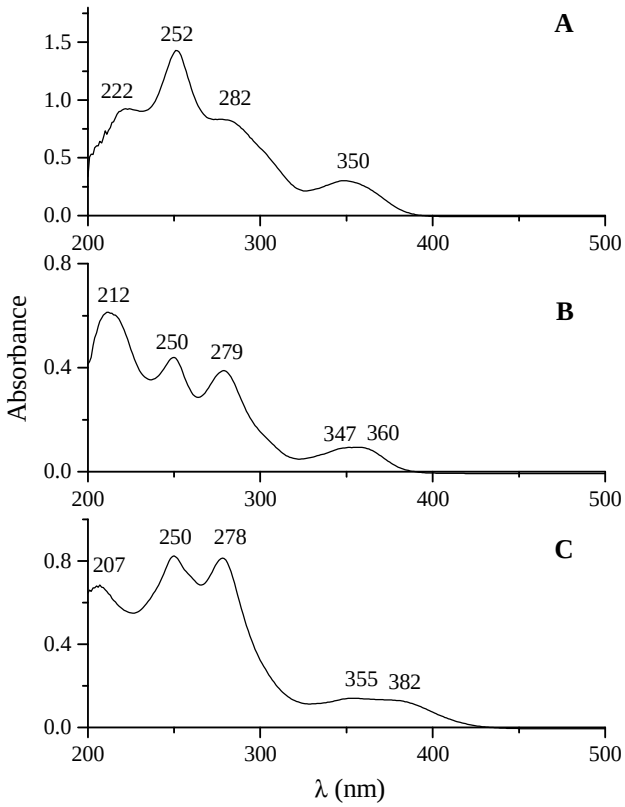

Figure 3.5. UV-visible spectra in CH_3CN of A) $[(CN)_2Py_2Quin]$, B) $[(CN)_2Py_2QuinPdCl_2]$, C) $[(CN)_2Py_2QuinPtCl_2]$.

Preliminary electrochemical measurements were made on the precursor $[(CN)_2Py_2Quin]$ and its metal complexes $[(CN)_2Py_2QuinPdCl_2]$ and $[(CN)_2Py_2QuinPtCl_2]$. Cyclic voltammograms of the three species in DMSO for the reduction range (0.0-2.0 V) are shown in Figure 3.6. Half-wave potentials ($E_{1/2}$, V vs SCE) of these species and the related

dicyanodipyridinopyrazine [$(CN)_2Py_2Pyz$] and its Pd^{II} and Pt^{II} derivatives are reported in Table 3.4.

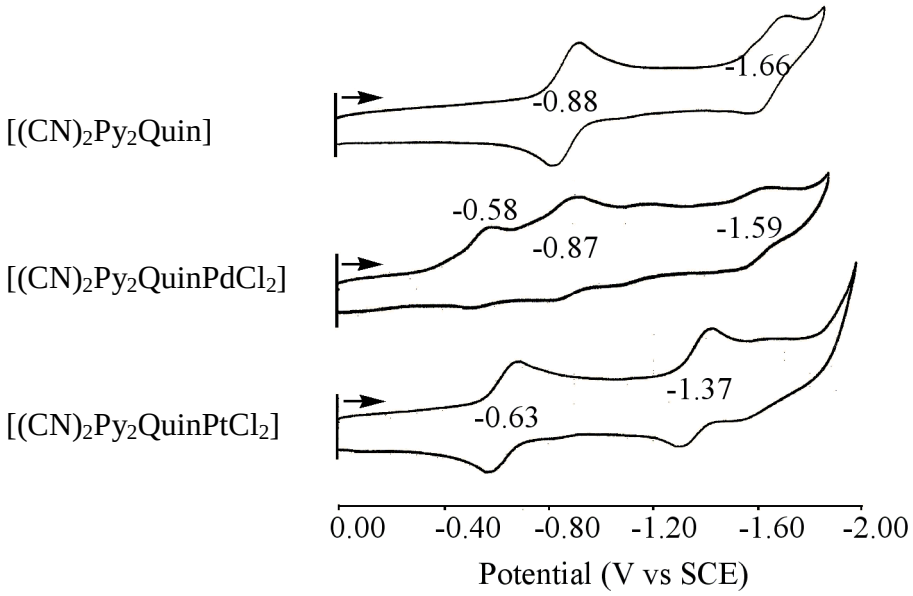

Figure 3.6. Cyclic voltammograms of [$(CN)_2Py_2Quin$], [$(CN)_2Py_2QuinPdCl_2$] and [$(CN)_2Py_2QuinPtCl_2$] in DMSO, 0.1 M TBAP. Scan rate 0.1 Vs^{-1}.

Table 3.4. Half-wave Potentials for Reduction of [$(CN)_2Py_2Quin$], [$(CN)_2Py_2QuinPdCl_2$], [$(CN)_2Py_2QuinPtCl_2$] and Related Compounds in DMSO containing 0.1 M TBAP. Scan rate 0.1 Vs^{-1}.

	$E_{1/2}$, V vs SCE	
Compound	1^{st} red	2^{nd} red
[$(CN)_2Py_2Quin$]	-0.88	-1.66
[$(CN)_2Py_2QuinPdCl_2$]	-0.58	
[$(CN)_2Py_2QuinPtCl_2$]	-0.63	-1.37
[$(CN)_2Py_2Pyz$]	-0.87	-1.72
[$(CN)_2Py_2PyzPdCl_2$]	-0.54	
[$(CN)_2Py_2PyzPtCl_2$]	-0.60	-1.25

Upon scanning the potential from 0.0 to -2.0 V, two reversible reductions at $E_{1/2}$ = -0.88 and -1.66 V, respectively, are obtained for a scan rate of 0.1 Vs^{-1}, involving stepwise one-electron additions, as described by eqs. 3.1 and 3.2:

$$[(CN)_2Py_2Quin] + e^- \rightleftharpoons [(CN)_2Py_2Quin]^- \quad (3.1)$$

$$[(CN)_2Py_2Quin]^- + e^- \rightleftharpoons [(CN)_2Py_2Quin]^{2-} \quad (3.2)$$

The $E_{1/2}$ values are similar to those observed for the dicyanodipyridinopyrazine already mentioned above $[(CN)_2Py_2Pyz]$ in the same solvent (see Table 3.4 and Figure 3.7), -0.87 and -1.72 V respectively for the first and second reduction. Noteworthy, in this case the second reduction is irreversible and involves a EC mechanism (an electron transfer (E) followed by a chemical reaction (C)), to give an unidentified product that is oxidized at E_p = -1.28 V in DMSO on the return anodic sweep.[23]

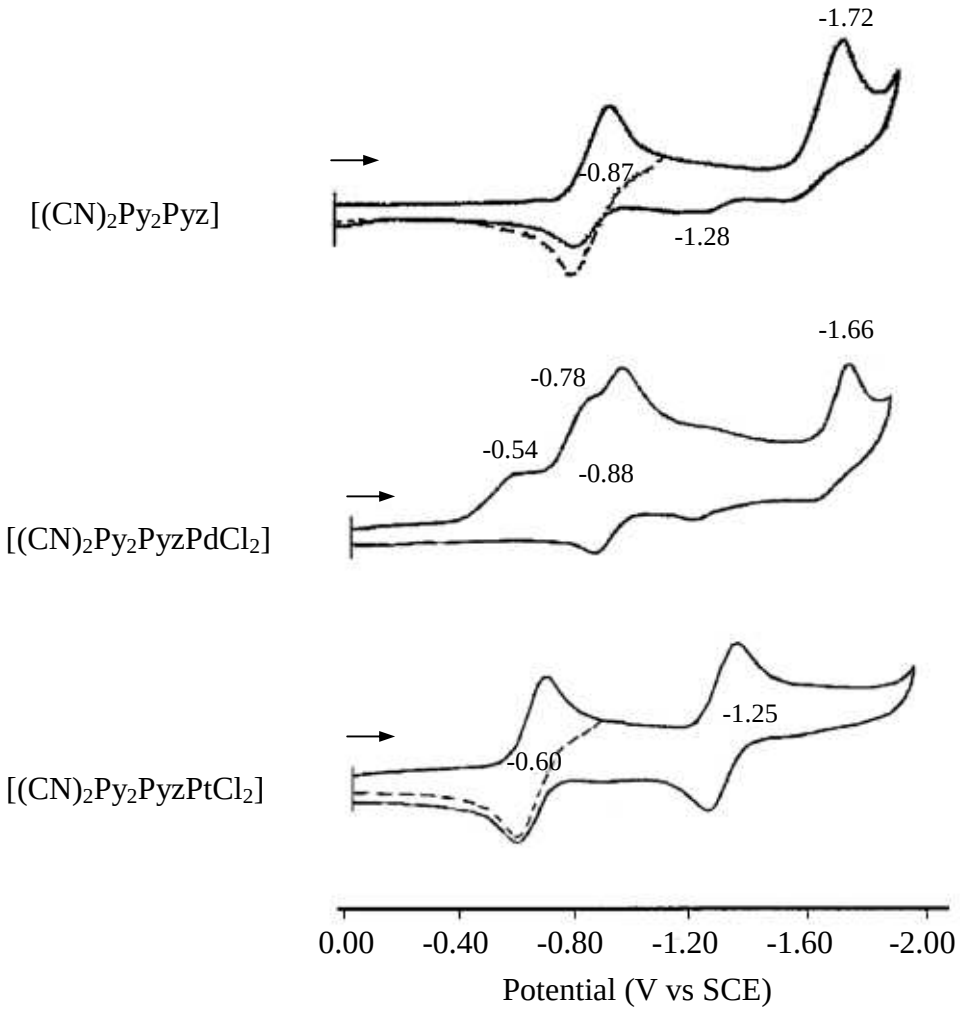

Figure 3.7. Cyclic voltammograms of $[(CN)_2Py_2Pyz]$, $[(CN)_2Py_2PyzPdCl_2]$ and $[(CN)_2Py_2PyzPtCl_2]$ in DMSO, 0.1 M TBAP. Scan rate 0.1 Vs^{-1}.

The cyclic voltammogram of the quinoxaline monoplatinated complex $[(CN)_2Py_2QuinPtCl_2]$ in DMSO is also shown in Figure 3.6. Two reversible one-electron reductions are present in this solvent. It is worth noting that the first one-electron addition at $E_{1/2}$ = -0.63 V is easier than that for reduction of the parent unmetalated compound (Figure 3.6 and Table 3.4) by 250 mV. This clearly indicates that coordination of the $PtCl_2$ unit at the two pyridine sites of $[(CN)_2Py_2Quin]$ causes electron-withdrawing effect, this significantly facilitating the reduction process of $[(CN)_2Py_2Quin]$ in the formation of the -1 charged species $[(CN)_2Py_2QuinPtCl_2]^{1-}$. The doubly reduced $[(CN)_2Py_2QuinPtCl_2]^{2-}$ ($E_{1/2}$ = -1.37 V) is also significantly easier to generate than the doubly reduced parent compound $[(CN)_2Py_2Quin]^{2-}$ ($E_{1/2}$ = -1.66 V), indicating that upon coordination of $PtCl_2$ the excess of negative charge is adequately redistributed within the organic fragment. The same trend was observed for the analogous monoplatinated complex $[(CN)_2Py_2PyzPtCl_2]$, which is easier to reduce than the corresponding unmetalated compound $[(CN)_2Py_2Pyz]$[23] (Figure 3.7 and Table 3.4). The absolute potential difference between $E_{1/2}$ values for the second reduction of $[(CN)_2Py_2Quin]$ and the platinated complex $[(CN)_2Py_2QuinPtCl_2]$ (290 mV) is similar to that observed for the first reduction of the same two compounds, this suggesting that $PtCl_2$ is retained on the molecule after the second electron transfer. In summary two electrons can be reversibly added to $[(CN)_2Py_2QuinPtCl_2]$ in the solvent examined, and these reactions are given by eqs. 3.3 and 3.4:

$$[(CN)_2Py_2QuinPtCl_2] + e^- \rightleftharpoons [(CN)_2Py_2QuinPtCl_2]^- \quad (3.3)$$

$$[CN)_2Py_2QuinPtCl_2]^- + e^- \rightleftharpoons [(CN)_2Py_2QuinPtCl_2]^{2-} \quad (3.4)$$

For the monopalladated complex $[(CN)_2Py_2QuinPdCl_2]$ the cyclic voltammogramm in DMSO (Figure 3.6) shows an irreversible first reduction located at E_p = -0.58 V for a scan rate of 0.1 Vs^{-1}. The electron transfer is easier by 300 mV, as compared to the first reduction of the unmetalated $[(CN)_2Py_2Quin]$. The similarity in the values of first reduction potential of $[(CN)_2Py_2QuinPdCl_2]$ (E_p = -0.58 V) and $[(CN)_2Py_2QuinPtCl_2]$ ($E_{1/2}$ = -0.63 V) is consistent with a similar site of electron transfer in both molecules, and is assigned at the conjugated π system. The chemical reaction following electron addition to

$[(CN)_2Py_2QuinPdCl_2]$ is consistent with a loss of the palladium fragment after the formation of Pd^I and Pd^0,[57] after which the uncomplexed parent compound undergoes reductions at $E_{1/2}$ = -0.87 and -1.59 V (see Figure 3.6). The similarity of this behaviour with the findings for the reduction of the analogous Pd^{II} complex $[(CN)_2Py_2PyzPdCl_2]$ is evident (see Figure 3.7).[23]

A.2 Synthesis and General Properties of $[(CN)_2Py_2Et]$ and its Complexes $[(CN)_2Py_2EtPdCl_2]$ and $[(CN)_2Py_2EtPtCl_2]$

The compound 1,2-di(2-pyridyl)-1,2-dicyanoethylene, $[(CN)_2Py_2Et]$ (Scheme 3.2A) was deeply studied in our laboratory and was used as starting material for the synthesis of a novel series of macrocyclic porphyrazines named here "pyridylporphyrazines".

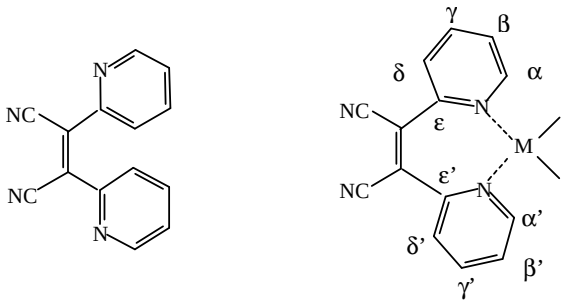

A: $[(CN)_2Py_2Et]$ **B**: "py-py"

Scheme 3.2

It was prepared according to a procedure already reported,[43] by mixing 2-pyridylacetonitrile and bisublimed iodine followed by a treatment of the reaction mixture with a methanolic solution of sodium methoxide. The reaction mechanism consists of an oxidative dehydrogenation process according to the following scheme:

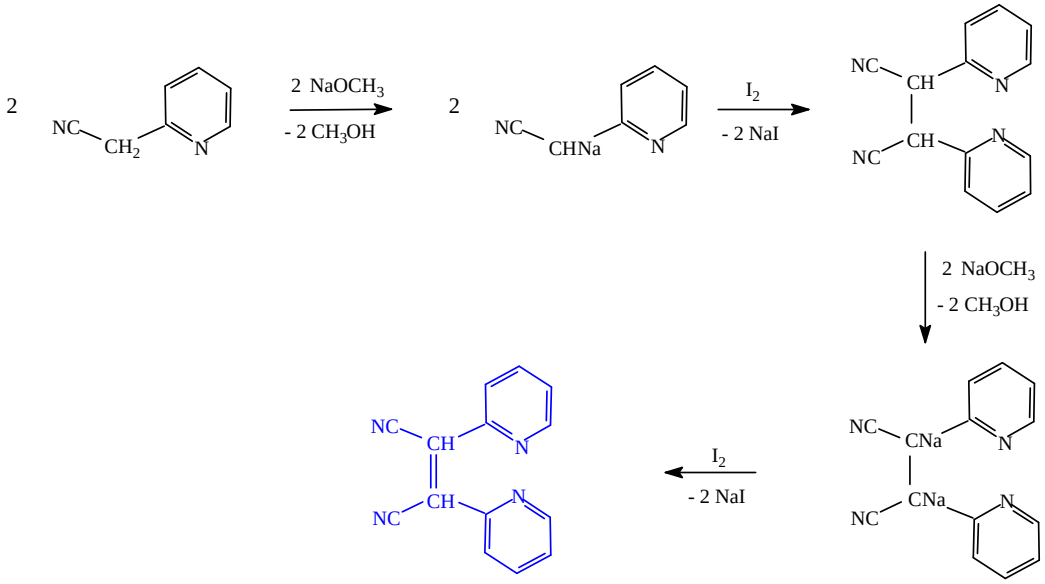

The solid is obtained with high yields as a microcrystalline, air stable brown powder. Attempts to obtain single crystals suitable for X-ray work were unsuccessful.

The reaction of $[(CN)_2Py_2Et]$ with $(C_6H_5CN)_2PdCl_2$ or $(C_6H_5CN)_2PtCl_2$ in CH_3CN leads to the formation of the monometalated complexes $[(CN)_2Py_2EtPdCl_2]$ and $[(CN)_2Py_2EtPtCl_2]$ as dark brown powders. Since the *cis* or *trans* arrangements predictable for $[(CN)_2Py_2Et]$ were not accurately studied in the literature, this aspect was not considered here, since, as it is obvious, upon successful metalation, the structure of the metalated species formed must have the two pyridine rings in their *cis*-arrangement, as shown in Scheme 3.2B ("py-py" coordination). The structure should see the M^{II} centre to adopt a square-planar coordination geometry provided by the N atoms of the two pyridine rings and the chlorine atoms, with the formation of the $N_{2(py)}MCl_2$ coordination site (M = Pd^{II}, Pt^{II}) lying almost orthogonal to the plane defined by the bond system NC-C=C-CN. Attempts to obtain single crystal suitable for single-crystal X-ray work, so far unsuccessful, are in due course in order to confirm the structure of the two metal derivatives, for which NMR spectra provided useful support.

^{1}H and ^{13}C NMR spectra of $[(CN)_2Py_2Et]$ and $[(CN)_2Py_2EtPdCl_2]$ were measured in DMSO-d_6 at 27 °C (see Figures 3.8 and 3.9 and Table 3.5 for the NMR assignments). For both the precursor and its Pd^{II} complex only one set of four resonance peaks is associated with the H atoms of the pyridine rings, which indicates that the pyridine rings are equivalent in both the systems, as expected. For data in Table 3.5 it can be notice that the external coordination of a $PdCl_2$ unit does not seem to influence the resonance peak positions, ie. no low-field shift is observed neither for the α proton, which is the one closest to the coordinated N atom (Scheme 3.2B), nor for the other β, γ, and δ protons. This is quite a different result from those seen for the other Pd^{II} derivatives of the "quinoxaline" and "pyrazine" precursors discussed above; this could be reasonably due to the absence in this case of delocalized electronic charge.

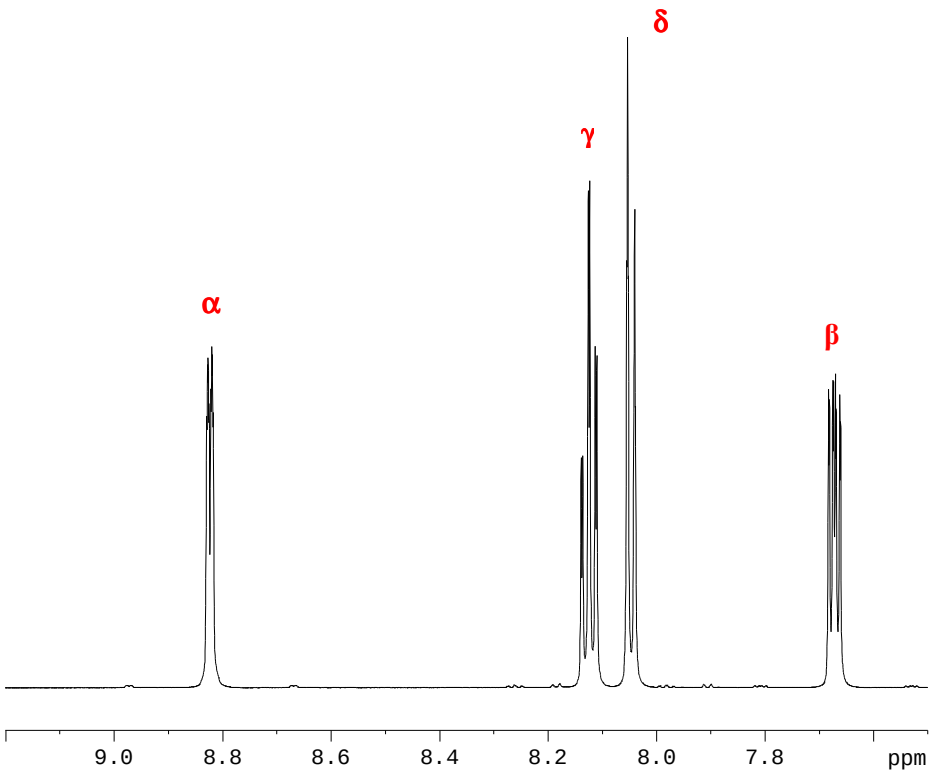

Figure 3.8. ^{1}H NMR spectrum of [$(CN)_2Py_2Et$] in DMSO-d_6 a 300 K.

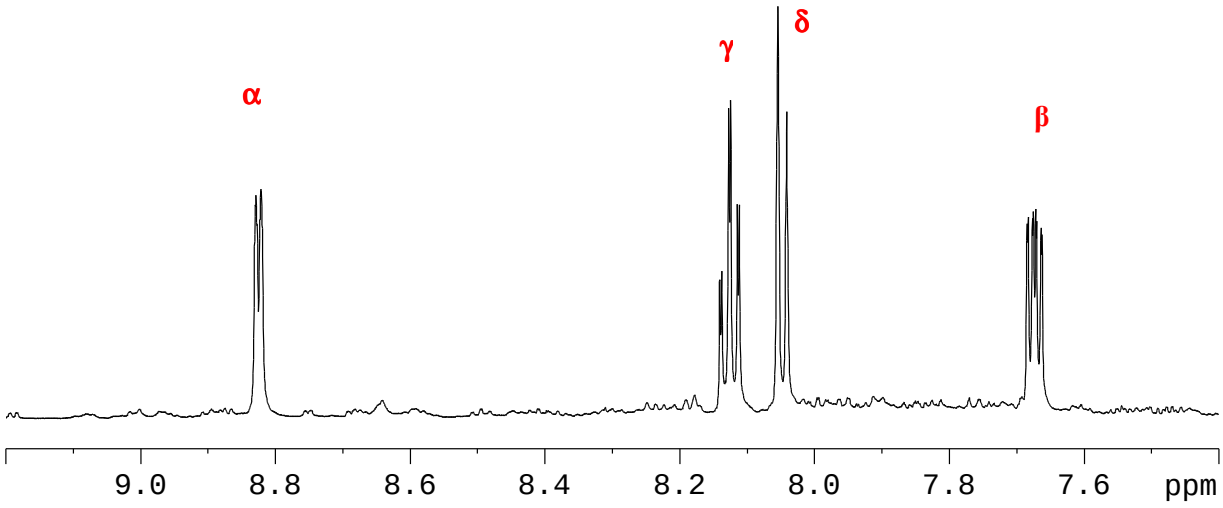

Figure 3.9. ^{1}H NMR spectrum of [$(CN)_2Py_2EtPdCl_2$] in DMSO-d_6 a 300 K.

Table 3.5. ^{1}H and ^{13}C NMR Assignments of [$(CN)_2Py_2Et$] and [$(CN)_2Py_2EtPdCl_2$] in DMSO-d_6 at 300

	[$(CN)_2Py_2Et$]				**[$(CN)_2Py_2EtPdCl_2$]**			
	^{1}H	**m**	***J* (Hz)**	**^{13}C**	**^{1}H**	**m**	***J* (Hz)**	**^{13}C**
α	8.823	ddd	4.8, 1.7, 1.0	150.5	8.824	bd	4.7	150.3
β	7.672	ddd	4.8, 7.8, 1.0	127.1	7.673	ddd	4.7, 7.7, 0.9	127.0
γ	8.124	ddd	7.8, 7.8, 1.7	138.8	8.125	ddd	7.7, 7.7, 1.7	138.9
δ	8.045	ddd	7.8, 1.0	125.1	8.047	ddd	7.9, 0.9, 0.9	125.1

The IR spectra in KBr in the range 1800-260 cm^{-1} are shown in Figure 3.10 for the precursor [$(CN)_2Py_2Et$] and its Pd^{II} and Pt^{II} derivatives. Important changes in the IR spectra are observed in going from [$(CN)_2Py_2Et$] to the two metalated derivatives. The spectrum of [$(CN)_2Py_2Et$] shows clean narrow absorptions throughout the range. The quality of the spectrum is not maintained for the two metal derivatives, and their spectra, similar to one another, indicative of closely existing structural features, appear with lower and broader absorptions.

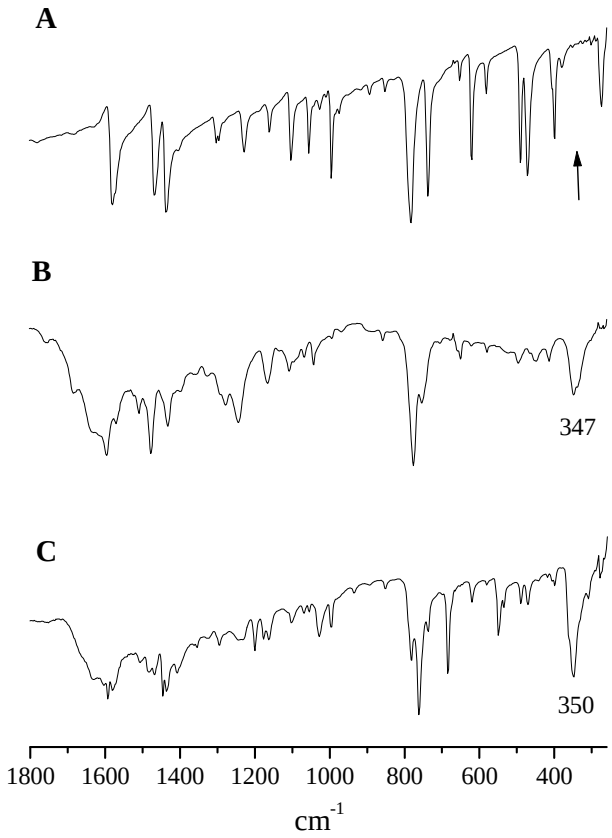

Figure 3.10. IR spectra in KBr of A) [$(CN)_2Py_2Et$], B) [$(CN)_2Py_2EtPdCl_2$] and C) [$(CN)_2Py_2EtPtCl_2$].

In the spectra of the two complexes, peaks are present at 347 and 350 cm^{-1}, in a region lacking of absorptions in the spectrum of the metal-free precursor, attributable as ν(Pd-Cl) and ν(Pt-Cl) for the Pd^{II} and the Pt^{II} complexes, respectively. Practically unchanged is the position of the intense absorption due to the stretching of the CN groups, at ca. 2210 cm^{-1} (see Experimental Section), not shown in the figure.

Quantitative UV-visible spectral data for $[(CN)_2Py_2Et]$ in CH_3OH and CH_3CN and for its Pd^{II} and Pd^{II} complexes $[(CN)_2Py_2EtPdCl_2]$ and $[(CN)_2Py_2EtPtCl_2]$ in CH_3CN are reported in Table 3.6. Figure 3.11 shows the spectra in CH_3CN for the three compounds in the range 200-600 nm. The spectrum of the dicyanodipyridylethylene compound $[(CN)_2Py_2Et]$ is characterized in both the examined solvents CH_3OH and CH_3CN by the presence of absorptions in the range 200-230 nm and a broad intense peak with maximum at 322-323 nm. In low donor solvents such as pyridine, DMSO and DMF only the absorption at 325-335 nm can be evidenced due to the solvent absorptions in the region 200-300 nm. The observed bands are assigned to $\pi \rightarrow \pi^*$ transitions of the molecular system. The spectra of the two metal complexes $[(CN)_2Py_2EtPdCl_2]$ and $[(CN)_2Py_2EtPtCl_2]$ are very similar to each other but different with respect to the spectrum of the metal-free precursor. The spectra show absorptions in the range 200-230 nm and a lower intensity absorption at 310-315 nm, possibly assigned as $\pi \rightarrow \pi^*$ transitions, plus a broad tale in a wide range of the visible (400-550 nm), more evident for the Pd^{II} complex, caused evidently by metalation (LMCT?).

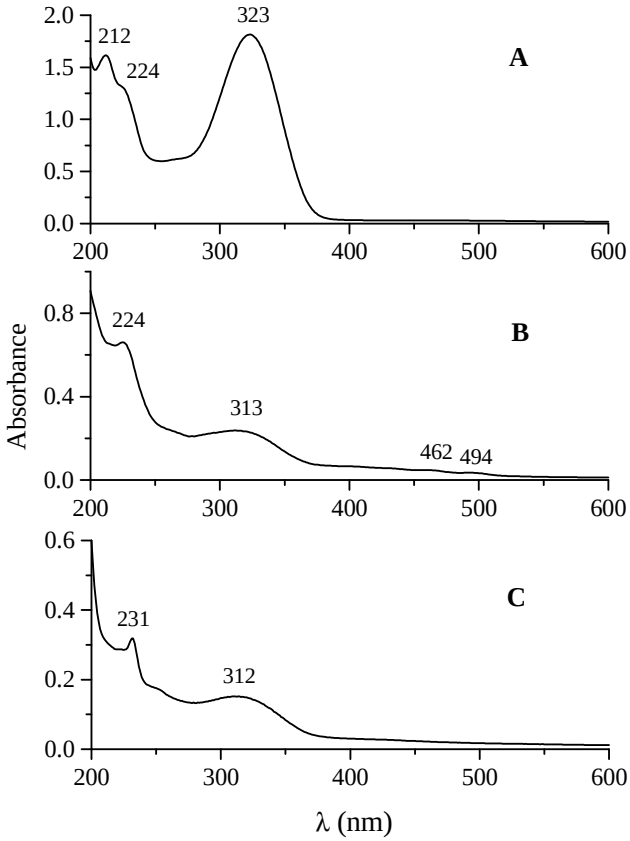

Figura 3.11. UV-Visible spectra in CH_3CN of A) $[(CN)_2Py_2Et]$, B) $[(CN)_2Py_2EtPdCl_2]$, C) $[(CN)_2Py_2EtPtCl_2]$.

Table 3.6. Quantitative UV-visible Spectral Data of $[(CN)_2Py_2Et]$ in CH_3OH, and CH_3CN and of $[(CN)_2Py_2EtPdCl_2]$ and $[(CN)_2Py_2EtPtCl_2]$ in CH_3CN.

Compound	Solvent	λ, nm (log ε)				
$[(CN)_2Py_2Et]$	CH_3OH	212 (4.17)	222 (sh) (4.10)	322 (4.22)		
	CH_3CN	212 (4.16)	224 (sh) (4.07)	323 (4.21)		
$[(CN)_2Py_2EtPdCl_2]$	CH_3CN	224 (4.17)	263 (sh) (3.92)	313 (3.72)	462 (3.03)	494 (2.89)
$[(CN)_2Py_2EtPtCl_2]$	CH_3CN	231 (4.18)	250 (sh) (3.72)	312 (3.86)		

Just preliminary electrochemical measurements were made on the ethylene precursor $[(CN)_2Py_2Et]$ and its metal complexes $[(CN)_2Py_2EtPdCl_2]$ and $[(CN)_2Py_2EtPtCl_2]$. Cyclic voltammograms of the three species in DMSO are illustrated in Figure 3.12; the half-wave potentials ($E_{1/2}$, V vs SCE) are reported in Table 3.7.

Table 3.7. Half-wave Potentials for Reduction of $[(CN)_2Py_2Et]$, $[(CN)_2Py_2EtPdCl_2]$, $[(CN)_2Py_2EtPtCl_2]$ in DMSO containing 0.1 M TBAP. Scan rate 0.1 Vs^{-1}.

	$E_{1/2}$, V vs SCE	
Compound	1st red	2nd red
$[(CN)_2Py_2Et]$	-0.71	-1.15
$[(CN)_2Py_2EtPdCl_2]$	-0.70	
$[(CN)_2Py_2EtPtCl_2]$	-0.70	-1.13

Upon scanning the potential from 0.0 to -2.0 V, two reversible one-electron reductions are seen at $E_{1/2}$ = -0.71 and -1.15 V for the metal-free precursor $[(CN)_2Py_2Et]$ at a scan rate of 0.1 Vs^{-1}, leading to the formation of the -1 and -2 charged species $[(CN)_2Py_2Et]^{1-}$ and $[(CN)_2Py_2Et]^{2-}$. This behaviour closely parallels what has been seen for the quinoxaline compound $[(CN)_2Py_2Quin]$. The less negative potentials measured for $[(CN)_2Py_2Et]$ indicate that the electron capture by this compound is greatly facilitated, particularly for the second reduction.

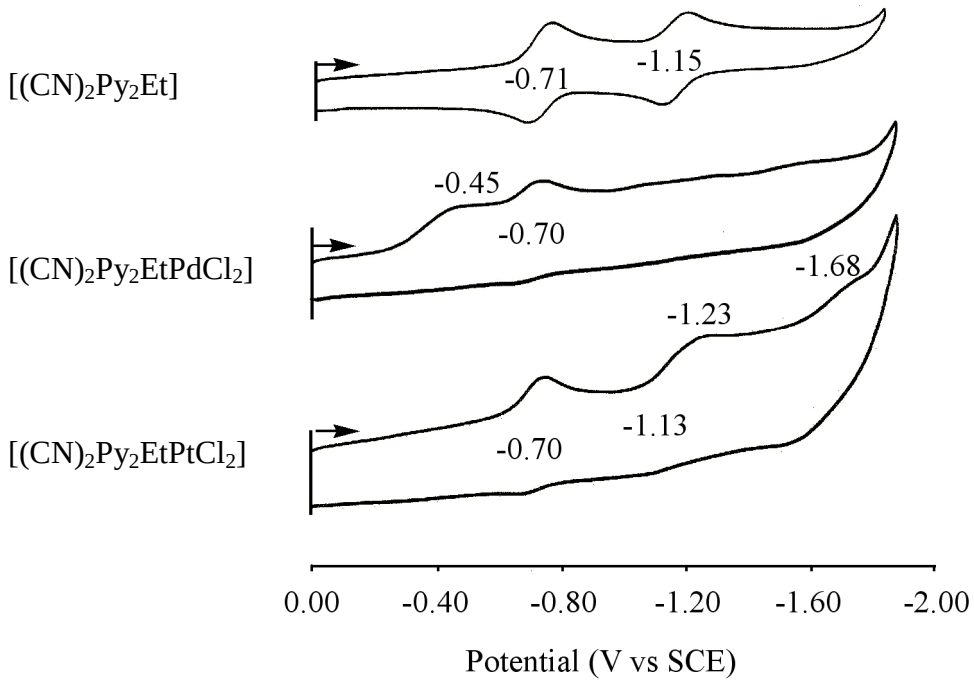

Figure 3.12. Cyclic voltammograms of $[(CN)_2Py_2Et]$, $[(CN)_2Py_2EtPdCl_2]$ and $[(CN)_2Py_2EtPtCl_2]$ in DMSO, 0.1 M TBAP.

As to the monoplatinated complex $[(CN)_2Py_2EtPtCl_2]$ two one-electron reductions are also observed at half-wave potential values ($E_{1/2}$ = -0.70 and -1.13 V) practically coincident with those measured for the parent precursor. Differently from the other examined systems (see above) these reductions are not reversible and other cathodic peaks are visible at E_p = -1.23 and -1.68 V, whose explanation needs more extensive studies to be done. Worth of notice is the fact that in this case the potentials of first and second reduction are not shifted at less negative values as observed above for the Pt^{II} derivative of the "quinoxaline" precursor and its analogous dicyanodipyridinopyrazine compound. In summary, this means that the one-electron reductions are not easier for the platinated species and that the electron-withdrawing effect of the $PtCl_2$ group upon coordination to the precursor $[(CN)_2Py_2Et]$ appears irrelevant. For the monopalladated complex $[(CN)_2Py_2EtPdCl_2]$ the situation in DMSO seem to be further complicated due to the poor response, and associated complicating elements, presumably due to the loss of the palladium fragment and irreversibility of the processes involved. Further studies to be conducted in different solvents are needed to design a more clear picture of the electrochemical behaviour of the monopalladated species.

Part B. Synthesis, General Properties and UV-visible Spectral Behaviour of Neutral Monometallic "Quinoxalinoporphyrazines", [Py_8TQuinPzM], and "Pyridylporphyrazines", [Py_8PzM]

B.1 "Quinoxalinoporphyrazines", [Py_8TQuinPzM] (M = $2H^I$, $Mg^{II}(H_2O)$, Zn^{II}, Co^{II})

On the basis of our research work it has been established that the title "quinoxalinoporphyrazines" having formula [Py_8TQuinPzM] (M = $2H^I$, $Mg^{II}(H_2O)$, Zn^{II}, Co^{II}) (Figure 3.13) can be obtained in the following sequence [Py_8TQuinPzMg(H_2O)] $\rightarrow$ [Py_8TQuinPzH_2] $\rightarrow$ [Py_8TQuinPzM] (M = Zn^{II}, Co^{II}).

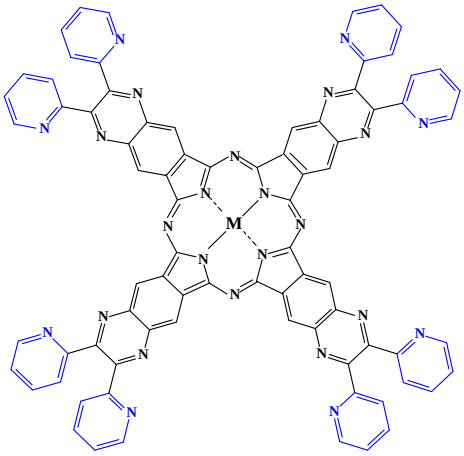

Figure 3.13. Structural formulation of the "quinoxalinoporphyrazines" [Py_8TQuinPzM] (M = $2H^I$, $Mg^{II}(H_2O)$, Zn^{II}, Co^{II}).

The Mg^{II} complex [Py_8TQuinPz$Mg^{II}(H_2O)$] was prepared by a template cyclotetramerization of its precursor 2,3-di(2-pyridyl)-6,7-dicyano-1,4-quinoxaline, [$(CN)_2Py_2$Quin], in the presence of magnesium propylate as described in the Experimental Section. The complex, which is formed in high yield as a stable-to-air hydrated dark-blue amorphous material, is formulated with one water molecule directly ligated to Mg^{II}, in line with a similar formulation for the complex [Py_8TPyzPzMg(H_2O)].[21] The presence of such a water molecule is difficult to be proved directly, but its presence is encouraged by the fact that the $Mg^{II}(H_2O)$ moiety is commonly observed in porphyrazine macrocycles. Examples

are the structures, elucidated by single-crystal X-ray work, of the complexes (aquo)(octakis(methylthio)porphyrazinato)-magnesium(II), [(omtp)Mg(H_2O)][58] and [PcMg(H_2O)]2py[59] (Pc = phthalocyaninato dianion, $C_{32}H_{16}N_8^{=}$). The same monoaquo moiety Mg(H_2O) was given some support of its presence for the previously reported Mg^{II} complexes of the tetrakis(thia/selenodiazole)porphyrazines[60] and tetrakis-2,3-(5,7-diphenyl-6*H*-diazepino)porphyrazine.[19,20] Interestingly, even the bis-hydrate [PcMg(H_2O)$_2$] has been recently reported[61] and a dimerized monohydrate of a low-symmetry porphyrazine macrocycle have been structurally elucidated,[37a] both these examples proving the tendency of Mg^{II}, if in the center of a porphyrazine macrocycle, to coordinate water molecules.

Demetalation of the Mg^{II} complex with formation of the corresponding free-base, ie. the process [Py_8TQuinPzMg(H_2O)] → [Py_8TQuinPzH_2], is obtained in boiling glacial acetic acid in fairly good yield. [Py_8TQuinPzH_2] is formed as a solid, dark-blue, air stable material. The used synthetic procedure is different from that reported elsewhere[41] by direct cyclotetramerization of the same "quinoxaline" precursor [$(CN)_2Py_2$Quin] in the presence of lithium pentoxide. Our attempts to reproduce this procedure were unsuccessful because of the difficulties encountered in the separation and purification of the macrocycle. Conversion of the free-base [Py_8TQuinPzH_2] to its dark blue stable-to-air Zn^{II} and Co^{II} derivatives [Py_8TQuinPzZn] and [Py_8TQuinPzCo], was obtained with good yields in DMSO in the presence of the pertinent metal acetate.

It is noticed here that all the new species [Py_8TQuinPzM] (M = $2H^I$, Mg^{II}(H_2O), Zn^{II}, Co^{II}) are obtained as hydrated species. In our experience this is a common feature for macrocycles carrying externally annulated heterocyclic rings, as has been frequently pointed out.[13,14,21,31b] Chlatrated water is variable from batch to batch for each single species. It can be easily eliminated by heating the macrocycles at ca. 100 °C under vacuum. After the loss of water, thermogravimetric analysis shows that the macrocycles are stable in an inert atmosphere at temperatures up to ca. 300 °C. Exposure of the heated samples to air leads to a rehydration of the material. Throughout the present thesis, chlatrated water will not be given in the formulated macrocycles unless strictly required, due to its unrelevant role played in the explored general physicochemical properties and studied photoactivity.

As a general observation, all the "quinoxalinoporphyrazines" prepared are not sublimable, and all the attempts made to isolate single crystals suitable for X-ray work were unsuccessful. The structural and electronic information was essentially achieved by IR and UV-visible spectral studies, as described below.

As illustrative examples, the IR spectra of the Mg^{II} complex [$Py_8TQuinPzMg(H_2O)$] and the free-base [$Py_8TQuinPzH_2$] are reported in the range 1800-260 cm^{-1} in Figures 3.14 and 3.15, respectively. The spectra are quite different form one another, which can facilitate the accomplishment of the preparation of the free base from the Mg^{II} complex. It is of interest that formation of the free-base determines the appearance of an absorption band at 3290 cm^{-1} (Figure 3.15, inset), which is assigned to the ν(NH) stretching of the central NH groups, similarly to what has been seen to occur for other porphyrazine macrocycles.[1,19,60a] This absorption disappears in the reverse process, ie. when the free-base is converted, for instance, into its Zn^{II} and Co^{II} metal derivatives. Indeed the IR spectra of the metal complexes [$Py_8TQuinPzM$] (M = $Mg^{II}(H_2O)$, Zn^{II}, Co^{II}) are very similar to each other, thus no matter which the type of metal center. The main differences between the spectrum of the free-base ligand and those of the metal complexes in the range 1800-260 cm^{-1} are located in the regions 1100-950 cm^{-1} and 850-650 cm^{-1}. Particularly in this latter region, the disappearance of absorptions at 856 and 775 cm^{-1} occurs on going from the free-base to the metal complexes.

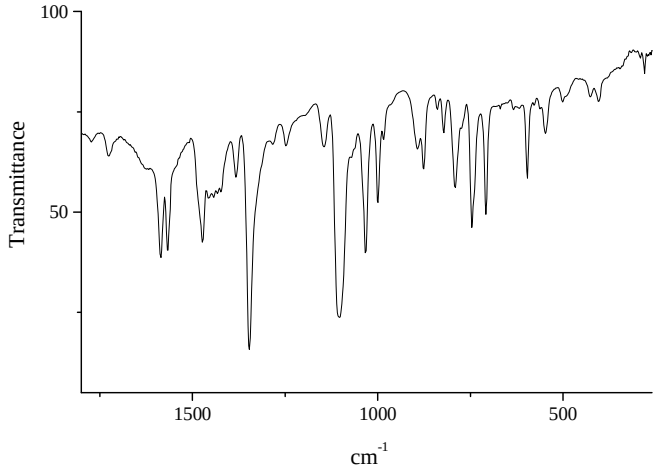

Figure 3.14. IR spectrum in KBr of [$Py_8TQuinPzMg(H_2O)$].

Concomitantly, new absorptions appear in the same region in the form of a clean triplet with peak positions at 791, 746 and 708 cm^{-1} for the Mg^{II} complex and practically fall in the same positions for the Zn^{II} and Co^{II} complexes.

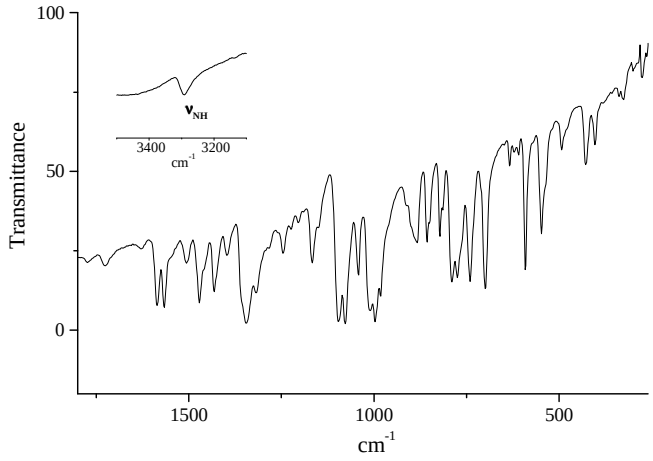

Figure 3.15. IR spectrum in KBr of [$Py_8TQuinPzH_2$].

<u>B.2</u> "Pyridylporphyrazines", [Py_8PzM] (M = $2H^I$, $Mg^{II}(H_2O)$, Zn^{II})

Template cyclotetramerization of 1,2-di(2-pyridyl)-1,2-dicyanoethylene, [$(CN)_2Py_2Et$] in refluxing propyl alcohol in the presence of magnesium(II) propylate gave the Mg^{II} complex [$Py_8PzMg(H_2O)$] (Figure 3.16). The crude material was purified by chromatography on alumina column by using as eluant a mixture of 20% CH_3OH in $CHCl_3$ for the first column, and a gradient from 5% to 30% of CH_3OH in $CHCl_3$ for the second column, as specified in the Experimental Section. The alternative method of separation and purification by centrifugation and washing of the solid sample, which is normally used for other porphyrazine macrocycles, could not be used, due to the high solubility of this compound in a variety of non-donor ($CHCl_3$, CH_3OH) or low-donor solvents such as pyridine, DMSO and DMF. Elemental analyses and an accurate control of its UV-visible spectrum were used for the definition of the level of purity of the compound. The Mg^{II} species is obtained with low yield as hydrated green stable-to-air amorphous powder, carrying chlatrated water. The amount of this water can vary significantly for different batches of preparation. It can be

easily removed by mild heating (ca. 100 °C) under vacuum. The Mg^{II} species is formulated as a monoaquo complex [$Py_8PzMg(H_2O)$] for reasons adequately detailed above for the quinoxaline Mg^{II} complex [$Py_8TQuinPzMg(H_2O)$].

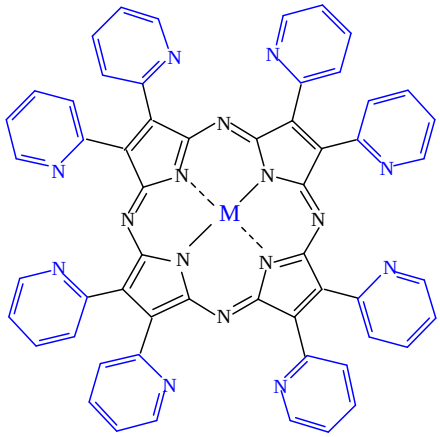

Figure 3.16. The "pyridylporphyrazines" [Py_8PzM] (M = $2H^I$, $Mg^{II}(H_2O)$, Zn^{II}).

The free-base macrocycle [Py_8PzH_2] can be easily obtained by demetallation of [$Py_8PzMg(H_2O)$] in glacial acetic acid at room temperature. The product was separated as a hydrated dark-green solid, stable to the air upon complete evaporation of the solvent and washings with water to neutrality.

The Zn^{II} complex, [Py_8PzZn], was prepared by a trasmetallation process, suspending the Mg^{II} species in glacial acetic acid at room temperature in the presence of an excess of zinc acetate. The solid was isolated, after evaporation of the solvent and washings with water to neutrality, as a hydrated dark-green powder, stable to air. The occurred exchange of the metal center was checked by elemental analyses for the content of C, H, N and Zn, which confirmed the given formulation. The complex could not be obtained by the process [Py_8PzH_2] $\rightarrow$ [Py_8PzZn] due to the poor amounts of the starting material and difficulties with purification. Presently, it has been verified that the Zn^{II} complex needs further studies and, due to the importance of this species for potential applications in photodynamic therapy, more research work is needed in order to obtain adequate amounts of enough pure material.

The observed high solubility in low-donor solvents (pyridine, DMSO, DMF) as well as in non donor solvents like $CHCl_3$ for the "pyridylporphyrazines" [Py_8PzM] so far prepared (M = $2H^I$, $Mg^{II}(H_2O)$, Zn^{II}) (the maximum concentration of a saturated solution was ca. 10^{-3}

M for the Mg^{II} complex and ca. 10^{-4} M for the free-base macrocycle in DMF), allowed to carry a preliminary NMR study on the macrocycles. ^{1}H and ^{13}C NMR spectra of the Mg^{II} complex were performed in DMF-d_7 using a saturated solution which shows a UV-visible spectrum indicative of the exclusive presence of the complex in its monomeric form, with no traces of aggregation. The ^{1}H NMR spectrum is shown in Figure 3.17 and the ^{1}H and ^{13}C NMR assignments are reported in Table 3.8, together with those of the respective precursor $[(CN)_2Py_2Et]$ in DMSO-d_6, for comparison. As can be seen from the figure only one set of four resonance peaks is associated with the H atoms of the pyridine rings, which indicates that the pyridine rings are equivalent, as expected.

Table 3.8. ^{1}H and ^{13}C NMR Assignments of $[(CN)_2Py_2Et]$ in DMSO-d_6,and of $[Py_8PzMg(H_2O)]$ in DMF-d_7.

	$[(CN)_2Py_2Et]$				**$[Py_8PzMg(H_2O)]$**			
	^{1}H	**m**	***J* (Hz)**	**^{13}C**	**^{1}H**	**m**	***J* (Hz)**	**^{13}C**
α	8.823	ddd	4.8, 1.7, 1.0	150.5	8.766	ddd	4.7, 1.8, 0.9	149.4
β	7.672	ddd	4.8, 7.8, 1.0	127.1	7.564	ddd	4.7, 7.6, 0.9	122.7
γ	8.124	ddd	7.8, 7.8, 1.7	138.8	8.201	ddd	7.6, 7.6, 1.8	135.7
δ	8.045	ddd	7.8, 1.0	125.1	8.998	ddd	7.6, 0.9, 0.9	129.0

If we compare the data for the precursor with those of the macrocycle, it is interesting to observe that, consequent to the formation of the macrocycle, the π-ring current induces a low field shift of the γ and δ resonances peaks of the pyridine rings, the magnitude of this shift depending upon the distances of the proton from the central macrocycle. The γ,γ' protons are shifted by 0.077 ppm, while the δ,δ' protons, being in the closest position to the central π-conjugated system, are shifted by 0.953 ppm.

This clearly indicates that the deshielding effect of the macrocycle on the δ,δ' protons overcome the influence of the pyridine N-atom on the α,α' protons. As a consequence, an inversion of the position of α,α' and δ,δ' proton resonances is observed (see Table 3.8). These results partially parallel those obtained on the precursor dicyanodipyridinopyrazine, $[(CN)_2Py_2Pyz]$ and the corresponding macrocycle $[Py_8TPyzPzH_2]$.[1]

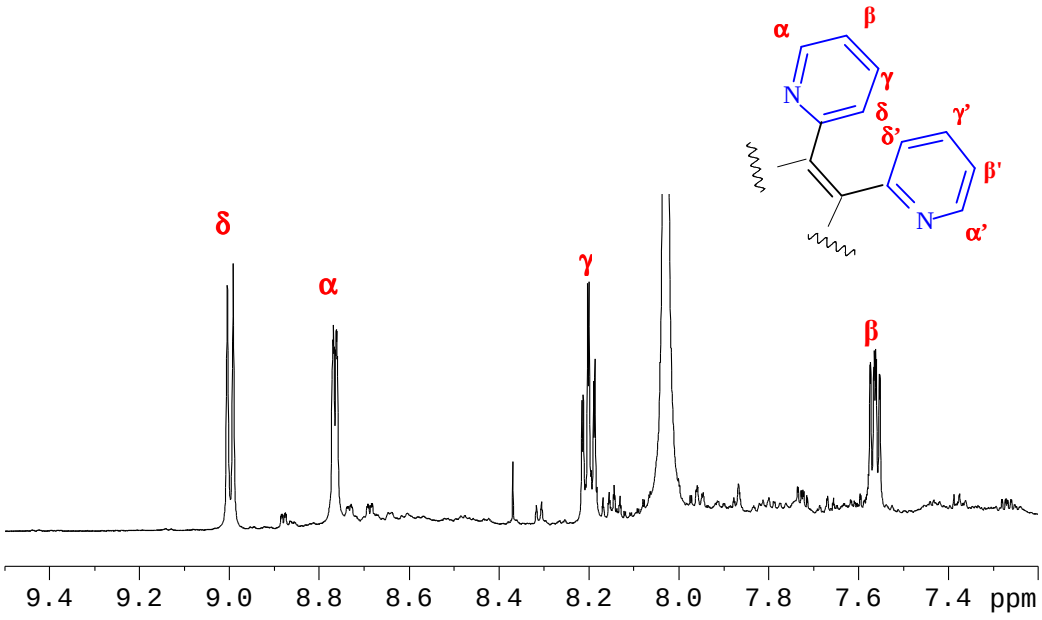

Figure 3.17. ^{1}H NMR spectrum of [$Py_8PzMg(H_2O)$] in DMF-d_7 at 300 K.

The IR spectra of the free-base macrocycle [Py_8PzH_2] and the Mg^{II} complex [$Py_8PzMg(H_2O)$] are reported in Figures 3.18 and 3.19, respectively (range 1800-260 cm^{-1}). The formation of the metal-free macrocycle from the Mg^{II} complex can be easily followed by the observed changes in the IR spectra in the process [$Py_8PzMg(H_2O)$] → [Py_8PzH_2]. The absorption found in the IR spectrum of [Py_8PzH_2] at 3310 cm^{-1} (Figure 3.18, inset) is assigned as ν(NH). This absorption disappears during the formation of the Zn^{II} complex in the reverse process [Py_8PzH_2] → [Py_8PzZn] as expected. The main differences between the spectrum of the free-base and that of magnesium complex in the range proposed in Figures 3.18 and 3.19 are located in the regions 1450-900 cm^{-1} and 800-700 cm^{-1}.

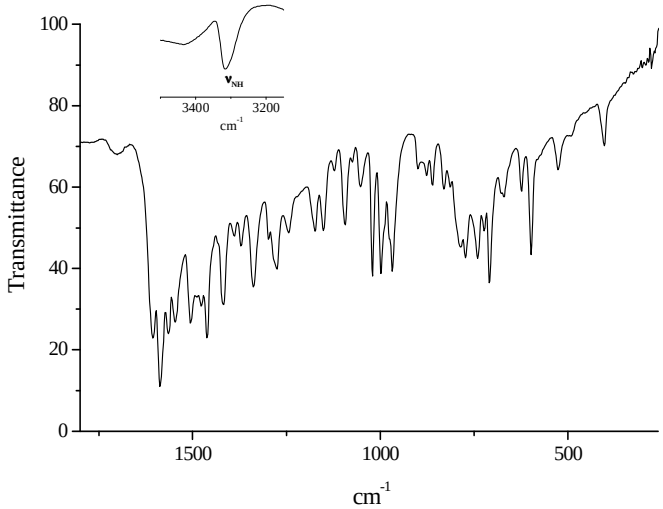

Figure 3.18. IR spectrum in KBr of [Py_8PzH_2].

The free-base [Py_8PzH_2], which displays a well resolved spectrum, shows absorptions at 1417, 1338, 1272, 1174 and 968 cm^{-1} and a peak at 707 cm^{-1} which are not present in the spectrum of the Mg^{II} complex.

The spectrum of this latter appears in general less rich of absorptions and less well defined. A doublet located at 1149 and 1095 cm^{-1} appears characteristic of the monometallic complexes, since it disappears going to the pentanuclear complexes formed by external coordination of four $PtCl_2$ units (see below).

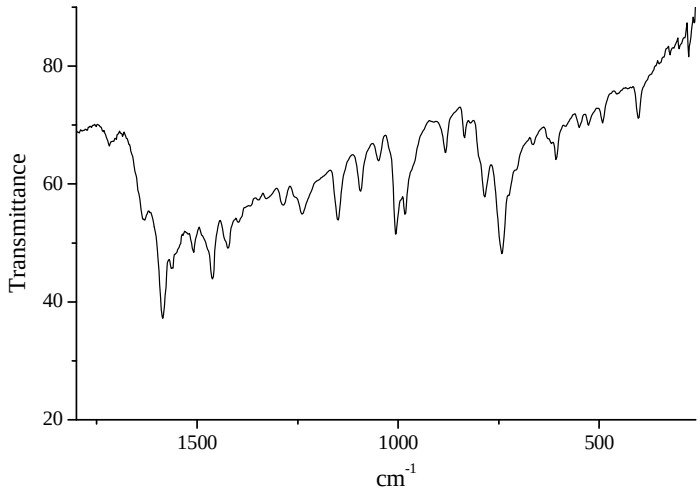

Figure 3.19. IR spectrum in KBr of [$Py_8PzMg(H_2O)$].

B.3 UV-Visible Spectral Behaviour of "Quinoxalinoporphyrazines" and "Pyridylporphyrazines"

B.3.a "Quinoxalinoporphyrazines", [$Py_8TQuinPzM$] (M = $2H^1$, $Mg^{II}(H_2O)$, Zn^{II}, Co^{II})

The examined "quinoxalinoporphyrazines" [$Py_8TQuinPzM$] are completely insoluble in water and exhibit very low solubility in nonaqueous nonpolar solvents ($CHCl_3$, CH_2Cl_2). This novel class of macrocycles, due to their more extended macrocyclic framework with respect to that present in the widely studied octapyridinated "pyrazinoporphyrazines",[1,21] are generally less soluble than these latter species. Concentrations ca. 10^{-5} M and in rare cases 10^{-4} M are possible for the "quinoxalinoporphyrazines" as metal derivatives in the low-donor solvents pyridine, DMSO and DMF. This allowed quantitative UV-visible spectra to

be accurately measured for the compounds [Py_8TQuinPzM] with the spectra showing in most cases, immediately or after a short time, the design typical of monomeric species. Data are summarized in Table 3.9. Reasons will be given specifically for those compounds and solutions for which only qualitative spectra could be taken.

The UV-visible spectra of the Mg^{II} complex [Py_8TQuinPz$Mg^{II}(H_2O)$] in pyridine, DMSO and DMF at concentration close to saturation (ca. 10^{-4} M) indicate the presence of highly aggregated macrocycles. At more diluted solutions ($c \leq 10^{-5}$ M) stable spectra are obtained with features expected for the monomeric species characterized by HOMO-LUMO π - π^* transitions, as indicated by an unsplit narrow Q band in the 700-800 nm region, accompanied by an absorption envelope in the Soret region (300-420 nm). These spectral features recall those normally observed for phthalocyanine and porphyrazine macrocycles.[62] A similar spectrum for the Mg^{II} complex is obtained in $CHCl_3$. The spectrum is stable for a few hours, but for longer times tends to change (lowering of the Q band and appearance of a shoulder around 800 nm), due to the probable formation of aggregates.

The Zn^{II} complex [Py_8TQuinPzZn] shows in general more tendency to molecular aggregation as compared to its Mg^{II} analogue. The spectrum in pyridine and DMF solution is only little disturbed by aggregation and stable with the time (24 h). It shows a Q band of comparable intensity with respect to the Soret band (see quantitative data in Table 3.9). In DMSO solution the Zn^{II} complex manifests strong aggregation also at $c \cong 10^{-5}$ M (or lower). Persistence of aggregation is seen also after heating the solution at 120 °C for 1 h, so that only qualitative UV-visible spectral data could be evaluated. The spectrum of the Zn^{II} complex in $CHCl_3$ indicates complete absence of aggregation. Interestingly, it shows a split Q band with peaks at 775 and 796 nm (Figure 3.20; quantitative data in Table 3.9).

Table 3.9. UV-visible Spectral Data (λ, nm (log ε)) of the Tetrakis[2,3-di(2-pyridyl)quinoxalino]porphyrazines, [$Py_8TQuinPzM$] (M = $2H^1$, $Mg^{II}(H_2O)$, Zn^{II}, Co^{II}).

Compound	Solvent	Soret region			Q-band region		
		λ, nm (logε)					
[$Py_8TQuinPzMg(H_2O)$]	Py	378(5.09)	534(4.10)	684 (4.47)	702 (4.56)	726(4.63)	765(5.21)
	DMSO	371(5.03)	533(4.05)	676sh (4.40)		707sh (4.61)	756(4.96)
	DMF	373(4.99)	535 (3.99)	677sh (4.32)	698 (4.45)	721(4.49)	759(5.07)
	$CHCl_3$	374(5.00)	535(3.94)	684 (4.22)	701 (4.21)	727(4.33)	766(5.11)
[$Py_8TQuinPzZn$]	Py	376(5.25)	528 (4.11)		702sh(4.98)	725sh(4.96)	763(5.29)
	DMSO	369	526		704sh	728	756
	DMF	373(4.93)	535(4.09)		699(4.61)	719(4.63)	757(4.94)
	$CHCl_3$	381(4.96)	546(4.23)		697sh(4.48)	774(4.93)	796(5.02)
	$CHCl_3$ [a]	379	540	683	696	724	762
[$Py_8TQuinPzCo$]	Py	360	483	536sh	674sh	712sh	746
	DMSO	355	460sh		683sh	707sh	743
	DMF [b]	365	519sh	668sh	684	708	746
[$Py_8TQuinPzH_2$]	$CHCl_3$	353(4.99)	509 (3.58)	686 (4.41)	702 (4.44)	729(4.55)	767(5.22)

[a] After addition of one drop of pyridine. [b] After addition of HCl.

This is similar to what was observed also for the Zn^{II} complex of the corresponding pyrazinoporphyrazine [$Py_8TPyzPzZn$].[21]Addition of one drop of pyridine to the solution determines the appearance of a narrow clean single Q band with maximum at 762 nm (Figure 3.20). It is likely that traces of HCl present in the $CHCl_3$ determine protonation of the meso N atoms with consequent some lowering of the symmetry of the macrocycle as has been seen in a work on the simple porphyrazine macrocycle.[63]

Unlike the Mg^{II} and Zn^{II} complexes, the Co^{II} complex [$Py_8TQuinPzCo$] shows heavy aggregation in DMSO. Nevertheless, a fairly good qualitative spectrum in this solvent can be obtained after long centrifugation and heating at 70 °C for 30 minutes. Aggregation is also disturbing in pyridine. Because of this, the spectrum in pyridine could not be quantitatively estimated for its monomeric form, despite the detection of its pertinent peaks.

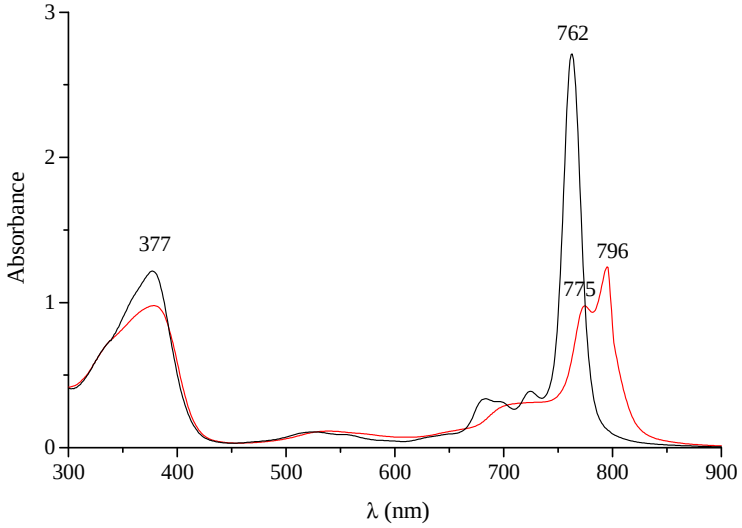

Figure 3.20. UV-visible spectra of [Py_8TQuinPzZn]: in $CHCl_3$ (red line) and in $CHCl_3$ after addition of one drop of pyridine (black line).

The spectrum of [Py_8TQuinPzCo] in DMF shows high aggregation (spectrum (a) in Figure 3.21). In addition the complex in DMF undergoes a spontaneous metal-centered one-electron reduction to its corresponding -1 species [$Py_8TQuinPzCo^{I}]^{1-}$. The reduction process, caused by the presence in DMF of a reducing agent (dimethylamine?), is similar to that observed (in the absence of aggregation) for the related Co^{II} pyrazinoporphyrazine complex [Py_8TPyzPzCo], for which one-electron reduction determines as the main spectral changes the total disappearance of the Q band with concomitant appearance of a peak in the region 540-560 nm, not detected for [$Py_8TQuinPzCo^{I}]^{1-}$, due to aggregation. Nevertheless, reoxidation of the Co^{I} monoanion [$Py_8TQuinPzCo^{I}]^{1-}$ to the neutral Co^{II} species [Py_8TQuinPzCo] in its clean monomeric form can be obtained upon addition to the solution of progressive amounts of HCl (see spectral evolution in Figure 3.21).

Persistent aggregation dominates the UV-visible spectral behaviour of the free-base [$Py_8TQuinPzH_2$] in pyridine, DMSO and DMF, no matter which the concentration of the compound. The UV-visible spectrum of [$Py_8TQuinPzH_2$] in DMSO and DMF presents broad featureless absorptions of low intensity throughout the explored region. Aggregation persists for this compound in DMSO or DMF even heating the solutions up to almost 100 °C or in the presence of HCl, addition of which was found resolutive in the case of other porphyrazine macrocycles for the disaggregation process and formation of the monomeric species. Interestingly, [$Py_8TQuinPzH_2$] is present in $CHCl_3$ solution in its practically pure monomeric form (Figure 3.22) with a Soret band having maximum at 353 nm and a more

intense sharp Q band at 767 nm (data in Table 3.9). This aspect will be discussed in more detail below in connection with the findings for the "pyridylporphyrazine" analogue [Py_8PzH_2] (data in Table 3.10) and the parallel pyrazinoporphyrazine macrocycle [$Py_8TPyzPzH_2$] (data in Table 3.11).

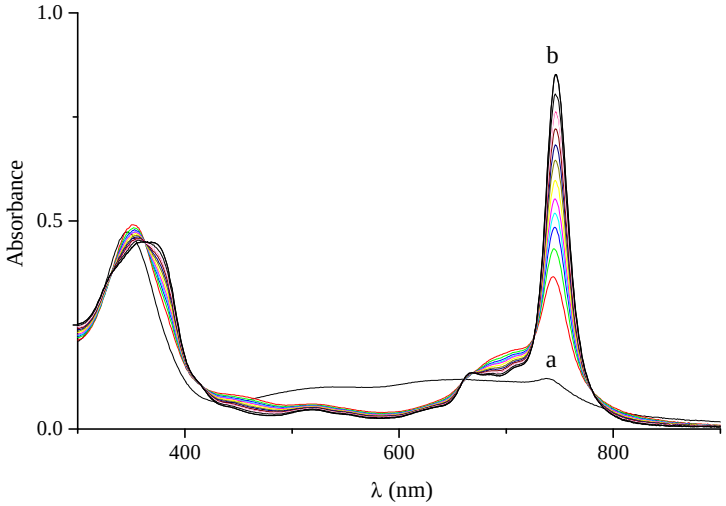

Figure 3.21. UV-visible spectra of [$Py_8TQuinPzCo$] in DMF: (a) spectrum of [$Py_8TQuinPzCo$] immediately after dissolution; (b) final spectrum upon addition of slight excess of HCl.

From the spectral data in Table 3.9, it can be seen that the Q-band peaks show a general scarce dependence from the type of solvent. The UV-visible spectra of the Mg^{II} and Zn^{II} complexes are quite similar to each other in terms of number of absorptions and their wavelength maxima. The Soret and Q bands of the two complexes vary over narrow ranges (371-381 and 756-766 nm, respectively). The spectra of the Co^{II} complex, [$Py_8TQuinPzCo$], in pyridine, DMSO or DMF are distinct from those of the other metal derivatives in that they exhibit peaks of the Soret and Q bands which are shifted to lower wavelengths by an average of 16 and 13-20 nm, respectively. These findings are in keeping with those observed for the corresponding pyrazinoporphyrazine Co^{II} complex, [$Py_8TPyzPzCo$] (see Table 3.11).[21,31b,22]

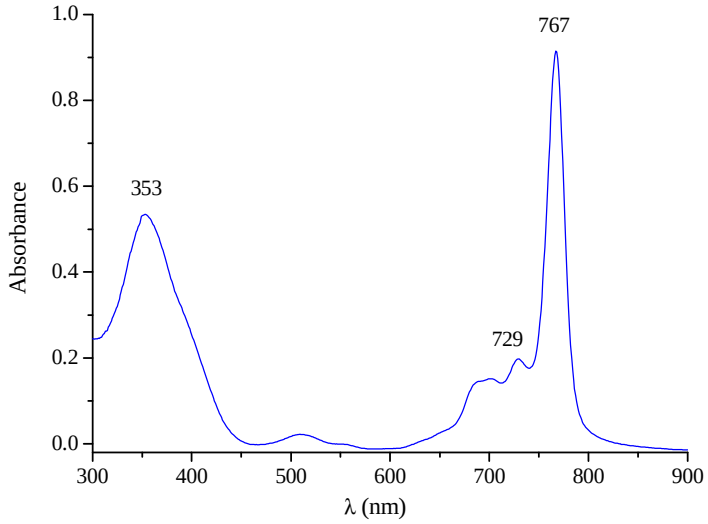

Figure 3.22. UV-visible spectrum of [$Py_8TQuinPzH_2$] in $CHCl_3$.

B.3.b "Pyridylporphyrazines", [Py_8PzM] (M = $2H^1$, $Mg^{II}(H_2O)$, Zn^{II})

The examined pyridylporphyrazine macrocycles of formula [Py_8PzM] (M = $2H^1$, $Mg^{II}(H_2O)$, Zn^{II}) exhibit better solubility (saturation limit in DMF for [$Py_8PzMg(H_2O)$] ca. 10^{-3} M) than the parallel series of quinoxalino- and pyrazinoporphyrazine macrocycles in the nonaqueous non-donor solvents ($CHCl_3$, CH_2Cl_2) and in the polar low-donor solvents pyridine, DMSO and DMF. In all these solvents the compounds [Py_8PzM] show spectra with Soret and Q bands in line with those found for quinoxalinoporhyrazines and pyrazinoporphyrazines, and porphyrazines in general, evidencing the monomeric form immediately after dissolution of the compounds or after short times. The available UV-visible spectral data for the all three compounds [$Py_8PzMg(H_2O)$], [Py_8PzZn] and [Py_8PzH_2] are summarized in Table 3.10.

The observed stable UV-visible spectra of the Mg^{II} complex [$Py_8PzMg(H_2O)$] in the solvents explored, ie. pyridine, DMSO, DMF and $CHCl_3$ normally indicate the formation of the exclusive monomeric form. The spectrum in $CHCl_3$ solution shown in Figure 3.23 presents an absorption of very low intensity, not vanishing with time, probably indicative of the presence of subtle traces of an aggregated species. As can be seen in Table 3.10, the quantitative UV-visible spectral data show little changes of the Soret and Q-band maxima for the different solvents. The monomeric form is retained also at the highest possible concentrations (ca. 10^{-3} M in DMF).

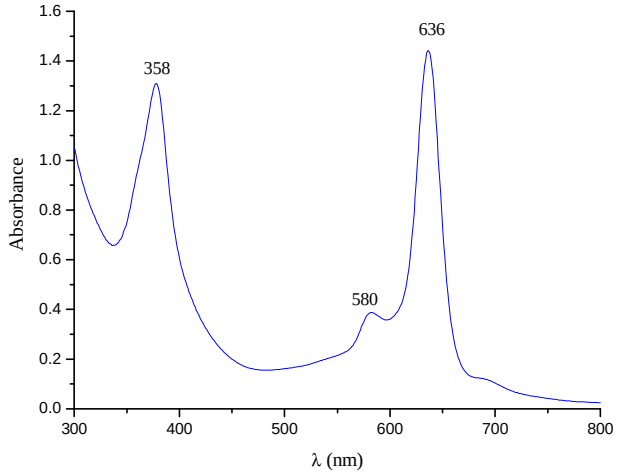

Figure 3.23. UV-visible spectrum of [$Py_8PzMg(H_2O)$] in $CHCl_3$.

Table 3.10. UV-visible Spectral Data (λ, nm (log ε)) of the Tetrakis[2,3-di(2-pyridyl)]porphyrazines of Formula [Py_8PzM] (M = $2H^1$, $Mg^{II}(H_2O)$, Zn^{II}) in Different Solvents.

Compound	Solvent	Soret region			Q-band region
		λ, nm (logε)			
[$Py_8PzMg(H_2O)$]	Py	380(4.66)	581sh(4.19)		638(4.66)
	DMSO	378(4.50)	579sh(4.04)		635(4.49)
	DMF	376(4.61)	578sh(4.17)		636(4.68)
	$CHCl_3$	377(4.49)	582sh(4.04)		637(4.47)
[Py_8PzZn]	Py	379	581		638
	DMSO	376	581		635
	DMF	378	580		635
[Py_8PzH_2]	Py	372(4.58)	554sh(4.10)	598(4.43)	664(4.58)
	DMSO	367		599	660
	DMF	367(4.72)	555sh(4.26)	595(4.53)	660(4.68)
	$CHCl_3$	368(4.59)	526(4.16)	595(4.40)	663(4.48)

As already detailed in the Experimental Section, the Zn^{II} complex can be contaminated by small amounts of its precursor and further purification is still needed. This is why in Table 3.10 only qualitative spectral data are reported. Comparison of the data in Table 3.10 for the Mg^{II} and Zn^{II} complexes shows that the two species have quite similar spectra in terms of Soret and Q-band positions in the regions 376-380 and 635-638 nm, respectively.

The free-base [Py_8PzH_2] exhibits stable spectra in solution of DMSO, DMF and $CHCl_3$ (24 h for DMSO and DMF, few hours for $CHCl_3$). The free-base behaves differently in pyridine. Figure 3.24 shows the spectral changes observed for the macrocycle in this solvent as a function of time (24 h). Most likely, the first spectrum is a mixture of the monomeric and dimeric form. This is strongly suggested by the formation, during spectral evolution, of isosbestic points at 403, 584, 614, 650 and 678 nm. The final spectrum, attributable to the macrocycle in its monomeric form, practically coincides with those observed for all the other solvents (compare the final spectrum of Figure 3.24 with the spectrum of [Py_8PzH_2] in $CHCl_3$ in Figure 3.25). As can be seen, the spectrum of the free-base shows then in all the solvents two intense highly separated absorptions in the region of the Q band at 595-599 and 660-664 nm (Table 3.10). The two absorptions, due to the presence of the central NH groups and the pertinent D_{2h} symmetry of the central porphyrazine core, are assigned as the two components of the Q band, ie. Q_x and Q_y, due to the transitions $a_u \rightarrow b_{2g}$ and $a_u \rightarrow b_{3g}$, respectively; the absorption in the Soret region at 367-372 nm is assigned as the B band.

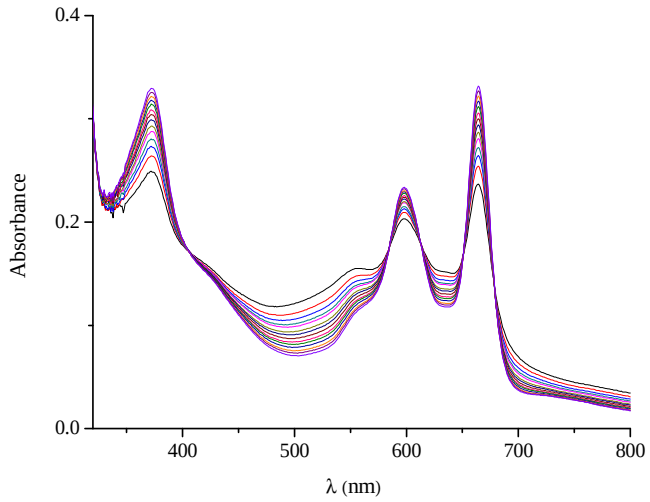

Figure 3.24. UV-visible spectral changes of [Py_8PzH_2] in pyridine solution as a function of the time.

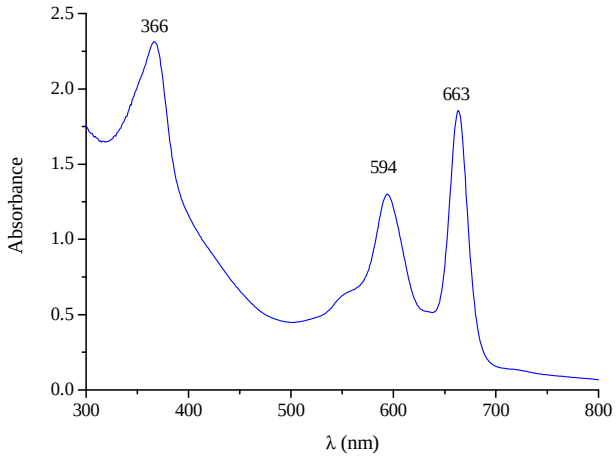

Figure 3.25. UV-visible spectrum of $[Py_8PzH_2]$ in $CHCl_3$.

As it has been noticed above, the spectrum of the quinoxalinoporphyrazine macrocycle $[Py_8TQuinPzH_2]$ shows an unsplit Q band at 767 nm in $CHCl_3$. Furthermore, the pyrazinoporphyrazine corresponding free-base $[Py_8TPyzPzH_2]$ shows in $CHCl_3$ solution a split Q band with peaks at 635 and 668 nm. Thus, in the sequence $[Py_8PzH_2] \rightarrow [Py_8TPyzPzH_2] \rightarrow [Py_8TQuinPzH_2]$, which sees a progressive increase of the extension of the central π-conjugated porphyrazine framework, the related difference in nanometers between the Q-band components decreases from 61-68 nm for $[Py_8PzH_2]$ to 33 nm for $[Py_8TPyzPzH_2]$, finishing with 0 nm for the quinoxaline macrocycle $[Py_8TQuinPzH_2]$. These findings seem to suggest that the splitting of the b_{2g} and b_{3g} HOMO energy levels decreases with the increase of the complexity of the π-delocalized system of the different macrocycles. In other words, the effect of the lowering of the symmetry $D_{4h} \rightarrow D_{2h}$ due to the asymmetry of the central porphyrazine core[1] vanishes with the expansion of the macrocycle.

The presence of a split Q band for $[Py_8PzH_2]$ suggests a higher relative stability of the neutral form with respect to that of its deprotonated form $[Py_8Pz]^{2-}$ in pyridine. Worth to notice, the corresponding pyrazinoporphyrazine free-base $[Py_8TPyzPzH_2]$, which shows a well seen split Q band (636/668 nm) in $CHCl_3$ and CH_2Cl_2 and in CH_3COOH (640/666 nm) indicative of the presence of the neutral species $[Py_8TPyzPzH_2]$ (D_{2h} symmetry), the same species exhibits a clean unsplit Q band (667 nm) in pyridine (see spectra in Figure 3 ref 1)

which addresses for the occurrence of the macrocycle in its dianionic form $[Py_8TPyzPz]^{2-}$ (D_{4h} symmetry) consequent to release of the central H atoms. Thus, the achieved information of the UV-visible spectral behaviour in pyridine solution of $[Py_8PzH_2]$ and $[Py_8TPyzPzH_2]$, seems to suggest that the former species, $[Py_8PzH_2]$, is less acidic than the latter, in which the presence of the external pyrazine rings, annulated to the central pyrrole rings, due to their electron-withdrawing properties, increase the electron-deficiency of the macrocycle, thus allowing release of the central protons. It is most unfortunate that the same level of information could not be obtained for the parallel quinoxalinoporphyrazine free-base for the very pooor response given under the all explored conditions in the same solvent.

One further aspect emerging from the consideration of the UV-visible spectral features of the "pyridylporphyrazines" and "quinoxalinoporphyrazines" (see Tables 3.9 and 3.10) is the different position of the entire barycentre of the explored region of the spectrum (300-800 nm) for these two new classes of macrocycles. Taking as reference the approximate average value (nm) of the Q-band position, it can be seen that in going from pyridylporphyrazines (635 nm) to the quinoxalinoporphyrazines (760 nm), the relative bathochromic shift for the latter species is 125 nm. This so relevant difference in the Q-band positions finds the series of "pyrazinoporphyrazines" (data in Table 3.11) placed just in between the two presented extremes, the average Q-band maximum being at 659 nm. These findings are well exemplified by the series of spectra shown in Figure 3.26 for the Mg^{II} complexes. It can be seen that the Q-band maxima positions incredibly well coincide with the average values reported above. This spectral behaviour finds strong support in the work directed to explain the influence on the energy level diagram for a series of macrocycles of the type shown in Figure 9 of ref. 64.[64] It is shown that with increasing the expansion of the delocalized π-conjugated framework the difference in energy of the HOMO-LUMO π - π^* orbitals progressively decreases.

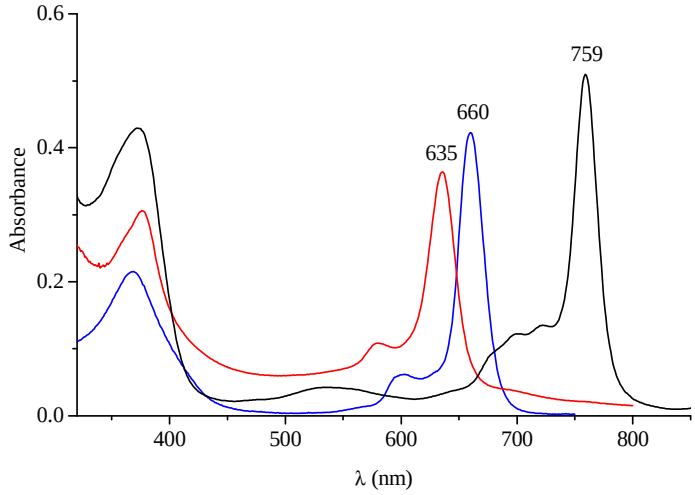

Figure 3.26. UV-visible spectra in DMF of [$Py_8PzMg(H_2O)$](red), [$Py_8TPyzPzMg(H_2O)$](blue), and [$Py_8TQuinPzMg(H_2O)$](black).

Table 3.11. UV-visible Spectral Data (λ, nm (log ε)) of Tetrakis-2,3-[5,6-di(2-pyridyl)pyrazino]porphyrazines of Formula [$Py_8TPyzPzM$] (M= $2H^1$, $Mg^{II}(H_2O)$, Zn^{II}, Co^{II}) in Different Solvents.

Compound	Solvent	Soret region		Q-band region				
		λ, nm (logε)						
[$Py_8TPyzPzH_2$]	$CHCl_3$	356(5.05)	400sh	582(4.40)	609(4.57)	618(4.61)	635(5.10)	668(5.21)
[$Py_8TPyzPz$]$^{2-}$	Py	362(4.83)	402sh		605(4.39)		643sh	667(5.06)
	DMSO	362	402sh		607		635sh	664
	DMF	360	402sh		606		632sh	662
[$Py_8TPyzPzMg(H_2O)$]	Py	375(5.23)		596(4.65)			631sh(4.64)	658(5.54)
	DMSO	374(5.08)		566sh(3.96)	594(4.36)		629sh(4.55)	653(5.34)
	DMF	370(4.94)		579(4.39)			628sh(4.43)	658(5.20)
[$Py_8TPyzPzZn$]	Py	378(4.90)		598(4.31)			630sh(435)	658(5.18)
	DMSO	372(5.10)		565 (4.54)	592(4.54)		629sh(4.61)	655(5.36)
	DMF	375(4.90)		600(4.38)			626sh(4.84)	657(5.15)
[$Py_8TPyzPzCo$]	Py	364(5.01)	441(4.40)	575sh			635(4.94)	
	DMSO	355(5.23)	450sh(4.65)		586sh(4.71)		634 (5.24)	
	DMF[a]	353	442	579			634	

[a] DMF added of HCl; spectrum perturbed by aggregation

Part C. Pentanuclear "Quinoxalinoporphyrazines" and "Pyridylporphyrazines" of Respective Formulae $[(M'Cl_2)_4Py_8TQuinPzM]$ (M = $Mg^{II}(H_2O)$, Zn^{II}, Pd^{II}, Pt^{II}; M' = Pd^{II}, Pt^{II}) and $[(PtCl_2)_4Py_8PzM]$ (M = $Mg^{II}(H_2O)$, Zn^{II})

The above reported mononuclear quinoxalinoporphyrazines and pyridylporphyrazines have offered the opportunity to explore the possible formation of pentanuclear species by exocyclic coordination of $PdCl_2$ and $PtCl_2$ units. The results of this research item are reported here below.

C.1 General Properties of $[(M'Cl_2)_4Py_8TQuinPzM]$ (M = $Mg^{II}(H_2O)$, Zn^{II}, Pd^{II}, Pt^{II}; M' = Pd^{II}, Pt^{II})

The heteropentametallic species $[(PdCl_2)_4Py_8TQuinPzM]$ (M = $Mg^{II}(H_2O)$, Zn^{II}) (Scheme 3.4A) having four externally coordinated $PdCl_2$ units have been prepared by reaction of the respective monometallic complex with $PdCl_2$ (molar ratio $PdCl_2$/macrocycle > 5:1) in DMSO at 120 °C for 7-8 h, as specified in the Experimental Section. Larger molar ratios (ca. 8:1) were used for the preparation of the homopentametallic Pd^{II} complex of formula $[(PdCl_2)_4Py_8TQuinPzPd]$ for which the starting material was the free-base ligand. These reaction conditions led systematically and reproducibly to the formation of a single porphyrazine product, as confirmed by elemental analyses for C, H, N and Pd.

All the compounds were obtained as hydrated dark-blue powders, stable to the air. As specified above for the parent "quinoxalinoporphyrazine" macrocycles, retention of clathrated water molecules by the solid material is a known feature for these and related porphyrazine systems. This water is normally eliminated by heating under vacuum at mild temperatures, but it is again at least partly recovered by exposure of the porphyrazine compounds to the air, as verified also for the present species. The number of retained water molecules can be different from batch to batch for each compound, and hence clathrated water is not shown in the formulation of the compounds $[(PdCl_2)_4Py_8TQuinPzM]$.

Analogous but more drastic reaction conditions (longer reaction times) were used for the synthesis of the homo- and heteropentanuclear platinated complexes of formula $[(PtCl_2)_4Py_8TQuinPzM]$ (M = $Mg^{II}(H_2O)$, Zn^{II}, Pt^{II}) (Scheme 3.4B), which were prepared in the same solvent (DMSO) by reaction of the mononuclear derivatives for Mg^{II} and Zn^{II}, and of the free-base ligand for the pentaplatinated species, with $PtCl_2$ (molar ratio $PtCl_2$/macrocycle 6-7:1). The purity of the compounds, which are dark-blue, air stable solids, has been systematically checked by elemental analysis for C, H, N, Pt. Also for these species all of the reported compounds carry clatharated water molecules of variable amount.

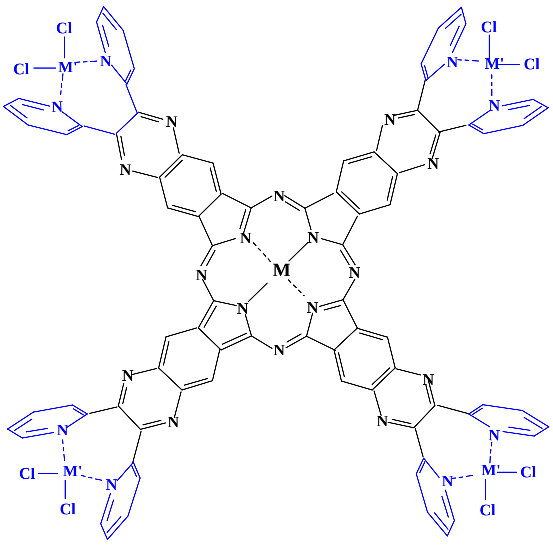

Scheme 3.4. A) M = $Mg^{II}(H_2O)$, Zn^{II}, Pd^{II}; M' = Pd^{II}
B) M = $Mg^{II}(H_2O)$, Zn^{II}, Pt^{II}; M' = Pt^{II}

A noteworthy feature in the IR spectrum of the palladated and platinated complexes is the presence of the stretching of the Pd-Cl and /or Pt-Cl respectively as a moderately intense absorption at 335-337 cm^{-1}. On going from the mononuclear to the pentametallic complexes the disappearance of absorptions at 1585, 999 and 710 cm^{-1} is also observed. Actually these absorptions were of some utility in discriminating the monometallic complex from the pentametallic species during the synthetic procedures. The IR spectrum in KBr of $[(PtCl_2)_4Py_8TQuinPzMg(H_2O)]$ is reported in Figure 3.27 as an example.

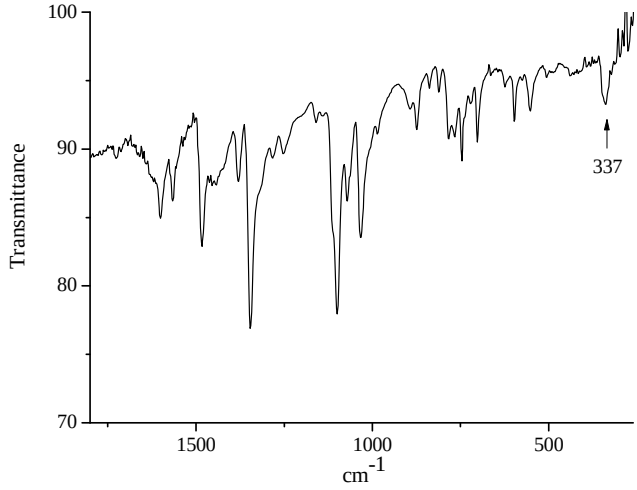

Figure 3.27. IR spectrum in KBr of $[(PtCl_2)_4Py_8TQuinPzMg(H_2O)]$.

All the pentanuclear palladated and platinated species are completely insoluble in water and generally show very poor solubility (lower than that of the parent mononuclear compounds, especially for the platinated species) in nonaqueous nondonor ($CHCl_3$) or low-donor (pyridine, DMSO, DMF) solvents, giving generally strong aggregation also at low concentrations (10^{-7} M). This is the reason why it was not possible to perform NMR measurements, nor to prepare single crystals suitable for an X-ray investigation useful to achieve information on the molecular structure of the compounds. Insights into the structural features of the palladated complexes were made possible from the ^1H NMR spectra and the X-ray data of the related earlier discussed palladated precursor $[(CN)_2Py_2QuinPdCl_2]$ which unequivocally indicate a "py-py" coordination mode of the dipyridinoquinoxaline fragment for Pd^{II}. Further support is also given by the data reported in the literature on the analogous palladated pyrazinoporphyrazine species $[(PdCl_2)_4Py_8TPyzPzM]$ (M = $Mg^{II}(H_2O)$, Cu^{II}, Zn^{II}, Cd^{II}, Pd^{II}).[24,26a] It can therefore be confidently concluded that the "py-py" coordination most likely occurs in the present pentanuclear quinoxalinoporphyrazine complexes $[(M'Cl_2)_4Py_8TQuinPzM]$ (M = $Mg^{II}(H_2O)$, Zn^{II}, Pd^{II}, Pt^{II}; M' = Pd^{II}, Pt^{II}) with the four square-planar $N_{2(pyr)}M'Cl_2$ moieties displaced out of plane and directed nearly perpendicular to the plane of the quinoxalinoporphyrazine ring. Also we can assume, in analogy with the case of the just mentioned pyrazinoporphyrazine complexes, that the largely prevalent isomer formed is the 4:0 isomer (C_{4v} symmetry) which carries the exocyclic dipyridino-$PdCl_2$ fragments on the same side of the macrocyclic porphyrazine framework (Figure 1.19). It should be noted that

for the series of externally platinated species $[(PtCl_2)_4Py_8TQuinPzM]$ NMR or X-ray data, not yet available, on the relative platinated precursor $[(CN)_2Py_2QuinPtCl_2]$, might provide further support to the structural features of the related pentanuclear macrocycles.

C.2 General Properties of $[(PtCl_2)_4Py_8PzM]$ (M = $Mg^{II}(H_2O)$, Zn^{II})

The $[(PtCl_2)_4Py_8PzM]$ complexes (M = $Mg^{II}(H_2O)$, Zn^{II}) (Scheme 3.5), were obtained by platination of the corresponding mononuclear $[Py_8PzM]$ derivatives by reaction with $PtCl_2$ (molar ratio $PtCl_2$/macrocycle ca. 5:1) in DMSO at 110 °C for 7 h, as detailed in the Experimental Section. These reaction conditions led systematically and reproducibly to the formation of a single porphyrazine product, as confirmed by elemental analyses for C, H, N and Pt, but the yields were very low especially for the Zn^{II} complex, and further studies are needed to improve reproducibility and yield of the reaction. Both the compounds were obtained as hydrated green-blue powders, stable to the air. The number of retained water molecules can be different from batch to batch for each compound. Interestingly, for the synthetic procedure reported in the Experimental Section the Mg^{II} is formulated just as monoaquo derivative with one water molecule directly bound to the metal center, and no clathrated water molecules were found present.

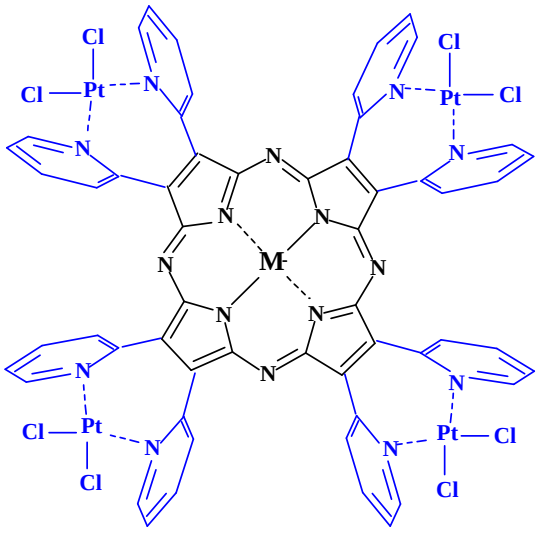

Scheme 3.5. $[(PtCl_2)_4Py_8PzM]$ (M = $Mg^{II}(H_2O)$, Zn^{II}).

A noteworthy feature in the IR spectrum of the tetraplatinated Mg^{II} and Zn^{II} complexes is the presence of the stretching of the Pt-Cl bond as a moderately intense absorption at 337 cm^{-1}. The IR spectrum of $[(PtCl_2)_4Py_8PzMg(H_2O)]$ in the range 1800-300 cm^{-1} is shown in Figure 3.28. The external platination leads to changes in the spectrum of the monometallic species with disappearance of absorptions at 1585, 1463, 1149, 1095, 821 and 742 cm^{-1} whereas new absorptions appear at 1560, 1471, 860 and 711 cm^{-1}. The absorptions at 983, 777 and 602 cm^{-1}, present in the spectrum of the starting Mg^{II} complex, show much higher intensities in the spectrum of the tetraplatinated species.

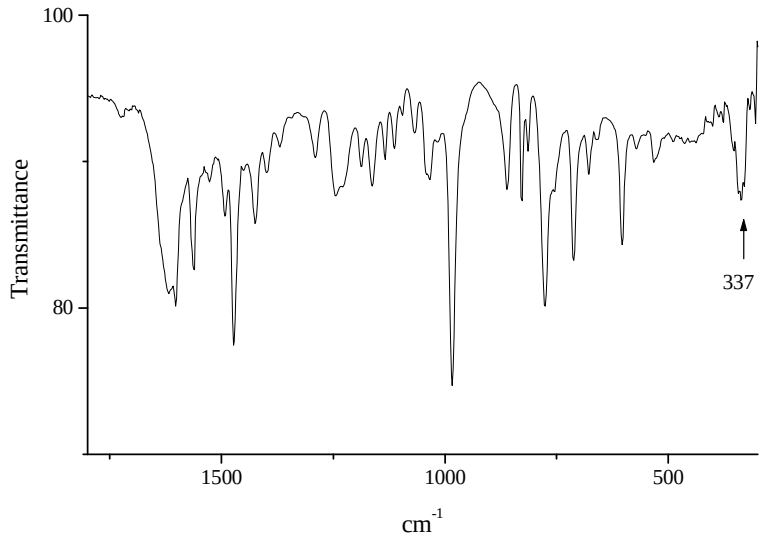

Figure 3.28. IR spectrum in KBr of $[(PtCl_2)_4Py_8PzMg(H_2O)]$.

As already pointed out for the two metal derivatives of the related precursor of formula $[(CN)_2Py_2EtMCl_2]$ (M = Pd^{II}, Pt^{II}), the ligation of the MCl_2 units to the porphyrazine macrocycle obviously takes place at the N atoms of the pyridine rings ("py-py" coordination) as strongly suggested by the above mentioned NMR spectral data for the compound $[(CN)_2Py_2EtPdCl_2]$. Again, the proposed overall structure of the pentanuclear species sees the four square-planar $N_{2(pyr)}MCl_2$ coordination sites all directed nearly perpendicularly to the plane of the porphyrazine core and oriented on the same side of macrocyclic framework (Figure 1.19). An unequivocal assignment of this structure waits for the ^{1}H and ^{13}C NMR spectral measurements, which should be facilitated by the higher solubility of these pyridylporphyrazines with respect to the pyridinated quinoxalino-analogues.

C.3 UV-Visible Spectral Behaviour of the Pentanuclear Compounds $[(M'Cl_2)_4Py_8TQuinPzM]$ (M = $Mg^{II}(H_2O)$, Zn^{II}, Pd^{II}, Pt^{II}; M' = Pd^{II}, Pt^{II}) and $[(PtCl_2)_4Py_8PzM]$ (M = $Mg^{II}(H_2O)$, Zn^{II})

The title pentanuclear quinoxalinoporphyrazines $[(M'Cl_2)_4Py_8TQuinPzM]$ (M = $Mg^{II}(H_2O)$, Zn^{II}, Pd^{II}, Pt^{II}; M' = Pd^{II}, Pt^{II}) exhibit even lower solubility than the corresponding mononuclear species. In addition they appear as highly aggregated species in solution of pyridine, DMSO, and DMF. Blue-green solutions are obtained in these solvents and their UV-visible spectral behaviour could be only qualitatively studied. It was verified that no spectral data could be taken in pyridine or DMSO solution for the pentanuclear complexes with central Mg^{II} and Zn^{II}, ie. $[(PdCl_2)_4Py_8TQuinPzMg(H_2O)]$ and $[(PdCl_2)_4Py_8TQuinPzZn]$, because both complexes, immediately after dissolution, release the external $PdCl_2$ units with formation of the respective mononuclear complexes. It is worth of notice that, analogous depalladation was observed in pyridine solution for the externally palladated pyrazinoporphyrazine macrocycles $[(PdCl_2)_4Py_8PyzPzM]$, but not in DMSO.[24,26a] The externally tetraplatinated Mg^{II} and Zn^{II} complexes, $[(PtCl_2)_4Py_8TQuinPzMg(H_2O)]$ and $[(PtCl_2)_4Py_8TQuinPzZn]$, exhibit stable solution spectra in that they do not manifest the tendency to loose the external $PtCl_2$ units. However, heavy aggregation, especially in the case of the Zn^{II} complex, is present in solution of all the solvents examined, including DMF (blue-violet solutions), and disaggregation is not obtained by heating the solutions at 70-80 °C or upon dilution (c = ca. 10^{-7} M). Slightly more stable solutions are obtained in DMF, where dissociation of $PdCl_2$ is observed after ca. 1 h. No different behaviour was seen for the homopentanuclear species $[(PdCl_2)_4Py_8TQuinPzPd]$ and $[(PtCl_2)_4Py_8TQuinPzPt]$. The qualitative spectral data collected for the species examined are given in Table 3.12.

Table 3.12. Qualitative UV-visible Spectral Data (λ, nm) for [(M'Cl_2)$_4$$Py_8$TQuinPzM] (M = $Mg^{II}(H_2O)$, Zn^{II}, Pd^{II}, Pt^{II}; M' = Pd^{II}, Pt^{II}) and [($PtCl_2$)$_4$$Py_8$PzM] (M = $Mg^{II}(H_2O)$, Zn^{II}) in Different Solvents.

Compound	Solvent	Soret region		Q-band region	
		λ, nm			
[($PdCl_2$)$_4$$Py_8$TQuinPzMg($H_2O$)]	DMF	385			777
[($PdCl_2$)$_4$$Py_8$TQuinPzZn]	DMF	362			777
[($PtCl_2$)$_4$$Py_8$TQuinPzMg($H_2O$)]	Py	392		733	788
	DMSO	393		721sh	776
	DMF	393		725sh	776
[($PtCl_2$)$_4$$Py_8$TQuinPzZn]	DMF	388			773
[($PtCl_2$)$_4$$Py_8$PzMg($H_2O$)]	Py	399	600sh	663	
	DMSO	394	607sh	660	
	DMF	395	596	651	
[($PtCl_2$)$_4$$Py_8$PzZn]	Py	399	600sh	648	

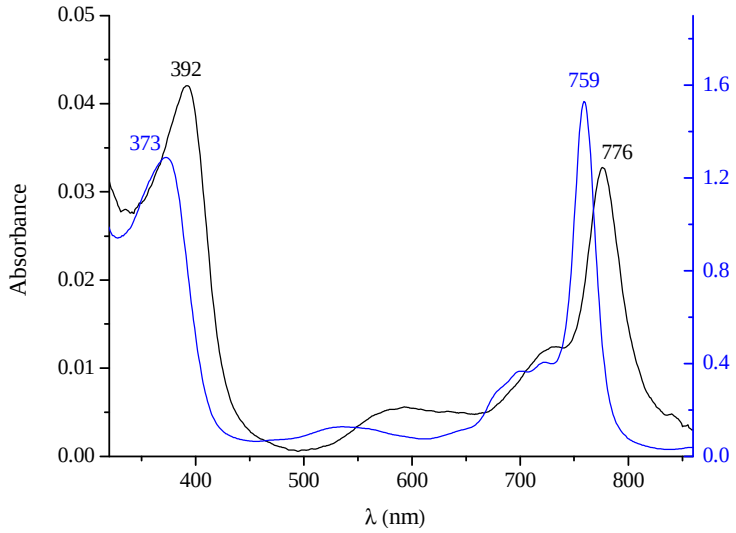

Figure 3.29. UV-visible spectra in DMF of [Py_8TQuinPzMg(H_2O)] (blue line), and [($PtCl_2$)$_4$$Py_8$TQuinPzMg($H_2O$)] (black line).

The spectra of all the pentanuclear species allow to identify the peaks attributable to the monomeric species, of which the Q band and the B band (Soret region), assigned to intraligand π-π* transitions, are found at 773-788 and 385-392 nm, respectively. It can be seen that, after external palladation or platination of the monometallic complexes at the dipyridinoquinoxaline fragments, the Q band of the resulting pentanuclear products is in each case shifted bathochromically of ca. 20 nm as compared to the position of the respective Q band of the corresponding mononuclear species [Py_8TQuinPzPM] with the same central metal ion (compare data in Table 3.9 and Table 3.12). In Figure 3.29 the UV-visible spectra in DMSO of the mono- and pentametallic Mg^{II} quinoxaline compounds are reported.

Table 3.13. UV-visible Spectral Data (λ, nm (log ε)) of [$(PdCl_2)_4Py_8$TPyzPzM] and [$(PtCl_2)_4Py_8$TPyzPzM] (M = $Mg^{II}(H_2O)$, Zn^{II}, Pd^{II}) in Different Solvents.

Compound	**Solvent**	**Soret region**		**Q-band region**		
		λ, nm (logε)				
[$(PdCl_2)_4Py_8$TPyzPzMg(H_2O)]	DMSO	342	368sh	597		656
	DMF	342		600		662
[$(PdCl_2)_4Py_8$TPyzPzZn]	DMSO	370(5.03)		598(4.47)		657(5.23)
	DMF	377(4.86)	420sh(4.57)		600(4.38)	662(5.26)
[$(PdCl_2)_4Py_8$TPyzPzPd]	DMSO	341(5.02)	370sh(4.69)	575(4.34)		636(5.03)
	DMF/HCl	343(5.00)		575(4.37)		635(5.11)
[$(PtCl_2)_4Py_8$TPyzPzMg(H_2O)]	Py	387(4.68)		608(4.22)	639sh(4.24)	671(4.96)
	DMSO	385(4.17)		600(4.22)	628sh(4.26)	659(5.00)
	DMF	383(4.69)		603(4.18)		664(4.96)
[$(PtCl_2)_4Py_8$TPyzPzZn]	Py	391(4.82)		607(4.36)		672(5.20)
	DMSO	382(4.91)		603(4.44)		667(5.30)
	DMF	382(4.91)		603(4.44)		667(5.30)
[$(PtCl_2)_4Py_8$TPyzPzPt]	Py	322(5.07)	368(5.08)	571(4.62)	631(5.36)	
	DMSO	323(4.99)	361(5.00)	568(4.48)	627(5.18)	
	DMF	321(5.05)	363(5.02)	566(4.51)	624(5.26)	

This trend is evidently the result of a lowering of the HOMO-LUMO gap upon going from [Py_8TQuinPzM] to [$(PdCl_2)_4Py_8$TQuinPzM] or to [$(PtCl_2)_4Py_8$TQuinPzM]; noteworthy these results parallel what is seen for the pyrazinoporphyrazine analogs [Py_8TPyPzM], for which the same bathochromic shift is observed upon external palladation[24,26a] or platination[39] (see data in Tables 3.11 and 3.13).

The UV-visible spectral behaviour of the [$(PtCl_2)_4Py_8$PzM] complexes (M = $Mg^{II}(H_2O)$, Zn^{II}), was studied in pyridine, DMSO and DMF. The Mg^{II} species [$(PtCl_2)_4Py_8$PzMg(H_2O)] shows in all solvents initial low aggregation which tends to increase with the time (24 h). The decreasing Q band is substituted by a new band on its red side and spectral changes evidence clean isosbestic points in pyridine and DMF (less well defined changes in DMSO) indicating an equilibrium between two species (monomer-dimer?). The initial spectra show the presence of a Q band at 651-663 nm (pyridine, DMSO) and a Soret band at 394-399 nm, the observed peaks due to intraligand π-π* transitions. The Q band is at 648 nm for the Zn^{II} companion species. The peaks of the monomeric species for both the Mg^{II} and Zn^{II} compounds could be easily identified and they are listed at the bottom of Table 3.12. After external platination of the monometallic complexes at the dipyridino-double bond C = C fragments, the Q band of the new formed pentanuclear species are shifted bathochromically by ca. 15-25 nm as compared to the [Py_8PzMg(H_2O)] complex in the same solvents (see data in Table 3.10 and Table 3.12). The initial spectra in DMF of [$(PtCl_2)_4Py_8$PzMg(H_2O)] and the related monometallic species [Py_8PzMg(H_2O)] are shown in Figure 3.30.

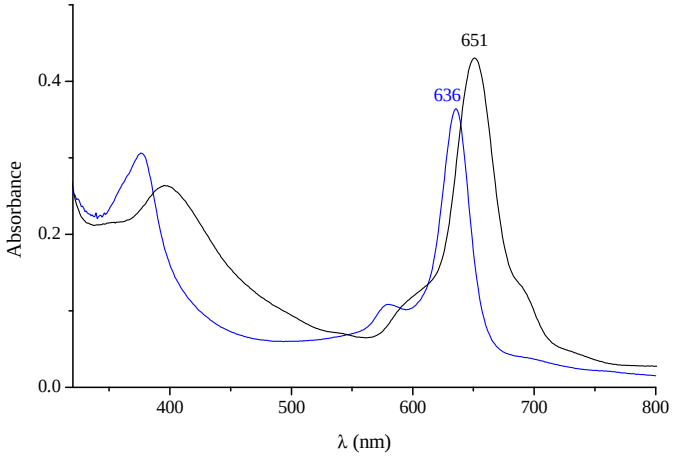

Figure 3.30. UV-visible spectra in DMF of [$(PtCl_2)_4Py_8$PzMg(H_2O)] (black line) and [Py_8PzMg(H_2O)] (blue line).

As observed for the "quinoxalinoporphyrazines" this tendency is evidently the result of a lowering of the HOMO-LUMO gap upon going from [Py_8PzM] to [$(PtCl_2)_4Py_8PzPM$]; noteworthy these results parallel what is seen for the pyrazinoporphyrazine analogs [$Py_8TPyPzM$] (see Tables 3.11 and 3.13).

Only preliminary studies have been conducted on the Zn^{II} complex [$(PtCl_2)_4Py_8PzZn$], whose behaviour needs further investigation. The initial spectrum in pyridine is a typical spectrum of a monomeric species with a narrow Q band with maximum at 648 nm shifted bathochromically of 10 nm with respect to the same band for the mononuclear [Py_8PzZn]. The spectral changes with time lead to a final spectrum in which the Q band almost disappears while a new narrow band, of lower intensity with respect to Q band, appears with maximum at 751 nm, accompanied by new absorptions at 509 and 578 nm. Clean isosbestic points are visible, indicative of the existence of an equilibrium between two species. In DMSO and DMF a spectrum stable with the time is observed, showing a narrow peak at 725-727 nm and low absorptions in the region 350-600 nm. This spectrum might be ascribed to a reduced form, but at the moment no electrochemical data are available to elucidate this aspect.

Part D. Quaternized "Quinoxalinoporphyrazines", [(2-Mepy)$_8$TQuinPzM](I)$_8$ and "Pyridylporphyrazines", [(2-Mepy)$_8$PzM](I)$_8$ (M = $Mg^{II}(H_2O)$, Zn^{II})

D.1 Quaternized "Quinoxalinoporphyrazines", [(2-Mepy)$_8$TQuinPzM](I)$_8$ (M = $Mg^{II}(H_2O)$, Zn^{II})

Octacationic quinoxalinoporphyrazine metal derivatives carrying external pyridines bearing N^+-methylated moieties having the formula $[(2\text{-Mepy})_8TQuinPzM]^{8+}$ (M = $Mg^{II}(H_2O)$, Zn^{II}) (Figure 3.31) were obtained in fairly good yields as hydrated iodide salts by reaction of the corresponding neutral species [$Py_8TQuinPzM$] with CH_3I in DMF, following the procedure already used for the pyrazinoporphyrazine analogues [(2-Mepy)$_8$TPyzPzM](I)$_8$.[31b] As for the neutral species, clathrated water molecules are

systematically present for the Zn^{II} complex but not for the Mg^{II} complex which is formulated with only one water molecule directly bound to the metal, i.e., $[(2\text{-Mepy})_8\text{TQuinPzMg}^{II}(H_2O)]^{8+}$. The aspect of water coordination to Mg^{II} has been previously discussed and is not further considered here.

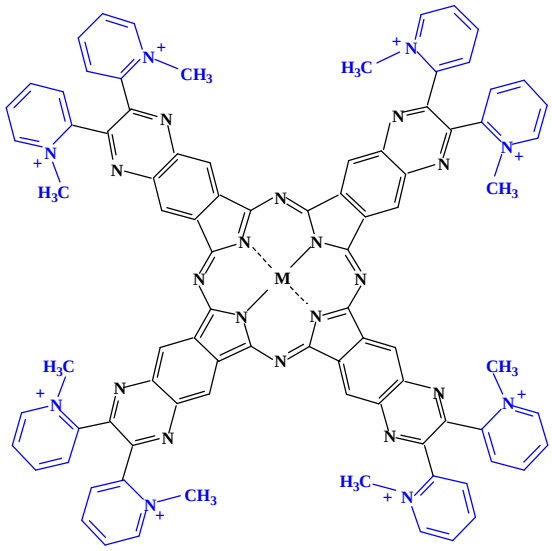

Figure 3.31. $[(2\text{-Mepy})_8\text{TQuinPzM}]^{8+}$ ($M = Mg^{II}(H_2O)$, Zn^{II}).

In the low-donor solvents pyridine, DMSO and DMF, the Mg^{II} octacation $[(2\text{-Mepy})_8\text{TQuinPzMg}(H_2O)]^{8+}$ shows initial aggregation (broad Q band) which tends to disappear along with the time (24 h) or by heating the solution, although it is finally still residually present. The Zn^{II} octacation behaves differently in that it shows, immediately after dissolution, the spectra expected for the monomeric form in all solvents, stable with the time (several hours). Table 3.14 (top) lists the spectral data of the two octacations in pyridine, DMSO and DMF solutions along with the data of the pyridinoporphyrazine $[(2\text{-Mepy})_8\text{PzM}](I)_8$ and pyrazinoporphyrazine $[[(2\text{-Mepy})_8\text{TPyzPzM}](I)_8$ analogues. The spectra of the two quinoxaline macrocycles in all solvents are very similar to each other in that they show an unsplit Q band in the range 772-787 nm accompanied by a B band at higher energy (379-385 nm). This spectral features suggest a D_{4h} symmetry for the macrocycle, independent of the type of the M^{II} center, as might be expected.[31b] The presence of axially ligated water evidently does not alter the overall D_{4h} symmetry of the macrocycle.

Table 3.14. UV-visible Spectral Data (λ, nm (logε)) of $[(2\text{-Mepy})_8\text{TQuinPzM}](I)_8$, $[(2\text{-Mepy})_8\text{PzM}](I)_8$ and related compounds, $[(2\text{-Mepy})_8\text{TPyzPzM}](I)_8$ (M = $Mg^{II}(H_2O)$, Zn^{II}) in Different Solvents.

Compound	Solvent	Soret region		Q-band region			
		λ, nm (logε)					
$[(2\text{-Mepy})_8\text{TQuinPzMg}(H_2O)]^{8+}$	H_2O	353				775	
	Py	385(5.01)	615(4.35)	725sh(4.53)	745sh(5.59)	787(5.14)	
	DMSO	379(5.19)	579sh(4.42)		732sh(4.83)	776(5.38)	
	DMF	379(5.08)	591sh(4.46)		730sh(4.76)	776(5.19)	
$[(2\text{-Mepy})_8\text{TQuinPzZn}]^{8+}$	Py	381(4.99)	577sh(4.24)	718(4.52)	742(4.52)	783(5.31)	
	DMSO	381(5.09)	558sh(4.23)	688(4.50)	731(4.58)	772(5.38)	
	DMF	383(5.07)	566sh(4.29)	709(4.59)	732(4.59)	774(5.43)	
$[(2\text{-Mepy})_8\text{PzMg}(H_2O)]^{8+}$	H_2O	374(4.43)	584sh(3.92)	642(4.38)			
	py			661			
	DMSO	378(4.56)	597sh(4.13)	656(4.58)			
	DMF			666			
$[(2\text{-Mepy})_8\text{PzZn}]^{8+}$	H_2O	363	595sh	657			
	DMF	360	584sh	642			
	DMSO	370		655			
$[(2\text{-Mepy})_8\text{TPyzPzMg}(H_2O)]^{8+}$	Py	368(4.06)	410sh(3.81)	578sh(3.22)	605(3.59)	642sh(3.66)	673(4.34)
	DMSO	370(4.83)	415sh(4.56)	562sh(3.80)	600(4.33)	630sh	660(5.15)
	H_2O				601(5.18)	631sh(5.35)	657(5.94)
$[(2\text{-Mepy})_8\text{TPyzPzZn}]^{8+}$	Py	373(4.92)	468sh(4.09)		607(4.38)	640sh(4.48)	673(5.23)
	DMSO	373(4.37)			600sh(3.86)	637sh(3.89)	666(4.74)
	H_2O	360(4.89)				626(4.69)	654(4.70)

It can be seen from Table 3.14 that the octacationic $[(2\text{-Mepy})_8\text{TQuinPzM}]^{8+}$ species (M = $Mg^{II}(H_2O)$, Zn^{II}) display a Q-band position in pyridine which is shifted bathochromically by ca. 10 nm as compared to the spectra in DMSO and DMF. This shift in λ_Q may result from different axial ligation in pyridine with respect to DMSO and DMF.

An additional and more important observation regarding the peak position of the Q band comes from the comparison of the data of the octacations with those of the corresponding unquaternized species shown in Table 3.9. It is observed that a bathochromic shift is systematically present (15-22 nm) in the direction unquaternized $\rightarrow$ quaternized in each

solvent. This shift must be ascribed to an electronic effect due to the quaternization of the pyridine N atoms, which determines a change in the electronic charge distribution on the entire macrocyclic framework in the direction of enhancement of the electron-deficient properties of the quaternized species. A similar bathochromic shift was observed also after external palladation or platination of the complexes [Py_8TQuinPzM], as discussed in the previous section, and this clearly suggests that both processes, ie. external metalation and quaternization of the mononuclear species [Py_8TQuinPzM] at the dipyridinoquinoxaline fragments results in a lowering of the HOMO-LUMO gap. These results parallel what was observed for the analogous pyrazinoporphyrazines [Py_8TPyzPzM] upon external palladation[24,26a] or quaternization[31b], which implies an enhancement of electron-deficiency of the macrocycles. It is expected that the appropriate electrochemical exploration of the behaviour of the octacationic quinoxalinoporphyrazines in pyridine, DMSO, or DMF might results in less negative potentials for the one-electron reductions than those of the respective neutral species. The electrochemical study is presently in due course.

The two Mg^{II} and Zn^{II} octacationic macrocycles exhibit moderate solubility in water with a maximum concentration (saturation limit) of ca. 10^{-5} M, a little higher at 50 °C. For both the complexes molecular aggregation is observed in water solution, evidenced by the presence of a broad absorption in the Q-band region (710-780 nm) and a B band at 350-365 nm (Table 3.14). The spectra at c ≅ 10^{-5} M do not change significantly as a function of time (24 h). Changes for the Mg^{II} complex are observed by dilution of the solution and consist of an increase of the intensity of the absorption at ca. 775 nm and a decrease of intensity for the absorption at ca. 720-730 nm, a behaviour which recalls that seen for the analogous class of octacationic species $[(2\text{-Mepy})_8\text{TPyzPzM}]^{8+}$ [31b] (Table 3.14). This allows to identify the first absorption as the Q band of the monomeric form while the second one is assigned to an aggregated form, probably the dimer. For both the Mg^{II} and Zn^{II} octacationic complexes, however, a high amount of aggregated species is still present at 10^{-7} M solutions.

D.2 Quaternized "Pyridylporphyrazines", $[(2\text{-Mepy})_8PzM](I)_8$ (M = $Mg^{II}(H_2O)$, Zn^{II})

The fully quaternized metal derivatives of the pyridylporphyrazine $[Py_8PzH_2]$ were obtained in fairly low yields as hydrated iodide salts having the formula $[(2\text{-Mepy})_8PzM](I)_8$ (M = $Mg^{II}(H_2O)$, Zn^{II}) (Figure 3.32). This was accomplished by methylation at the pyridine N atoms of the corresponding neutral $[Py_8PzM]$ by using CH_3I in DMF under experimental conditions milder (room temperature) than those used for the corresponding quinoxaline derivatives. Due to the high solubility of these octacationic species, it was not possible in the case of the Zn^{II} complex to separate it in a pure form from the mother liquors by centrifugation. The complex has been extracted in water and then left to evaporate, as described in the Experimental Section. The difficulty of separation is also responsible of the low reaction yield. Samples of the compound were obtained as dark-green powders stable to the air. Also in this case clathrated water molecules are systematically present with variable amount from preparation to preparation. The Mg^{II} cationic fragment is formulated with one water molecule directly bound to the metal, i.e., $[(2\text{-Mepy})_8PzMg^{II}(H_2O)]^{8+}$.

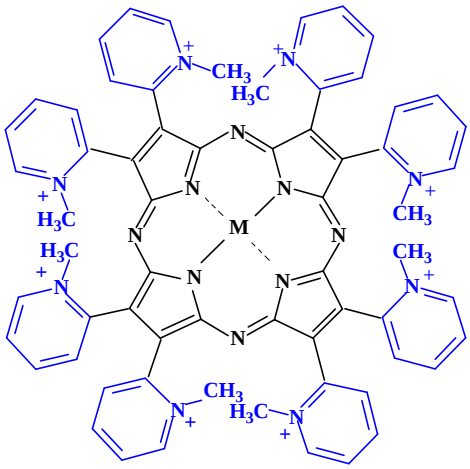

Figure 3.32. $[(2\text{-Mepy})_8PzMg^{II}(H_2O)]^{8+}$ (M = $Mg^{II}(H_2O)$, Zn^{II}).

The Mg^{II} complex is soluble in water giving, at concentration of ca. 10^{-5} M or little higher, a stable spectrum conform to that expected for the monomeric form of the compound with a narrow unsplit Q band (D_{4h} symmetry) at 642 nm and a B band at 374 nm (Figure 3.33). The spectrum is stable as a function of time (24 h). Molecular aggregation is

observed at higher concentrations (≥ 10^{-4} M). This behaviour is different from that observed for the analogous octacationic quinoxalino- and pyrazinoporphyrazines. For these macrocycles, as discussed above, a second band of comparable intensity is always present at concentration of 10^{-5}-10^{-6} M on the blue side of the Q band, belonging to an aggregated species that shows the tendency to disappear upon dilution (10^{-7} M).

Table 3.14 lists the spectral data of the two complexes $[(2\text{-Mepy})_8\text{PzM}](I)_8$ (M = $Mg^{II}(H_2O)$, Zn^{II}) in H_2O, pyridine, DMSO and DMF solutions. The initial spectrum of the Mg^{II} complex in DMSO is typical of a monomeric species with a narrow Q band at 756 nm and a B band at 378 nm. Upon staying of the solution, the appearance of a peak at ca. 730 nm is observed with the concomitant lowering of the Q band at 756 nm; the final spectrum (24 h) shows the two peaks with almost the same intensity and clean isosbestic points are detectable. The solution behaviour is more heavily complicated by aggregation in pyridine and DMF and only the Q-band position could be detected. Comparing the data in DMSO for the octacationic species $[(2\text{-Mepy})_8\text{PzMg}(H_2O)]^{8+}$ and the neutral $[\text{Py}_8\text{PzMg}(H_2O)]$ a bathochromic shift, as expected, is observed (ca. 20 nm) in the direction unquaternized → quaternized species and this once again is attributable to the enhancement of the electron deficient properties of the macrocycle due to the quaternization at the pyridine N atoms.

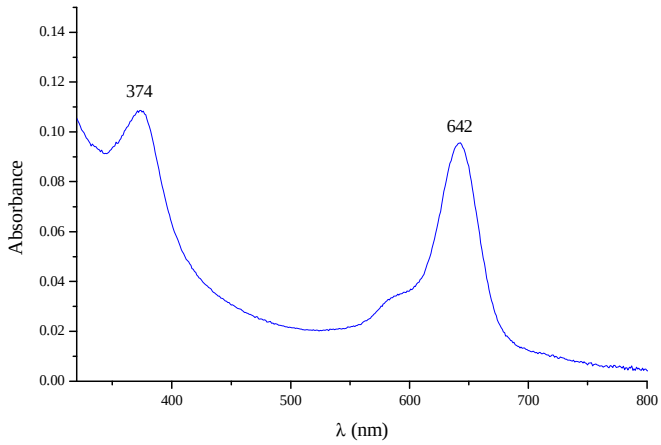

Figure 3.33. UV-visible spectrum of $[\text{Py}_8\text{PzMg}(H_2O)]^{8+}$ in H_2O.

The Zn^{II} octacationic complex $[(2\text{-Mepy})_8\text{PzZn}]^{8+}$ is less soluble in water than the respective Mg^{II} species, the solubility slightly raising with temperature (50 °C). Molecular aggregation, persisting also upon dilution, is observed in the other solvents (pyridine, DMSO

and DMF). In addition, the UV-visible spectra confirm that the complex is not at the highest level of purity and further work is needed to better define the preparative aspects and its spectroscopic behaviour.

Part E. PDT and Fluorescence Measurements of "Quinoxalinoporphyrazines" and "Pyridylporphyrazines"

The use of porphyrins and phthalocyanines in photodynamic therapy (PDT) of cancer has been intensively studied[32] as already outlined in Part D of the Introduction, but porphyrazines have received in general only limited attention in this regard.[36,38,25,52,26b] The efficiency of a porphyrazine photosensitizer, measured by the quantum yield value of its singlet oxygen production (Φ_Δ), will depend on its tendency to achieve, upon light irradiation, the triplet state T_1 with high quantum yield, and have for T_1 adequate energy and lifetime to allow a proper energy transfer to dioxygen for the process $^3O_2 \rightarrow {}^1O_2$.

The type of the central metal ion in the macrocycles can strongly influence this process and it is known that closed shell ions like Zn^{II} and Mg^{II}, and in some cases, open-shell diamagnetic d^8 metal centers, like Pd^{II} or Pt^{II}, give rise to complexes with good photosensitizing capabilities. In this contest the research group has recently demonstrated that Pd^{II} [25,67] and Pt^{II}-pyridinated "pyrazinoporphyrazines" [26b] are photoactive in DMF solutions and act as singlet oxygen sensitizers.

In the present thesis work we have explored the photosensitizing activity of the Zn^{II} and Mg^{II} complexes of the new quinoxalino- and pyridylporphyrazine macrocycles, [Py_8TQuinPzM] and [Py_8PzM], respectively. The measurements were made in DMF ([complex] $\cong 10^{-5}$ M) by an absolute method, using a laser source at 635 nm for the pyridyl compounds and at 760 nm for the quinoxaline species, close to the maximum of the Q-band absorption peaks of the corresponding compounds (Figure 3.34). A drawing exemplifying a typical Stern-Volmer plot used to calculate the singlet oxygen quantum yield (Φ_Δ) of the sensitizers, according to Eq.2.1 (reported in the Experimental Section), is shown in Figure 3.34B for [Py_8PzMg(H_2O)]. The inset illustrates the related experimental data

corresponding to the absorption decay at 414 nm for the $^1O_2$ scavenger, DPBF, recorded during the irradiation time of the solution. The data of Φ_Δ are reported in Table 3.15. Fluorescence quantum yields (Φ_F) and Stokes shifts ($\Delta\lambda$) obtained in DMF ([complex] $\leq 10^{-6}$ M) are also listed in the table.

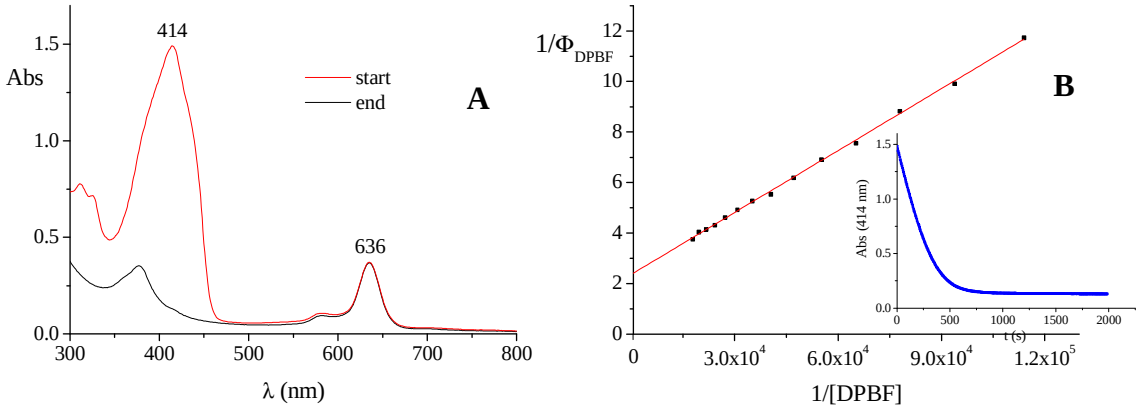

Figure 3.34. UV-visible data recorded during a typical experiment of a Φ_Δ measurement. A: Spectra of a solution containing [$Py_8PzMg(H_2O)$] and DPBF before (red line) and after (black line) laser irradiation (635 nm); B: Stern-Volmer data analysis of the DPBF photooxidation (see inset).

Table 3.15. Singlet Oxigen (Φ_Δ) and Fluorescence Quantum Yields (Φ_F) in DMF of [Py_8TQuinPzM] and [Py_8PzM] with (M = $Mg^{II}(H_2O)$, Zn^{II}).

		Singlet oxygen		**Fluorescence**		
Compound	λ_{max} [nm]	λ_{irr} [nm]	Φ_Δ [a]	λ_{exc} [nm]	λ_{em} ($\Delta\lambda$) [b] [nm]	Φ_F [a]
[Py_8TQuinPzZn]	757	778	0.22	620	763(5)	0.04
[Py_8PzZn]	635	635	0.54	580	647(14)	0.14
[Py_8TQuinPzMg(H_2O)]	759	778	0.08	620	767(7)	0.10
[Py_8PzMg(H_2O)]	636	635	0.41	580	647(13)	0.23

[a] Mean value of at least three measurements. Uncertainty is half dispersion and it is typically ± 0.03.
[c] $\Delta\lambda$ is the Stokes shift.

Solutions in DMF of the complexes [Py_8PzM] (M = $Mg^{II}(H_2O)$, Zn^{II}) are generally stable under irradiation. The quinoxalinporphyrazines [Py_8TQuinPzM] (M = $Mg^{II}(H_2O)$, Zn^{II}) present instead marked instability, showing some degree of decomposition (ca. 15%) within the time of a run.

The DMF solutions of the complexes [Py_8PzM] with M = $Mg^{II}(H_2O)$ or Zn^{II} generally present some scattering material, probably due to insoluble impurities, which determines a highly disturbing noise in the spectrum. This implies an error in the evaluation of the exact absorbance and consequently an undervalutation of the Φ_Δ and Φ_F values. This is the reason why the absorption spectra have been baselined by the Morton-Stubbs three point correction.[65] The Φ_Δ and Φ_F values reported in Table 3.15 are the corrected ones and can be considered fairly reliable values (see Experimental Section for the k_d/k_r values).

The observed Φ_Δ values for the Zn^{II} and Mg^{II} complexes of both quinoxalino- and pyridylporphyrazine macrocycles follow the order $Zn^{II} > Mg^{II}$; higher Φ_Δ values for the Zn^{II} species as compared to those of the Mg^{II} compounds are in line with expectation, in view of the "heavy atom effect" which enhances the triplet excited state quantum yield for the Zn^{II} with respect to Mg^{II}. The Φ_Δ value of the Zn^{II} complex, [Py_8PzZn] (0.54) is in the range 0.4-0.7 observed for a number of Zn^{II} porphyrazines,[36,37,38] and this qualify it as excellent photosensitizer for the generation of singlet oxygen. The comparison of the Φ_F values observed for the two metal centers also seems to be in line with expectation, i.e., the value of the Mg^{II} complexes (0.10-0.23) are higher than those of the Zn^{II} analogs (0.04-0.14), which is coherent with the reverse order found for Φ_Δ.

Worth of notice, higher Φ_Δ and Φ_F values are observed for the same metal center going from the quinoxalino- to the pyridylporphyrazines. This suggests that the more extended quinoxaline macrocycle has higher facility to dissipate the excitation energy by non radiative internal conversion processes, which lead to a decrease of the singlet and triplet excited state lifetime (τ_{S1} and τ_T) and of their quantum yields (Φ_{S1}, Φ_T). The effect is the decrease of both Φ_F and Φ_Δ values. Furthermore the presence of more extended π-π interactions causes a higher tendency to molecular aggregation which leads to a decrease of photoactivity.[66]

Additional considerations refer to the trend of the observed Φ_Δ values upon increasing of the macrocycle dimensions. On going from quinoxalino- to pyrazino- and to pyridylporphyrazines, i.e. decreasing of the extension of the π-conjugated system in the macrocycle, the Φ_Δ variations are $[Py_8TQuinPzZn]_{DMF}$ (0.22) → $[Py_8TPyzPzZn]_{DMF}$ (0.55)[67] → $[Py_8PzZn]_{DMF}$ (0.54) for the Zn^{II} complexes and $[Py_8TQuinPzMg(H_2O)]_{DMF}$

(0.08) → $[Py_8TPyzPzMg(H_2O)]_{DMF/HCl}$ (0.29)[67] → $[Py_8PzMg(H_2O)]_{DMF}$ (0.41) for the Mg^{II} species. It is important to notice that the gradual contraction of the macrocycle determines an increasing of the singlet oxygen quantum yield production. The effect is particularly evident in the case of the Mg^{II} derivatives.

This behaviour has been observed also for other tetrapyrrolic macrocycles such as naphthalocyanines (Nc) and phtalocyanines (Pc); see for comparison the data reported in Table 3.16 for the Zn^{II} complexes of different couples of Nc/Pc systems.

Table 3.16. Singlet Oxigen Quantum Yields (Φ_Δ) of Naphthalocyanines (Nc) and Phtalocyanines (Pc) in Different Solvents.

	Φ_Δ	solvent	Ref.
NcZn	0.36	DMF	35e
PcZn	0.49		
$(t\text{-}Bu)_4$NcZn	0.48	DMF	38
PcZn	0.56		
S_4NcZn	0.25	H_2O	66
S_4PcZn	0.70		

Fluorescence emission spectra typical of porphyrazine macrocycles are obtained for both the series of systems. Figures 3.35A and 3.35B show the absorption and excitation spectra of the Mg^{II} complexes $[Py_8TQuinPzMg(H_2O)]$ and $[Py_8PzMg(H_2O)]$, respectively. The overall coincidence of the narrow Q band as to the absorption and excitation spectra in the case of $[Py_8PzMg(H_2O)]$, indicates that the monomeric species is almost exclusively present in solution. A different behaviour is observed for the quinoxaline compound $[Py_8TQuinPzMg(H_2O)]$, for which the correspondence of the excitation with the absorption spectrum is not observed in all the Q-band range. This is particularly evident in the range 650-750 nm, where the low intensity bands present in the absorption spectrum could be assigned to a form of molecular aggregation.

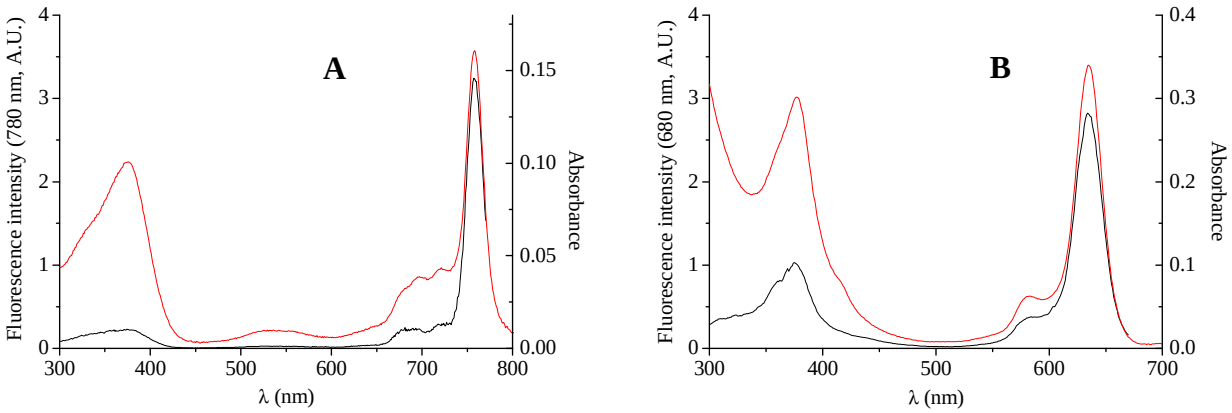

Figure 3.35. Fluorescence excitation (black lines, left hand ordinates) and absorption (red lines, right hand ordinates) spectra of [Py_8TQuinPzZn] (A) and [Py_8PzMg(H_2O)] (B) in DMF.

Part F. Tetrakis[di(2-thienyl)pyrazino]porphyrazines

The synthesis and general physicochemical characterization of the new class of thienyl pyrazinoporphyrazines [Th_8TPyzPzM] (M = $2H^I$, $Mg^{II}(H_2O)$, Co^{II}, Cu^{II}, Zn^{II}) (Figure 3.36A) and their heteropentametallic derivatives [$(PdCl_2)_4Th_8$TPyzPzM] (M = $Mg^{II}(H_2O)$, Zn^{II}) (Figure 3.36B) were described in the graduation thesis work of the candidate. In this Section only the new aspects pertaining to work developed during the PhD thesis will be referred to as follows: Par. **F.1**: Electrochemical behaviour of [Th_8TPyzPzM] in a very brief manner; Par. **F.2**: PDT and Fluorescence Measurements on [Th_8TPyzPzM] and [$(PdCl_2)_4Th_8$TPyzPzM] (PDT data were partially illustrated in the graduation thesis); Par. **F.3**: DFT and TDDFT calculations and the EXAFS spectrum collected in the context of the investigation of the Pd^{II} complex of the precursor 2,3-dicyano-5,6-di(2-thienyl)-1,4-pyrazine, [$(CN)_2Th_2$Pyz]. Almost all the material presented here has been the object of two recent publications.[40]

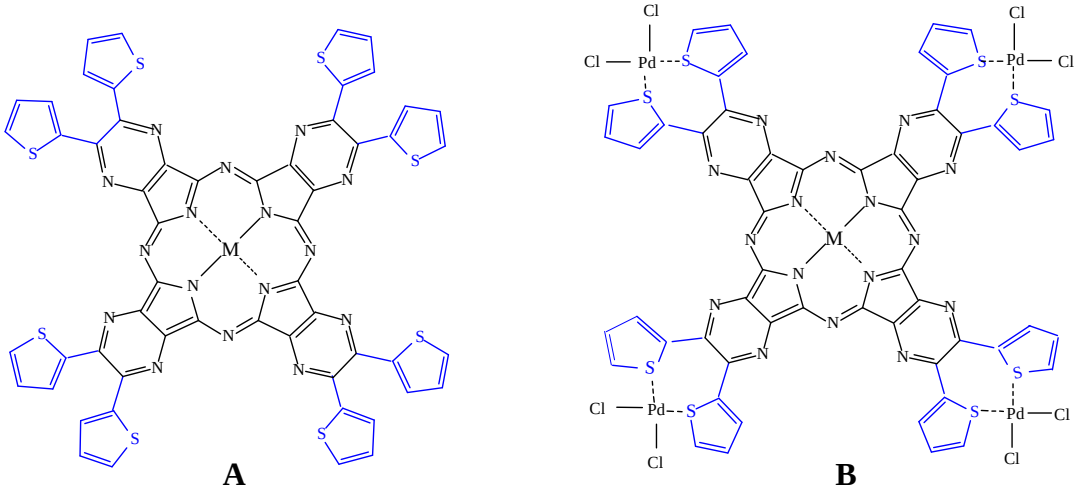

Figure 3.36. A) [Th_8TPyzPzM]; B [$(PdCl_2)_4Th_8$TPyzPzM].

The work on the octathienyl pyrazinoporphyrazine systems involved pheripheral modifications of the tetrapyrazinoporphyrazine macrocycle, focusing on the ligating properties of the S atoms inserted in the external 2-thienyl rings, in an interesting comparison with those seen for the pyridine rings in the pyridinated "pyrazinoporphyrazines" [Py_8TPyzPzM].

All the mono- and multimetallic compounds, completely insoluble in water, were characterized by their UV-visible spectra in solutions of DMF, DMSO and pyridine. Molecular aggregation occurs at concentrations of ca. 10^{-4} M or less, but monomers are formed in more dilute solutions of 10^{-4} M or less. The examined octathienyl compounds [Th_8TPyzPzM] behave as electron-deficient macrocycles, and UV-visible spectral measurements provide useful information about how the peripheral thienyl rings influence the electronic distribution over the entire macrocyclic framework. Electrochemical data for [Th_8TPyzPzM] (see below) confirm the easier reducibility of the compounds as compared to the related phthalocyanine analogues, and the overall redox behaviour is similar to that of the octapyridinated analogues [Py_8TPyzPzM].

Spectroscopic data on the tetrapalladated compounds [$(PdCl_2)_4Th_8$TPyzPzM] strongly suggest an equivalent employment of vicinal 2-thienyl rings through their sulphur atoms and formation of exocyclic $S_{2(th)}PdCl_2$ coordination sites ("th-th" coordination). This is similar to what was found for the corresponding octapyridinated analogues ("py-py" coordination)

and different from the findings for the bis-palladated derivative formed from the precursor [$(CN)_2Th_2Pyz(PdCl_2)_2$] (see below).

It is noteworthy that the mono- and pentametallic octathienyl compounds exhibit both the Soret and Q-band positions bathochromically shifted with respect to what is observed for the corresponding octapyridino analogues. This seems to indicate that the thienyl residues behave as stronger electron-withdrawing groups than the pyridine rings in the respective macrocycles. An interesting aspect of the spectra is that the Soret and Q bands remain unshifted upon exocyclic coordination of the $PdCl_2$ units. This is different from what has been seen for the parallel series of octapyridino analogues, for which peripheral coordination of $PdCl_2$ units leads to a bathochromic shift of 7-9 nm in DMSO and in other solvents. In an attempt to explain this, these findings require a knowledge of the precise local geometry at the Pd^{II} coordination sites as well as an understanding of how the pyridyl and thienyl rings are positioned with respect to the central pyrazinoporphyrazine core, a fact which may influence the σ/π electronic contact between the central macrocyclic framework and the peripheral metalated fragments.

F.1 Electrochemical behaviour of [Th_8TPyzPzM] (M = $Mg^{II}(H_2O)$, Co^{II}, Cu^{II}, Zn^{II})

Electrochemical and spectroelectrochemical measurements were carried out in pyridine, DMSO and DMF. Figures 3.37 and 3.38 exemplify the voltammograms in these solvents for [Th_8TPyzPzZn]. Table 3.17 list the half-wave potentials (V vs SCE) of the compounds examined. A detailed discussion of the electrochemical and spectroelectrochemical results have been reported in ref. 40a and will be referred to here very briefly.

Referring to the electrochemistry of the mononuclear "octathienyl-pyrazinoporphyrazines" [Th_8TPyzPzM], it is clear from the measured $E_{1/2}$ values in Table 3.17 that the stepwise addition of electrons to the series of [Th_8TPyzPzM] compounds takes place at much more positive $E_{1/2}$ values than for the related phthalocyanine analogues,[68] a fact which is attributed to the presence of the strongly electron-withdrawing

dithienylpyrazino fragments which replace the benzene rings of the phthalocyanine macrocycle (see Figure 3.36A).

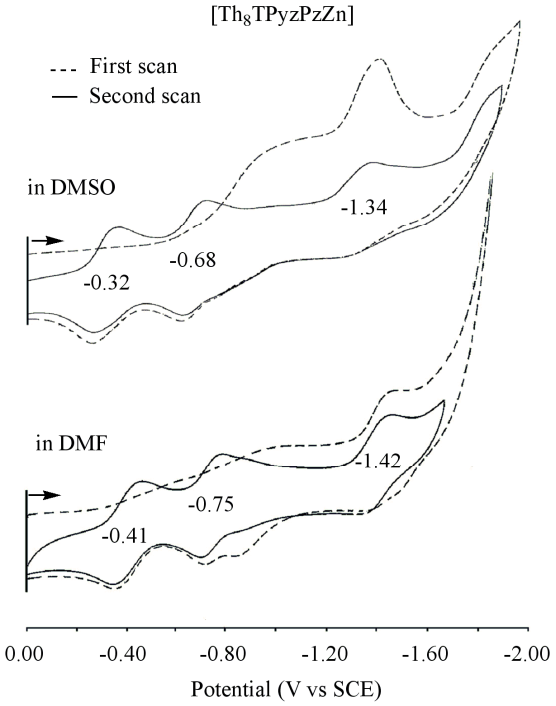

Figure 3.37. First scan (---) and second scan (—) thin-layer cyclic voltammograms of [Th_8TPyzPzZn] in DMSO and DMF, 0.2 M TBAP.

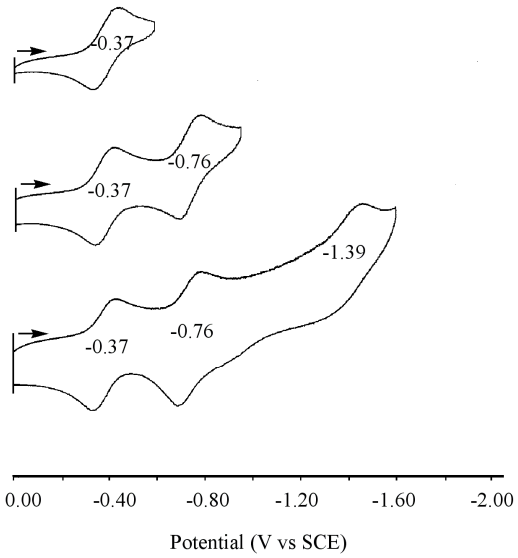

Figure 3.38. Second scan thin-layer cyclic voltammograms of [Th_8TPyzPzZn] in pyridine, 0.2 M TBAP.

Table 3.17. Half-wave Potentials ($E_{1/2}$, V *vs* SCE) for Reduction of [Th_8TPyzPzM] (M = Zn^{II}, $Mg^{II}(H_2O)$, Cu^{II}, Co^{II}) in DMSO, DMF and pyridine, 0.2 M TBAP.

Metal ion	**Solvent**	1^{st} red	2^{nd} red	3^{rd} red
Zn^{II}	DMSO	-0.32	-0.68	-1.34
	DMF	-0.41	-0.75	-1.42
	pyridine	-0.37	-0.76	-1.39
$Mg^{II}(H_2O)$[a]	DMSO	-0.37	-0.68	-1.40
	DMF	-0.43	-0.77	-1.41
	pyridine	-0.46	-0.79	-1.49
Cu^{II}	DMSO	-0.30	-0.67	-1.34
	DMF	-0.26	-0.60	-1.24
	pyridine	-0.35	-0.67	-1.36
Co^{II}	DMSO[b]	-0.12	-0.78	-1.36
	DMF	-0.13	-0.82	-1.36
	pyridine	-0.25	-0.85	-1.35

[a] Unknown impurity or side reaction seen for Mg^{II} complex at $E_{1/2}$ = -0.98 to -1.04 V vs SCE in all solvents. [b] The oxidization of [Th_8TPyzPzCo^{II}] to [Th_8TPyzPzCo^{III}]$^+$ occurs at $E_{1/2}$ = 0.57 V in DMSO.

This shift of $E_{1/2}$ values towards more positive potentials is a feature shared by the related diazepino-[20] and thiadiazolporphyrazine[18b] macrocycles, with parallel results also being obtained for related macrocyclic compounds having peripheral dipyridinopyrazine fragments[1,21,24] and their corresponding octacationic[24,31b] and the homo-[24] and heteropentametallic[26a] derivatives.

F.2 PDT and Fluorescence Measurements on [Th_8TPyzPzM] and [$(PdCl_2)_4Th_8$TPyzPzM] (M = $Mg^{II}(H_2O)$, Zn^{II})

In the present study, Φ_Δ values were calculated from Eq. 2.1 (see Experimental Section) using Stern-Wolmer plots of the type shown in Figure 3.39 for the compound [Th_8TPyzPzZn]. The data obtained for the octathienyl Zn^{II} and Mg^{II} porphyrazine compounds [Th_8TPyzPzM] and the corresponding tetrapalladated species [$(PdCl_2)_4Th_8$TPyzPzM] in DMF ($c \cong 10^{-5}$ M), and in DMF acidified with HCl (DMF/HCl; [HCl] = $1x10^{-4}$ M) are listed in Table 3.18. Regardless of the presence or absence of HCl, the observed Φ_Δ values follow the order $Zn^{II} > Mg^{II}(H_2O)$. As can be seen in Table 3.18, the same order is mantained for the Zn^{II} and Mg^{II} octapyridinated analogues, [Py_8TPyzPzZn] and [Py_8TPyzPzMg(H_2O)] [67] and their corresponding tetrapalladated complexes [$(PdCl_2)_4Py_8$TPyzPzM] (M = $Mg^{II}(H_2O)$, Zn^{II}).

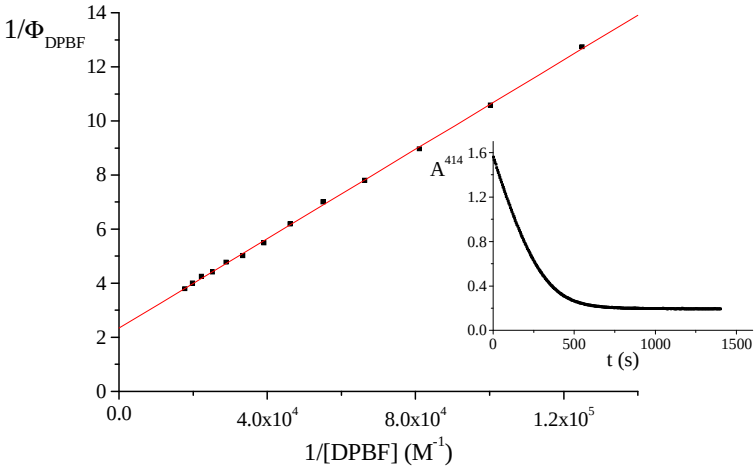

Figure 3.39. Stern-Volmer data analysis of the DPBF decay (see inset) recorded during a Φ_Δ measurement of the complex [Th_8TPyzPzZn] in DMF.

Higher Φ_Δ values for the Zn^{II} species as compared to those of the Mg^{II} compounds are in line with expectation, in view of the heavy atom effect which favors Zn^{II}. The Φ_Δ values of the Zn^{II} species (0.4-0.6) are in the range 0.4-0.7 observed for a number of Zn^{II} porphyrazines,[36,37,38] and qualify them as excellent photosensitizers for the generation of singlet oxygen.

Table 3.18. Singlet Oxygen (Φ_Δ) and Fluorescence (Φ_F) Quantum Yields in DMF for [Th_8TPyzPzM] and [$(PdCl_2)_4$TPyzPzM] (M = Zn^{II}, $Mg^{II}(H_2O)$) and related species.

Compound	[HCl] (M)	λ_{max} (Q band) (nm)	λ_{irr} [a] (nm)	Φ_Δ [b]	k_d/k_a*10^5 [c,d] (M)	λ_{em} ($\Delta\lambda$)[e] (nm)	Φ_F [b]
[Th_8TPyzPzZn]	0	672	670	0.43[f]	3.5	679(7)	0.15[g]
	$1x10^{-4}$	672	670	0.51	3.1	680(8)	0.17[g]
[Th_8TPyzPzMg(H_2O)]	0	672	670	0.14	3.1	679(7)	0.11[g]
	$1x10^{-4}$	669	670	0.27	3.1	677(8)	0.40[g]
[$(PdCl_2)_4Th_8$TPyzPzZn]	0	672	670	0.43	3.5	680(8)	0.11[g]
	$1x10^{-4}$	672	670	0.54	3.3	680(8)	0.10[g]
[$(PdCl_2)_4Th_8$TPyzPzMg(H_2O)]	0	675	670	0.13	2.9	679(4)	0.12[g]
	$1x10^{-4}$	669	670	0.27	2.9	678(9)	0.20[g]
[Py_8TPyzPzZn]	0	657	660	0.55	3.4	664(7)	0.23[h]
	$1x10^{-4}$	657	660	0.58	2.7	664(7)	0.17[h]
[Py_8TPyzPzMg(H_2O)]	0	658	660	0.09	2.9	665(7)	0.10[h]
	$1x10^{-4}$	653	660	0.29	3.0	663(10)	0.43[h]
[$(PdCl_2)_4$TPyzPzZn]	0	662	670	0.48	3.4	671(9)	-
	$1x10^{-4}$	662	670	0.52	2.7	671(9)	0.16[h]
[$(PdCl_2)_4$TPyzPzMg(H_2O)]	0	662	670	0.23	3.2	673(11)	-
	$1x10^{-4}$	660	670	0.37	3.3	671(11)	-

[a] Wavelength of laser source irradiation. [b] Mean value of at least three measurements. Uncertainty is half dispersion and it is typically ± 0.02. [c] The list of reported values, which depend exclusively on the scavenger and the solvent used, are close to the previously published data for similar measurements: $(2.9 \pm 0.3) \times 10^{-5}$ M (DMF), $(3.7 \pm 0.4) \times 10^{-5}$ M (DMF), and $(3.0 \pm 0.2) \times 10^{-5}$ M (DMF/HCl)· [d] Uncertainty: ± 0.1. [e] $\Delta\lambda$ is the Stokes shift which move in the range 4-10 nm. [f] The value measured in pyridine for this compound was 0.635. [g] Excitation wavelength: 620 nm. [h] Excitation wavelength: 600 nm.

Among the compounds listed in Table 3.18 there are no cases for which preacidification with HCl ($1x10^{-4}$ M) was strictly required, since no tendency to reduction was in general observed in DMF for the mono- and pentametallic octathienyl Zn^{II} and Mg^{II} compounds. This reduction process is ascribed to small amounts of reducing agents normally present in the solvent at a level of concentration comparable with that of the macrocycles, and it is was shown[25] that HCl is able to reoxidize the reduced forms or to avoid reduction with preacidification. So, the increment of Φ_Δ observed in the presence of HCl might be attributed to the elimination of residual forms of aggregation which are not observed by UV-visible and spectroelectrochemical studies of the compounds. Although the relatively small increase of

Φ_Δ for the Zn^{II} species might be explained in such a way, it appears difficult to justify the observed variations for the Mg^{II} compounds on the same basis.

Fluorescence quantum yields, Φ_F, and Stokes shifts ($\Delta\lambda$) obtained in DMF and DMF/HCl for the Zn^{II} and Mg^{II} mono- and pentametallic species ($\leq 10^{-6}$ M) are also listed in Table 3.18 The values for the octapyridino pyrazinoporphyrazine analogues are also reported for comparison. Small Stokes shifts (4-10 nm) are observed for all in the compounds series, as is normally found for porphyrazine macrocycles. Figure 3.40 shows, as a representative example, the absorption, excitation and emission spectra of the Zn^{II} complex [Th_8TPyzPzZn] in DMF solution. The overall coincidence of the narrow Q-band as to the absorption and excitation spectra, common to all the compounds, indicates that monomeric species are almost exclusively present in solution.

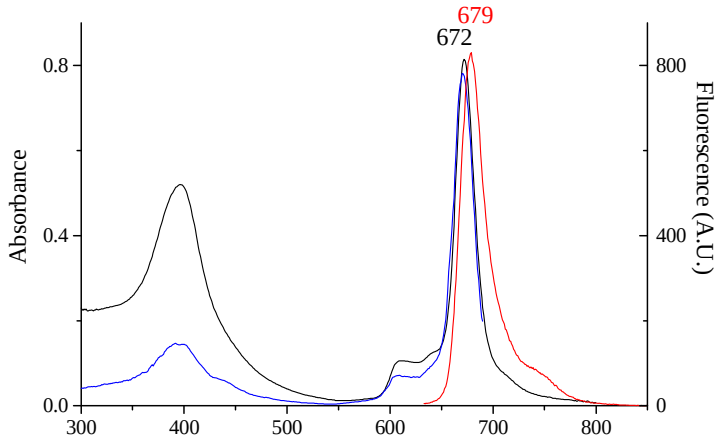

Figure 3.40. UV-visible absorption (black line), excitation (blue line; λ_{em} = 690 nm) and emission (red line; λ_{exc}= 620 nm) spectra of the complex [Th_8TPyzPzZn] in DMF.

The Φ_F values of the Zn^{II} species in DMF or DMF/HCl are lower than the corresponding Φ_Δ values, which is in line with expectation. The small changes of Φ_F values for the Zn^{II} species determined by acidification are in striking contrast with the parallel changes of the Mg^{II} monometallic species. For these latter ones, Φ_F variations are 0.11 (DMF) $\rightarrow$ 0.40 (DMF/HCl) and 0.10 (DMF) $\rightarrow$ 0.43 (DMF/HCl) for the octathienyl and the octapyridino compounds, respectively (Table 3.18). In the light of these data, the hypothesis that the observed changes might be due to disaggregation phenomena appears inadequate.

The observed behavior suggests that more advanced studies are needed, especially in the light of fluorescence values (0.40-0.43) in DMF/HCl which appear to be of interest in the area of the medical imaging response and diagnosis.

F.3 Structural Studies and Theoretical Calculations on the Dinuclear Pd(II) Derivatives of the Precursor 2,3-Dicyano-5,6-di(2-thienyl)-1,4-pyrazine, $[(CN)_2Th_2Pyz(PdCl_2)_2]\cdot H_2O$

The target of the work on the precursor 2,3-dicyano-5,6-di(2-thienyl)-1,4-pyrazine, $[(CN)_2Th_2Pyz]$, was to establish the type of metal coordination to the di(2-thienyl)pyrazino site. The involvement of the thienyl residues of $[(CN)_2Th_2Pyz]$ in the Pd^{II} coordination of $[(CN)_2Th_2Pyz(PdCl_2)_2]\cdot H_2O$ was studied by NMR and extended X-ray absorption fine structure (EXAFS) measurements and was supported by density functional theory (DFT) and time-dependent DFT (TDDFT) calculations. As detailed below, two different coordination sites occur in the complex, in which the two $PdCl_2$ units are bound to a pyrazine N atom and to a S atom, generating different local environments for the Pd^{II} centers and an overall asymmetric structure. This behaviour is different from what has been observed for its monopalladated bispyridine analogue $[(CN)_2Py_2PyzPdCl_2]$[24] and the tetrapalladated thienyl macrocycles as illustrated above.

EXAFS Results. A quantitative determination of the coordination geometry of Pd^{II} in $[(CN)_2Th_2Pyz(PdCl_2)_2]$ was obtained by assuming the first coordination sphere of each Pd^{II} center in the compound as being composed of two Cl atoms, one N atom of the pyrazine ring and possibly the S atom of one thienyl ring. Fitting procedures were applied to the whole set of structural and nonstructural parameters to improve, as far as possible, the agreement between the calculated signals and the experimental EXAFS spectrum. In particular, we optimized four structural parameters for each single shell contribution and least-squares fits were performed in the range k = 2.5-12.8 $Å^{-1}$. The best-fit analysis is shown in the upper panel of Figure 3.41 The first four curves from the top are the Pd-N, Pd-Cl and Pd-S first shell two-body contributions, and the reminder of the figure shows the total theoretical signal compared with the experimental spectrum, and the resulting residual.

Overall, the fitted EXAFS spectrum matches the experimental data well enough, and the dominant contribution to the total EXAFS signals is given by the two Pd-Cl first shell signals, and by the Pd-N signal. Moreover, one of the S atoms also provides a detectable contribution well above the experimental noise of the spectrum. The FT moduli of the experimental spectra extracted with a three segmented cubic spline are shown in the lower panel of Figure 3.41. The FTs have been calculated in the interval k = 2.5-12.5 $Å^{-1}$ with no phase-shift correction applied. The agreement between the theoretical and experimental curves is quite good, reinforcing the validity of the following structural results. Elaboration of EXAFS experimental data provide evidence of the occurrence of two different Pd^{II} coordinations sites. In one of them, Pd^{II} first shell was fitted with one Pd-N contribution with a distance of 2.03 ± 0.03 Å, two Pd-Cl contributions with a distance of 2.36 ± 0.03 Å and one Pd-S contribution with a distance of 2.25 ± 0.04 Å (Table 3.19). The presence of a short Pd-S bond distance hinders a comparable approach for the second S atom to the Pd^{II} center, the coordination site of which sees the S atom at a much longer distance (3.21 ± 0.05 Å), in an overall asymmetric arrangement of the entire molecular framework. The relatively low intensity of both the Pd-S signals is probably due to the coexistence of two different Pd^{II} coordination environments.

Table 3.19. Palladium(II) First Shell Geometrical Parameters Obtained by EXAFS on $[(CN)_2Th_2Pyz(PdCl_2)_2]$. N is the Coordination Number, R the Average Distance, σ^2 the Distance Variance and β is the Skewness. The last column reports the bond distances obtained by DFT calculations.

	N	R (Å)	σ^2 ($Å^2$)	β	R (Å)
Pd-N	1	2.03(3)	0.020(4)	0.9(3)	2.12-2.14
Pd-Cl	2	2.36(3)	0.011(4)	0.9(3)	2.28-2.29
Pd-S1	0.5	2.25(4)	0.019(5)	1.1(3)	2.46-3.5
Pd-S2	0.5	3.21(5)	0.025(5)	1.2(3)	

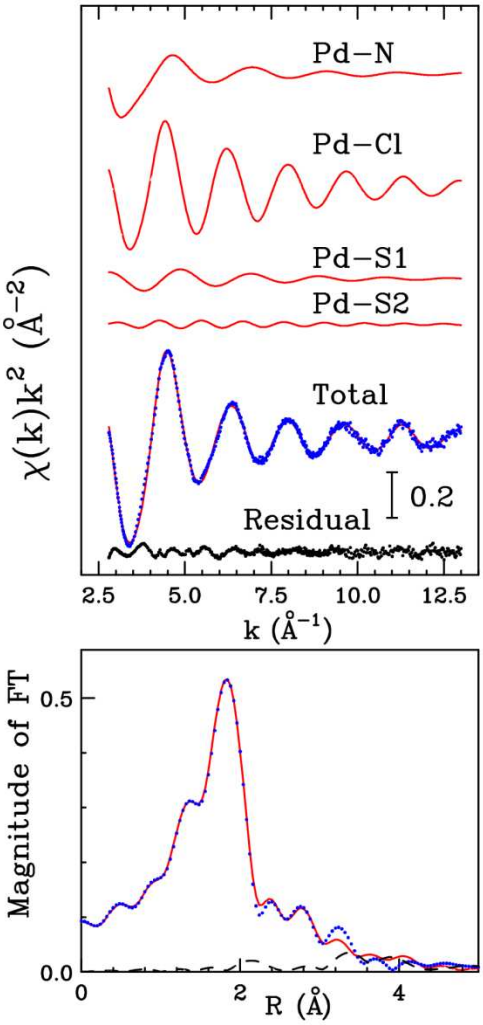

Figure 3.41. Analysis of the Pd K-edge EXAFS spectrum of solid $[(CN)_2Th_2Pyz(PdCl_2)_2]$. Upper panel: theoretical Pd-N, Pd-Cl, and Pd-S first shell contributions, total theoretical signal (full red line) compared with the experimental spectrum (dotted blue line), and residual curve (full black line). Lower panel: nonphase-shift-corrected Fourier transforms of the experimental data (dotted blue line), of the total theoretical signal (full red line), and of the residual curve (dashed-dotted black line).

DFT and TDDFT Calculations. Data from DFT studies of $[(CN)_2Th_2Pyz(PdCl_2)_2]$ concerning the Pd-N, Pd-Cl and Pd-S bond distances are reported in Table 3.19 (last column). As can be seen, the Pd-N and Pd-Cl bond distances of the optimized structure are in good agreement with those obtained from elaboration of the EXAFS experiments. Two Pd-S bond distances are obtained from calculations, both sufficiently close to those obtained from the EXAFS spectrum. This generates the structurally distorted arrangement shown in Figure 3.42, where it can be seen that the two thienyl rings are oriented with the S atoms on the same side, displaying a quite different approach to the two Pd^{II} centers. Formation of this non-symmetrical arrangement might be explained by assuming that after the binding of the first $PdCl_2$ unit at a distance of 2.25(4) Å (Table 3.19). The second unit binds preferably the N atom, but the S atom of the second thienyl ring is at a longer distance.

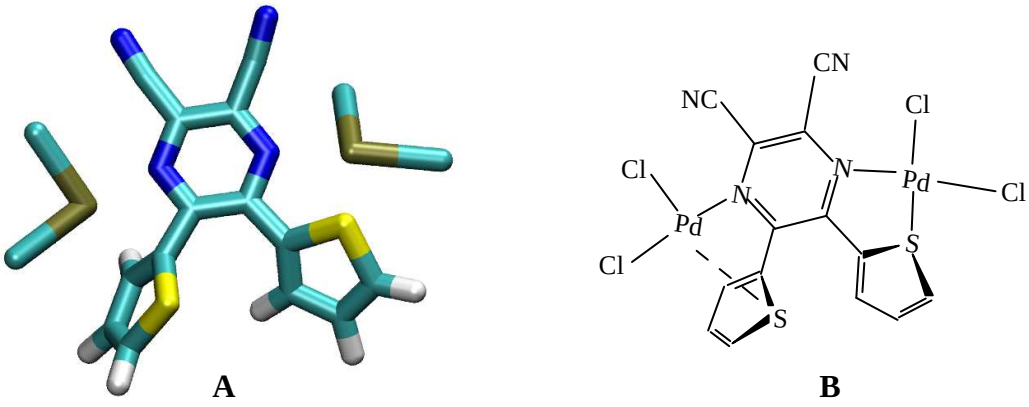

Figure 3.42. Calculated optimized structure (A) and schematic representation (B) for the bis-palladate compound $[(CN)_2Th_2Pyz(PdCl_2)_2]$.

CONCLUSIONS

The target of the present thesis work has been centered on the synthesis of two novel series of porphyrazine macrocycles carrying peripherally pyridine rings, either directly attached to the central tetrapyrrolic core (pyridylporphyrazines; Figure 3.43A) or bridged to it through quinoxaline rings (quinoxalinoporphyrazines; Figure 3.43C). Concomitantly with the investigation of their stability in the solid state and in solution and their general physicochemical behaviour, it was of interest for the two series of mononuclear compounds, to explore the effect on the UV-visible spectral behaviour caused respectively by the reduction of the π-conjugated macrocyclic framework, in the pyridylporphyrazines, and/or by the extension of the same π-delocalized electronic arrangement in the quinoxalinoporphyrazine compounds, with respect to the level of delocalization of the previously studied series of pyrazinoporphyrazines (Figure 3.43B); in other words the target was to establish a possible relationship between UV-visible spectral response and dimension of the π-delocalized system.

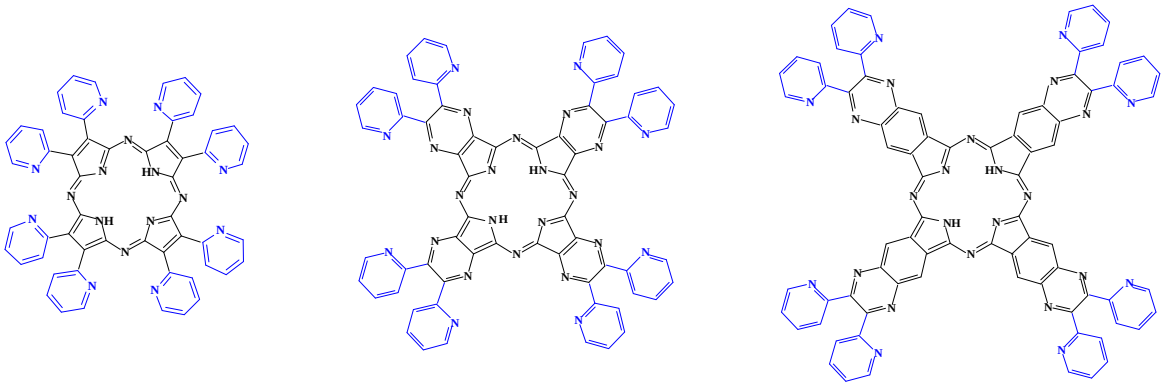

A B C

Figure 3.43

Following the accurate work conducted by elemental analyses, IR and NMR spectral studies, the detailed UV-visible spectral behaviour in the nonaqueous solvents pyridine, DMSO, DMF and in water was deeply explored. UV-visible spectral data in the low-donor nonaqueous solvents, in which occurring aggregation phenomena and/or reducibility of the compounds were often faced and accurately examined, indicate that there is a progressive highly remarkable bathochromic shift of the barycentre of the overall spectrum in the

direction pyridylporphyrazines → pyrazinoporphyrazines → quinoxalinoporphyrazines, in line with the parallel enhanced extension of the π-conjugated system of the macrocycles in the order given. These results are in line with expectation as seen on the basis of theoretical results developed on a parallel series of macrocyclic systems.[64]

The eight external pyridines, each two of them located in a vicinal relative position, allow the accomplishment of exocyclic coordination and formation of pentanuclear species carrying externally $PdCl_2$ and $PtCl_2$. Figure 3.44 proposes the pentametallic species for the pyridyl- (A) and quinoxalinoporphyrazines (B). Data at hand indicate that coordination of the Pd^{II} or Pt^{II} units takes place in all cases at the pyridine N atoms, and sites of the type $N_{2(pyr)}M'Cl_2$ (M' = Pd^{II}, Pt^{II}; "py-py" coordination) are generated, displaying a square planar geometry and directed nearly perpendicularly to the plane of the central π-conjugated macrocyclic system. External ligation modifies the UV-visible spectrum of the initial mononuclear species, the effect evidencing a bathochromic shift of the original main Q band by an average value of 15-20 nm. This remarkable shift is surprising if account is taken that exocyclic coordination of Pd^{II} and Pt^{II}, particularly for the pyrazino- and even more for the quinoxalinoporphyrazine compounds, takes place at the extreme periphery of the macrocycle and progressively more far away from the central metal. In addition, the external sites are oriented nearly perpendicularly to the plane of the macrocycle, a situation which appears unfavourable to the σ/π electronic contact of the Pd^{II} and Pt^{II} metal ions with the central porphyrazine core.

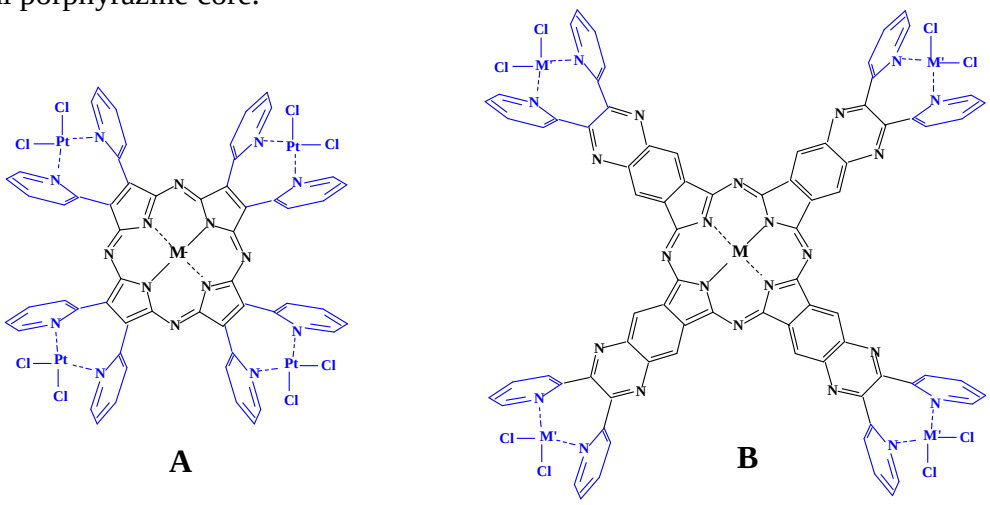

Figure 3.44. A) $[(PtCl_2)_4Py_8PzM]$ (M = $Mg^{II}(H_2O)$, Zn^{II}); B) $[(PtCl_2)_4Py_8TQuinPzM]$ M = $Mg^{II}(H_2O)$, Zn^{II} , Pd^{II}, Pt^{II}.; M' = Pd^{II}, Pt^{II}.

Further extension to the present work focused on the synthesis of supercharged macrocycles for the pyridyl- and quinoxalinoporphyrazines. The new octacationic compounds were prepared from the mononuclear species upon reaction with CH_3I, a process which results in the full N-methylation of the pyridine rings (Figure 3.45). Mention is deserved by the fact that the new charged species are water soluble (moderately) and examination of these species could be conducted in water solution and in the low-donor solvents pyridine, DMSO and DMF. In these latter solvents interesting effects are seen from the UV-visible spectra, which parallel those determined by the external metalation. In fact the spectra evidence in the process from neutral to octacationic species a bathochromic shift of the Q bands more or less of the order already encountered for the change mononuclear → pentanuclear species. As a result, this means that the charged macrocycles enhance their electron deficiency, a fact that should be confirmed by the electrochemical behaviour in terms of the expected less negative half-wave potentials with respect to those pertinent to the neutral mononuclear species. The electrochemical study of the neutral, pentanuclear and octacationic species is an obvious further step of investigation necessary for a better understanding of the role played by external metalation or quaternization of the macrocyclic periphery.

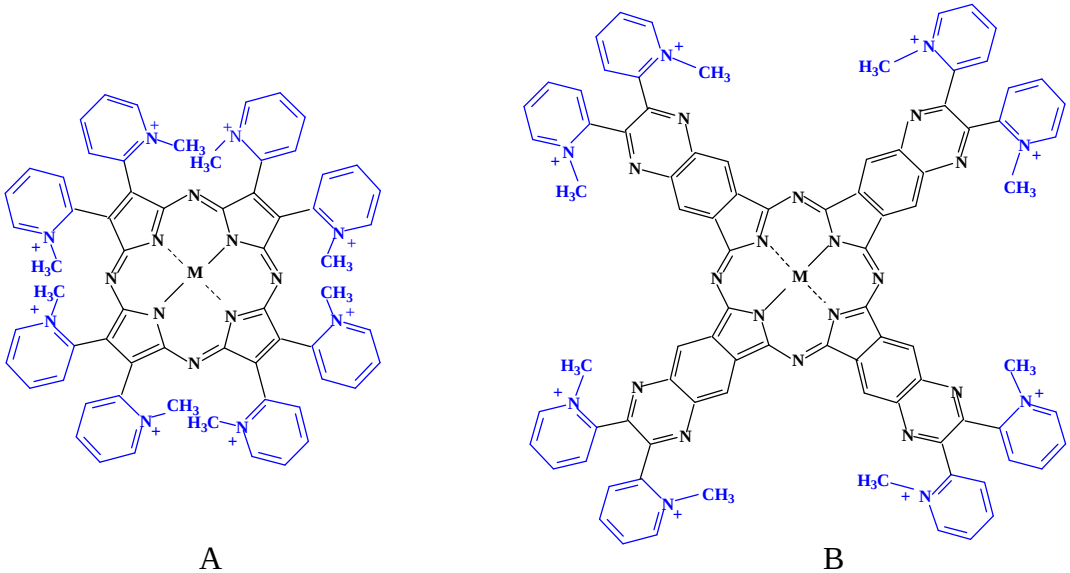

A B

Figure 3.45. A) $[(2\text{-Mepy})_8PzM]^{8+}$ and B) $[(2\text{-Mepy})_8TQuinPzM)]^{8+}$ (M = $Mg^{II}(H_2O)$, Zn^{II}).

The final certainly important challenge of some of the pyridyl- and quinoxalinoporphyrazines, especially those carrying centrally Zn^{II}, Mg^{II} (closed shell metal ions) or Pd^{II} and Pt^{II} (d^8 electronic structure and diamagnetic in a square planar arrangement), is their measured photoactivity for the generation in DMF of singlet oxygen, $^1O_2$, the citytoxic agent in the photodynamic therapy of cancer (PDT). The quantum yields of $^1O_2$ measured, particularly for the two pyridylporphyazines having centrally Zn^{II} and Mg^{II}, qualify these compounds as excellent photosensitizers. A combination of purity of the samples, water solubility, stability under the appropriate irradiation (600-750 nm), absence of aggregation in solution may be profitable for application in the PDT curative modality. The species carrying outside $PtCl_2$ units may open perspectives for applications as bimodal PDT/cis-platin anticancer agents. An effort for a further development of the work carried out in the present thesis, focusing on the applicative biomedical aspects, is believed necessary.

The parallel work on the new class of thienylporphyrazine macrocycles, allowed to provide information about the multifaceted mode of coordination of vicinal thienyl rings to a metal center for the precursor and corresponding macrocyclic systems. On the other hand the singlet oxygen and fluorescence response of the mono- and pentametallic complexes open perpectives for their potential use in PDT of cancer and for medical imaging and diagnosis.

REFERENCES

[1] Donzello, M. P.; Ou, Z.; Monacelli, F.; Ricciardi, G.; Rizzoli, C.; Ercolani, C.; Kadish, K. M. *Inorg. Chem.*, **2004**, *43*, 8626.

[2] *"The Porphyrins"*, Dolphin, D.; Ed.; Academic Press: New York, **1979**, *Vols. I-VII*.

[3] a)*"The Porphyrin Handbook"*, Kadish, K. M.,; Smith, K. M.; Guilard, R.; Eds; Academic Press: New York, **2000**, *Vols. 1-10*. b) *"The Porphyrin Handbook"*, Kadish, K. M., Smith, K. M.; Guilard, R.; Eds; Academic Press: New York, **2003**, *Vols. 11-20*.

[4] Kostenich, G. A.; Zhuravkin, I. N.; Zhavrid, E. A. *J. Photochem. Photobiol., B: Biol.*, **1994**, *22*, 211.

[5] (a) Byrne, G. T.; Linstead, R. P.; Lowe, A. W. *J. Chem. Soc.*, **1934**, 1017; (b) Linstead, R. P.; Lowe, A. W. *J. Chem. Soc.*, **1934**, 1022; (c) Linstead, R. P. *J. Chem. Soc.*, **1953**, 2873 and refs therein.

[6] (a) Robertson, J. M.; Linstead, R. P.; Dent, C. E. *Nature*, **1935**, 506; (b) Robertson, J.M.; Woodward, I. *J. Chem. Soc.*, **1937,** 219; (c) Robertson, J. M.; Woodward, I. *J. Chem. Soc.*, **1940**, 36.

[7] Gouterman, M. in *"The Porphyrins"*, Dolphin, D.; Ed.; Academic Press: New York, **1978**, *Vol. III*, 1.

[8] Linstead, R. P.; Whalley, M. *J. Chem. Soc.*, **1952**, 4839.

[9] Luk'yanets, E. A. *Zh. Org. Khim*., **1971,** *7*, 369.

[10] Michel, S. L. J.; Hoffman, B. M.; Baum, S. M.; Barrett, A. G. M. *Progress in Inorganic Chemistry*, **2001,** *50*, 473.

[11] a) Bilton, J. A., Linstead, R. P. *J. Chem. Soc.*, **1937**, 922; b) Linstead, R. P.; Noble, E. G.; Wright, J. M. *J. Chem. Soc.*, **1937**, 911.

[12] a) Christie, R. M.; Freer, B. G. *Dyes Pigm.*, **1997**, *33*, 107; b) Cook, M. J.; Jafari-Fini, A. *J. Mater. Chem.*, **1997**, *7*, 5; c) Cook, M. J.; Jafari-Fini, A. *Tetrahedron*, **2000**, *56*, 4085. Nemykin, V. N.; Polshina, A. E.; Kobayashi, N. *Chem. Lett.*, **2000**, 1236.

[13] Kudrevichvan, S. V.; Lier, J. E. *Coord. Chem. Rev.*, **1996**, *156***,** 163.

[14] Stuzhin, P. A.; Ercolani, C. "Porphyrazines with annulated heterocycles" in "*The Porphyrin Handbook*", Kadish, K. M.; Smith, K. M.; Guilard, R.; Eds. Academic Press: New York, **2003**, *Vol. 15*, p. 263.

[15] Mørkved, E. H.; Neset, S. M.; Kjøsen, H.; Hvistendahl, G.; Mo, F. *Acta Chem. Scand.*, **1994**, *48*, 912.

[16] Donzello, M. P.; Ercolani, C.; Stuzhin, P. A. *Coord. Chem. Rev.*, **2006**, *250*, 1530, and refs therein.

[17] a) Fujimori, M.; Suzuki, Y.; Yoshikawa, H.; Awaga, K. *Angew. Chem. Int. Ed.*, **2003**, *42*, 5863; b) Suzuki, Y.; Fujimori, M.; Yoshikawa, H.; Awaga, K. *Chem. Eur. J.*, **2004**, *10*, 5158.

[18] a). Donzello, M. P.; Ercolani, C.; Kadish, K. M.; Ricciardi, G.; Rosa, A.; Stuzhin, P. A. *Inorg. Chem*., **2007**, *46*, 4145; b) Donzello, M. P.; Ercolani, C.; Cai, X.; Kadish, K. M.; Ricciardi, G.; Rosa, A. *Inorg. Chem.*, **2009**, *48*, 9890.

[19] Donzello, M. P.; Ercolani, C.; Stuzhin, P. A; Chiesi-Villa, A.; Rizzoli, C. *Eur. J. Inorg. Chem.*, **1999**, 2075.

[20] Donzello, M. P.; Dini, D.; D'Arcangelo, G.; Ercolani, C.; Zhan, R.; Ou, Z.; Stuzhin, P. A.; Kadish, K. M. *J. Am. Chem. Soc*., **2003**, *125*, 14190.

[21] Donzello, M. P.; Ou, Z.; Dini, D.; Meneghetti, M.; Ercolani, C.; Kadish, K. M. *Inorg. Chem.*, **2004**, *43*, 8637.

[22] Viola, E.; Donzello, M. P.; Ciattini, S.; Portalone, G.; Ercolani, C. *Eur. J. Inorg. Chem.*, **2009**, *12*, 1600.

[23] Cai, X.; Donzello, M. P.; Viola, E.; Rizzoli, C.; Ercolani, C.; Kadish, K. M. *Inorg. Chem.*, **2009**, *48*, 7086 and refs therein.

[24] Donzello, M. P.; Viola, E.; Cai, X.; Mannina, L.; Rizzoli, C.; Ricciardi, G.; Ercolani, C.; Kadish, K. M.; Rosa, A. *Inorg. Chem.*, **2008**, *47*, 3903.

[25] Donzello, M. P.; Viola, E.; Bergami, C.; Dini, D.; Ercolani, C.; Giustini, M.; Kadish, K. M.; Meneghetti, M.; Monacelli, F.; Rosa, A.; Ricciardi, G. *Inorg. Chem*., **2008**, *47*, 8757.

[26] a) Donzello, M. P.; Viola, E.; Cai, X.; Mannina, L.; Ercolani, C.; Kadish, K. M. *Inorg. Chem*., **2010**, *49*, 2447; b) Donzello, M. P.; Viola, E.; Mannina, L.; Barteri, M.; Fu, Z.; Ercolani, C. *J. Porphyrins Phthalocyanines*, **2011**, *15*, 984.

[27] Hambright, H. in "The Porphyrin Handbook", Kadish, K. M.; Smith, K. M.; Guilard, R.; Eds; Academic Press: New York, **2003**, *Vols. 1-20*, p. 130.

[28] "*Phthalocyanines: Properties and Applications*", *Vols. 1-4* (Edrs.: C.C. Leznoff, A.B.P. Lever), VCH Publishers, New York, **1989**-**1996**.

[29] "The Porphyrin Handbook", *Vols. 15-20*, Kadish, K. M.; Smith, K. M; Guilard, R.; Eds; Academic Press: New York, **2003.**

[30] Anderson, M. E.; Barrett, A. G. M.; Hoffman, B. M. *Inorg. Chem*., **1999**, *38*, 6143.

[31] a) Bergami, C.; Donzello, M. P.; Ercolani, C.; Monacelli, F.; Kadish, K. M.; Rizzoli, C. *Inorg. Chem.*, **2005**, *44*, 9852; b) Bergami, C.; Donzello M. P.; Monacelli, F.; Ercolani, C.; Kadish, K. M. *Inorg. Chem.*, **2005**, *44*, 9862.

[32](a) Moreira, L. M.; Vieira dos Santos, F.; Pereira Lyon, J.; Maftoum-Costa, M.; Pacheco-Soares, C.; Soares da Silva, N. *Aust. J. Chem.*, **2008**, *61*, 741; (b) O'Connor, A. E.; Gallagher, W. M.; Byrne, A. T. *Photochem. Photobiol.*, **2009**, *85*, 1053; (c) Szacilowski, K.; Macyk, W.; Drzewiecka-Matuszek, A.; Brindell, M.; Stochel, G. *Chem. Rev.*, **2005**, *105*, 2647; (d) Detty, M. R.; Gibson, S. L.; Wagner, S. J. *J. Med. Chem.*, **2004**, *47*, 3897; (e) De Rosa, M. C.; Crutchley, R. J. *Coord. Chem. Rev*., **2002**, *233-234*, 351-371; (f) Pandey, R. K.; Zheng, G. in "The Porphyrin Handbook", Kadish, K. M., Smith, K. M., Guilard, R. Eds., **2000**, Vol. 6, Chapter 43, pp.157-230.

[33] (a) Redmond, R. W.; Gamlin, J. N. *Photochem. Photobiol*., **1999**, *70*, 391; (b) Ali, H.; van Lier, E. *Chem. Rev.*, **1999**, *99*, 2379-2450.

[34] Sharman, W. M.; Allen, C. M.; van Lier, J. E. *Drug Discovery Today*, **1999**, *4*, 507; (b) Bellner, B. A.; Dougherty, T. J. *J. Clin. Laser Med. Surg.*, **1996**, *14*, 311.

[35] (a) Shinohara, H.; Tsaryova, O.; Schnurpfeil, G.; Wöhrle, D. *J. Photochem. Photobiol. A*: *Chemistry*, **2006,** *184*, 50; (b) Spiller, W.; Kliesch, H.; Wöhrle, D.; Hackbarth, S.; Röder, B.; Schnurpfeil, G. *J. Porphyrins Phthalocyanines*, **1998**, *2*, 145; (c) Schnurpfeil, G.;

Sobbi, A. K.; Spiller, W.; Kliesch, H.; Wöhrle, D. *J. Porphyrins Phthalocyanines*, **1997**, *1*, 159;

(d) Fernandez, D. A.; Awruch, J.; Dicelio, L. E. *Photochem. Photobiol.*, **1996**, *63*, 784; e) Müller, S.; Mantareva, V.; Stoichkova, N.; Kliesch, H.; Sobbi, A.; Wöhrle, D.; Shopova, M. *J. Photochem. Photobiol. B: Biology*, **1996**, *35*, 167; f) Maree, S. E.; Nyokong, T. *J. Porphyrins Phthalocyanines*, **2001**, *5*, 782; g) Lawrence, D.S.; Whitten, D. G. *Photochem. Photobiol.*, **1996**, *64*, 923.

[36] (a) Zimcik, P.; Novakova, V.; Miletin, M.; Kopecky, K. *Macroheterocycles*, **2008**, *1*, 21, and refs. therein; (b) Mitzel, F.; Fitzgerald, S.; Beeby, A.; Faust, R. *Eur. J. Org. Chem.*, **2004**, 1136.

[37] a) Baum, S. M.; Trabanco A. A.; Montalban, A. G.; Micallef, A. S.; Zhong, C.; Meunier, H. G.; Suhling, K.; Phillips, D.; White, A. J. P.; Williams, D. J.; Barrett, A. G. M.; Hoffman, B. M. *J. Org. Chem.*, **2003**, *68*, 1665; b) Sakellariou, E. G.; Montalban, A. G.; Meunier H.; Rumbles, G.; Philips, D.; Ostier, R. B.; Suhling, K.; Barrett, A. G. M.; Hoffman, B. M. *Inorg. Chem.*, **2002**, *41*, 2182; c) Montalban, A. G.; Baum, S.M.; Barrett, A. G. M.; Hoffman, B. M. *Dalton Trans.*, **2003**, 2093.

[38] Michelsen, U.; Kliesch, H.; Schnurpfeil, G.; Sobbi, A. K.; Wöhrle, D. *Photochem. Photobiol.*, **1996**, *64*, 694.

[39] Donzello, M. P. et al. Manuscript submitted.

[40] a) De Mori, G.; Fu, Z.; Viola, E.; Cai, X.; Ercolani, C.; Donzello, M. P.; Kadish, K. M. *Inorg. Chem.*, **2011**, *50*, 8225. b) Donzello, M.P.; De Mori, G.; Viola, E.; Ercolani, C.; Bodo, E.; Mannina, L.; Capitani, D.; Rizzoli, C.; Gontrani, L.; Aquilanti, G.; Kadish, K. M.; D'Angelo, P. *Inorg. Chem*, **2011**, *50*, 12116.

[41] Hass, M.; Liu, S.; Neels, A.; Decurtins, S. *Eur. J. Org. Chem.*, **2006**, 5467.

[42] Kharascg, M. S.; Seyler, R. C.; Mayo, F. R. *J. Am. Chem. Soc.*, **1938,** *60*, 882.

[43] Piechucki, C.; Michalski, J. *Bull. Acad. Pol. Sci., Ser. Sci. Chim.*, **1970**, *18*, 605.

[44] Morkved, E. H.; Ossletten, H.; Kjosen, H. *J. Prakt. Chem.*, **2000,** *342*, 83.

[45] a) Filipponi, A.; Di Cicco, A.; Natoli, C. R. *Phys. Rev. B*, **1995**, *52*, 15122; b) Filipponi, A.; Di Cicco, A. *Phys. Rev. B*, **1995**, *52*, 15135.

[46] Sheldrick, G. M. *Acta Cryst.* 2008, A**64**, 112.

[47] Frisch, M. J.; Trucks, G. W.; Schlegel, H. B.; Scuseria, G. E.; Robb, M. A.; Cheeseman, J. R.; Scalmani, G.; Barone, V.; Mennucci, B.; Petersson, G. A.; Nakatsuji, H.; Caricato, M.; Li, X.; Hratchian, H. P.; Izmaylov, A. F.; Bloino, J.; Zheng, G.; Sonnenberg, J. L.; Hada, M.; Ehara, M.; Toyota, K.; Fukuda, R.; Hasegawa, J.; Ishida, M.; Nakajima, T.; Honda, Y.; Kitao, O.; Nakai, H.; Vreven, T.; Montgomery J. A., Jr.; Peralta, J. E.; Ogliaro, F.; Bearpark, M.; Heyd, J. J.; Brothers, E.; Kudin, K. N.; Staroverov, V. N.; Kobayashi, R.; Normand, J.; Raghavachari, K.; Rendell, A.; Burant, J. C.; Iyengar, S. S.; Tomasi, J.; Cossi, M.; Rega, N.; Millam, J. M.; Klene, M.; Knox, J. E.; Cross, J. B.; Bakken, V.; Adamo, C.; Jaramillo, J.; Gomperts, R.; Stratmann, R. E.; Yazyev, O.; Austin, A. J.; Cammi, R.; Pomelli, C.; Ochterski, J. W.; Martin, R. L.; Morokuma, K.; Zakrzewski, V. G.; Voth, G. A.; Salvador, P.; Dannenberg, J. J.; Dapprich, S.; Daniels, A. D.; Farkas, Ö.; Foresman, J. B.; Ortiz, J. V.; Cioslowski, J. and Fox, D. J. *Gaussian 09*, Revision A.1, Gaussian, Inc., Wallingford CT, 2009.

[48] Becke, A. D. *J. Chem. Phys.*, **1993**, *98*, 5648.

[49] McLean A. D. and Chandler, G. S. *J. Chem. Phys.*, **1980**, *72*, 5639.

[50] Hay, P. J.; Wadt, W. R. *J. Chem. Phys.*, **1985**, *82*, 299.

[51] Lin, X. Q.; Kadish, K. M. *Anal. Chem.*, **1985**, *57*, 1849.

[52] Donzello, M. P.; Viola, E.; Giustini, M.; Monacelli, F.; Ercolani C. *Dalton Trans.*, **2012**, *41*, 6112.

[53] Zimcik, P.; Miletin, M.; Musil, Z.; Kopecky, K.; Kubza, L.; Brault, D. *J. Photochem. Photobiol. A: Chemistry*, **2006**, *183*, 59.

[54] Nicole, F.; Cusumano, M.; Di Pietro, M. L.; Scopelliti, R.; Bruno, G. *Acta Crystallogr*., **1998**, *C54*, 485.

[55] Granifo, J.; Vargas, M. E.; Garland, M. T.; Baggio, R. *Inorg. Chim. Acta*, **2002**, *305*, 143.

[56] Granifo, J.; Vargas, M. E.; Rocha , H.; Garland, M. T.; Baggio, R. *Inorg. Chim. Acta*, **2001**, *321*, 209.

[57] Miedaner, A.; Haltiwanger, R. C.; Dubois, D. L. *Inorg. Chem*., **1991**, *30*, 417.

[58] Velasquez, S. V.; Fox, G. A.; Broderick, W. E.; Anderesen, K. a.; Anderson, O. P.; Barret, A. g. M.; Hoffman, B. M. *J. Am. Chem. Soc.*, **1992**, *114*, 7416.

[59] Fischer, M. S.; Templeton, D. H.; Zalkin, A.; Calvin, M. *J. Am. Chem. Soc.*, **1971**, *93*, 2622.

[60] a) Stuzhin, P.A.; Bauer, E. M.; Ercolani, C. *Inorg. Chem*., **1998**, *37*, 1533; b) Bauer, E. M.; Ercolani, C.; Galli, P.; Popkova, I.A.: Stuzhin, P. A. *J. Porphyrins Phthalocyanines*, **1999**, *3*, 371.

[61] Matzumoto, S.; Endo, A.; Mizuguchi, J.Z. *Krystallogr.* **2000**, *215*, 182.

[62] a) Stillman, M.J. In *Phthalocyanines: Properties and Applications;* Leznoff, C. C.; Lever, A. B. P., Eds.; VCH Publisher: New York, **1989**; Vol. 1, pp 133-289. b) Mack, J.; Stillman, M. J. In *The Porphyrin Handbook;* Kadish, K. M., Smith, K.M., Guilard, R., Eds.; Academic Press: New York, **2003**; Vol. 16, pp 43-116.

[63] Stuzhin, P.A. *J. Porphyrins Phthalocyanines*, **1999**, *3*, 500.

[64] Kobayashi, N.; Konami, H. in "*Phthalocyanines: Properties and Applications*", Vol. 4, pp 349-404, Edrs.: C.C. Leznoff, A.B.P. Lever, VCH Publishers, New York, **1996**.

[65] Owen, A. J. *Agilent Tecnologies Application Note*, **1995**, pub. N. 5963-3937E.

[66] Spikes, J. D.; van Lier, J. E.; Bommer, J. C. *J. Photochem. Photobiol. A: Chem.*, **1995**, *91*, 193.

[67] Donzello, M. P.; Vittori, D.; Viola, E.; Manet, I.; Mannina , L.; Cellai, L.; Monti, S.; Ercolani, C. *Inorg. Chem*., **2011**, *50*, 7391.

[68] Clark, D.W.; Hush, N.S.; Yandle, J. R. *Inorg. Chem.*, **1972**, *11*, 1738.

AKNOWLEDGEMENTS

Firstly, I would like to thanks Dr. Maria Pia Donzello for assisting me with her professional and personal advice and Prof. Claudio Ercolani for his professional guidance, and extensive scientific discussions throughout these years.

My thanks are also due to Dr. Enrico Bodo for the theoretical calculations, to Prof. Karl M. Kadish for the electrochemical measurements, to Prof. Luisa Mannina for NMR spectra and the related discussion, to Prof. Mario Barteri for his kindness in the use of fluorescence instrument, to Prof. Paola D'Angelo for the EXAFS calculations and to Dr. Maria Luisa Astolfi for ICP-Plasma analyses.

I wish also to thank Dr. Elisa Viola for her help in the measurements of singlet oxygen quantum yields, and for her friendship and support in these years. Finally, my special gratitude goes to my family for the encouragement throughout these years.